

ISSET JOURNAL OF EARTHQUAKE TECHNOLOGY

Vol. 45

No. 3-4

September-December 2008

CONTENTS

No.	Paper	Page
497	GIS-Based Urban Seismic Risk Assessment Using RISK.iitb Ravi Sinha, K.S.P. Aditya and Achin Gupta	41
498	Ground Vibration from Rigid Foundation by BEM-TLM Badreddine Sbartaï and Ahmed Boumekik	65
499	A Modal Combination Rule for Ordered Peak Response under Multi-component Ground Motion Ayan Sadhu and Vinay K. Gupta	79
	Technical Note	
	Mode-Based Procedure to Interpolate Strong Motion Records of Instrumented Buildings Rakesh K. Goel	97

Financial Assistance from AICTE and DST, New Delhi for the Publication of ISET Journals for 2008–2009 is duly acknowledged.

GIS-BASED URBAN SEISMIC RISK ASSESSMENT USING RISK.IITB

Ravi Sinha, K.S.P. Aditya and Achin Gupta

Department of Civil Engineering
Indian Institute of Technology Bombay
Powai, Mumbai-400076

ABSTRACT

The earthquake risk or damage potential of an area is due to a combination of seismic hazard, and vulnerability of the built environment and its exposure. The damage during recent earthquakes worldwide has demonstrated the need for seismic risk assessment for disaster management applications. It is also often observed that the complex risk assessment carried out in the scientific domain does not easily provide information and data amenable to policy making or for disseminating seismic risk to the public. In this paper, a newly developed GIS-based system for seismic risk assessment, namely RISK.iitb, has been described. RISK.iitb quantifies seismic hazard, structural vulnerability, and exposure and loss estimation. This system considers the requirements of disaster management community, and results can be easily understood by the various stakeholders while maintaining scientific rigour. An example analysis has been performed for the Mumbai municipal region to illustrate the uses of RISK.iitb.

KEYWORDS: Disaster Management, Seismic Hazard, Vulnerability, Economic Loss, Mumbai Scenario

INTRODUCTION

The past few decades have witnessed an increase in the number of damaging earthquakes in India, with nine damaging earthquakes occurring during the last two decades itself. The vast extent of damage and the consequent loss of life associated with these events reflect the poor construction practices in India. Before the 2001 Bhuj earthquake, constructions with poor seismic resistance were assumed to be a feature of non-urban areas, with urban structures considered safer due to the use of engineering knowledge and modern construction materials. However, this earthquake shattered the myth of urban seismic safety through widespread damage to modern buildings. The low awareness among the general public towards structural safety and the inability of regulatory bodies and technical professions in maintaining quality standards in constructions has created an urgent need to educate the leaders, public, city planners, architects, and the engineering professionals about the consequences of earthquakes. Advocacy of the importance of seismic safety requires understanding of seismic risk and the adverse consequences of earthquakes by all the stakeholders. This issue assumes particular importance due to the long return period of damaging earthquakes in India, resulting in diminishing public memory of earthquake disasters with time. Recent earthquakes, such as the 2001 Bhuj earthquake that had followed the damaging Anjar earthquake in 1957 in the same area, have shown that the vulnerability of the constructions did not get reduced despite the experiences of the 1957 earthquake. As a result, the same tragic lessons had to be re-learned in 2001 as during 1957 (Sinha et al., 2001).

The evaluation of consequences of earthquakes using a rigorous scientific approach does not automatically provide useful data for advocacy, policy-making, or for implementation of the earthquake risk management initiatives. These results must be interpreted in a manner that makes the various non-expert stakeholders understand the factors contributing to the damage and losses due to earthquake and their influence on the affected area. One approach that has been successfully used in the recent past is based on developing earthquake scenarios in which losses and other consequences are estimated due to different potential earthquakes. In this the results are presented in the form of charts and colour coded maps, which can be easily understood by the various stakeholders in disaster management without requiring them to understand the intricacies of the mathematical modelling and other scientific details. Some recent scenario studies that have been found useful for advocacy and policy-making include RMS (1995), Chen et al. (1997), and Erdik et al. (2005).

Scientifically realistic earthquake damage scenarios, if available for India, can be invaluable for the advocacy of seismic safety and for disaster management. The disaster scenario information can be used to sensitize various stakeholders regarding the risk and potential consequences of earthquakes. The information can thus overcome some of the limitations due to the absence of earthquake disaster memory in the society. The disaster scenario can also help in identifying the most vulnerable areas and population groups that will require the most assistance in the aftermath of a damaging earthquake. The pros and cons of various disaster management interventions can also be evaluated using earthquake disaster scenario tools by simulating the effectiveness of these measures in reducing the losses over time. The use of disaster scenarios is very useful for both urban and rural areas. Their use for effective disaster management planning is essential in urban areas because of the intense concentration of people, infrastructure, and resources that may be affected by a damaging earthquake. As a result, disaster management plans that are prepared without carrying out rigorous risk assessment and scenario development, such as those described herein, are unable to take advantage of this information for optimal prioritization of resources and for monitoring long-term reduction of risk.

Several methodologies have been developed to estimate the consequences of scenario earthquakes. These methodologies can be probabilistic, wherein the probability of exceeding different levels of losses with corresponding uncertainties are evaluated, or deterministic wherein the losses due to a given scenario earthquake are estimated. The loss estimation can include the extent of damage to the buildings, the number of people injured, the number of fatalities, and the economic losses occurring in the region under study. The probabilistic assessment is often used by insurance companies to manage their risk portfolio. However, the probabilistic assessment does not easily provide information and data useful for policy making or for public advocacy. Recent publications also indicate that deterministic scenario-based assessment can provide a suitable basis for carrying out probabilistic risk assessment (Klügel et al., 2006). Hence, in this study only the deterministic analysis procedure has been considered whose results are realistic and easier to understand by the non-technical stakeholders.

Various efforts have been globally made to develop software systems that quantify the losses caused due to natural hazards like earthquakes, hurricanes, floods, etc. The most well known tools for the estimation of losses associated with earthquakes include HAZUS (NIBS, 1999), RADIUS (IDNDRS, 1999), HAZ-Taiwan (Yeh et al., 2006), and RISK-UE (Spence and Le Brun, 2006).

HAZUS is a tool that can be used for earthquake-related mitigation, emergency preparedness, response and recovery planning, and disaster response operations. It has been implemented on GIS platforms such as Arc View and MapInfo. It provides the user ability to perform different levels of analysis, ranging from estimates based on simplified models using default inventory to very refined studies based on detailed engineering and geotechnical data for a specific study region. Its methodology is comprehensive, and it generates maps and calculates losses with different probabilities. Various US agencies use HAZUS for earthquake risk management. The HAZUS approach has been used for HAZ-Taiwan and RISK-UE projects with modifications based on local hazard and vulnerability in Taiwan and Europe, respectively.

RADIUS is a risk assessment tool, which has been implemented in MS-Excel software. The user selects rectangular meshes, which roughly represent the area under study. Properties are assigned to each mesh, and the tool estimates the losses due to a scenario earthquake using factors, the default values of which are provided in the tool. The user has the freedom to change the values of these factors as per the area under study. However, the tool gives very approximate estimates for losses, and the results are also not properly displayed. RADIUS has been widely used for simulation training of engineers, architects and public officials, particularly in developing countries, since it is freely available and requires minimal computing resources.

Even though the software tools such as HAZUS give very detailed results, those are not suitable for loss estimation simulations from earthquakes in India because the hazard and vulnerability assessment in HAZUS has been carried out using the data applicable for USA, Taiwan, and Europe. Further, the financial models for determining the damage to social and economic losses are not applicable to India. Another problem with the HAZUS method is that it requires extensive urban data regarding buildings, population, and economic activities that are typically not available in India. On the other hand, even though the method is simple requiring limited inputs, RADIUS does not have advanced processing capabilities and only gives approximate loss estimates. Earthquake risk assessment tools that consider the

special requirements of India and other similar developing countries are not available in the public domain.

The authors have recently developed a seismic risk assessment system known as RISK.iitb at the Indian Institute of Technology Bombay (Gupta and Sinha, 2006; Aditya and Sinha, 2006). This risk assessment system uses Geographical Information System (GIS) kernel and is amenable to convenient graphical inputs and outputs. The physical inventory data for carrying out risk assessment can be specified for each structure as individual objects or grid-wise inventory after dividing the entire study area into small-square grids. The simulation capabilities where each structure is considered as a separate object is not very useful for policy-making and public advocacy due to its excessive detail. In this paper, the methodology for seismic risk assessment and loss estimation in RISK.iitb for grid-wise simulation, which is more useful for policy-making, public policy and disaster management applications, is described. Various options for specification of inputs are also described. The procedure for estimation of injuries, deaths, and economic losses is also briefly presented. It may be noted that RISK.iitb is undergoing constant enhancement, and additional mathematical models for hazard, vulnerability, and losses are being implemented. The main aim of this paper is to illustrate the importance of disaster scenario studies using GIS platform for advocacy and policy-making and for the preparation of disaster management plans.

RISK.iitb has been used for carrying out seismic risk assessment of an urban area for a scenario earthquake. The city of Mumbai has been selected for the example assessment and to illustrate the features of the risk assessment system. The results have been presented in tables and easy-to-understand figures to demonstrate the effectiveness of using RISK.iitb for advocacy and to communicate with decision-makers and other non-technical stakeholders. The results presented here are in form of a postulated scenario for a given earthquake on the basis of available data, which can be improved further by using RISK.iitb based on more detailed inputs as and when those become available.

METHODOLOGY FOR SEISMIC RISK ASSESSMENT

The assessment of seismic risk involves the estimation of consequences of an earthquake in the chosen area in terms of the expected damage and loss from a given hazard to a given element at risk. For deterministic risk assessment, the estimation is typically carried out for a hazard event, such as an earthquake of a particular magnitude at a specified location. For probabilistic risk assessment, the consequences can be assessed over a specified period in future (Bendimerad, 2001). The risk assessment involves evaluation of seismic hazard, vulnerability of structures, exposure, and finally loss estimation. Thus, the total risk can be expressed simply in the following pseudo-mathematical form:

$$\text{Risk} = \text{Hazard} \times \text{Vulnerability} \times \text{Exposure} \tag{1}$$

The methodology has been outlined in Figure 1. Various components used in risk assessment in RISK.iitb have been explained below.

1. Seismic Hazard

Seismic hazard quantifies ground motions generated due to an earthquake in terms of peak ground acceleration (PGA) or other similar parameters associated with a scenario earthquake (Kramer, 1996). In this paper, a deterministic seismic hazard assessment has been carried out, where hazard is evaluated at the centre of each grid. The ground-motion parameters in deterministic assessment are estimated for the specified earthquake event that is assumed to occur at the specified location and depth. The computation of seismic hazard requires the following inputs (Gupta and Sinha, 2006):

- i) Source characterization, which includes (a) point source model—epicentre and hypocentral depth, or (b) line source model—epicentre, fault orientation (or bearing), and type of fault. For strike-slip fault, the fault rupture model based on Wells and Coppersmith (1994) has been implemented.
- ii) Attenuation relationships that define how ground motions decrease as a function of distance. The following attenuation relationships that have been found to be suitable for Deccan and peninsular India have been implemented in RISK.iitb:
 - a) The relationship by Iyengar and Raghukanth (2004) for PGA in terms of acceleration due to gravity is given by

$$\ln \text{PGA} = 1.6858 + 0.9241 \times (M - 6) - 0.076 \times (M - 6)^2 - \ln R - 0.0057R + \ln \varepsilon \tag{2}$$

where $\ln \varepsilon$ is the error in the estimation of \ln PGA, whose standard deviation is given as $\sigma(\ln \varepsilon) = 0.468$; R is the hypocentral distance; and M is the moment magnitude. The above attenuation relationship is valid for hard rock exposed on the surface, with shear wave velocity V_s exceeding 3.6 km/s.

- b) The relationship by Atkinson and Boore (1995) for PGA in terms of cm/s^2 is given by

$$\ln \text{PGA} = 3.79 + 0.298 \times (M - 6) - 0.0536 \times (M - 6)^2 - \ln R - 0.00135R + \ln \varepsilon \quad (3)$$

where $\ln \varepsilon$ is the error in the estimation of \ln PGA, whose standard deviation is given as $\sigma(\ln \varepsilon) = 0.250$; R is the hypocentral distance; and M is the moment magnitude. The relationship is derived from an empirically based stochastic ground motion model. The expression is valid for hard rock sites with shear wave velocity V_s exceeding 3.8 km/s.

- c) The relationship by Toro et al. (1997) for PGA in terms of acceleration due to gravity is given by
- $$\ln \text{PGA} = 2.20 + 0.81 \times (M - 6) - 1.27 \times \ln R + 0.11 \times \max[\ln(R/100), 0] - 0.0021R \quad (4)$$

where R is the source-to-site distance, i.e., $R = \sqrt{R_{jb}^2 + C_7^2}$, with R_{jb} taken as the closest horizontal distance to the earthquake rupture in kilometres, and $C_7 = 9.3$, while M is the moment magnitude. This expression is valid for hard rock sites with shear wave velocity V_s exceeding 1.8 km/s at the surface.

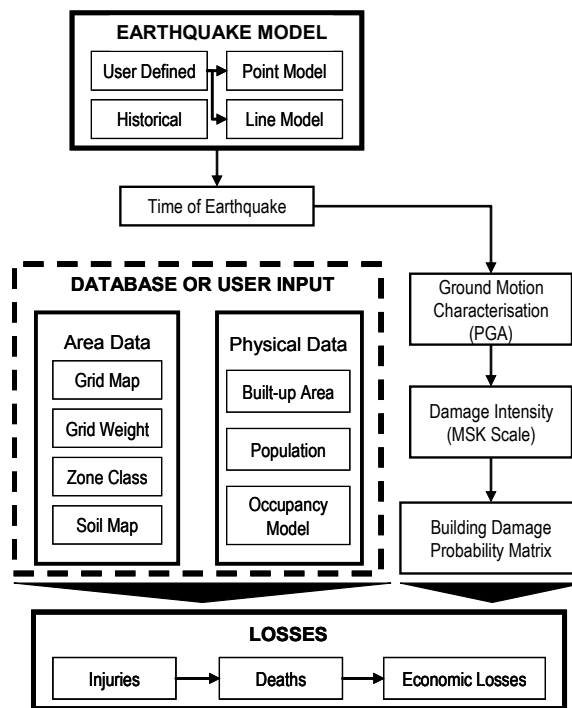


Fig. 1 Methodology for loss estimation using grid-wise assessment in RISK.iitb

- iii) Site characteristics, which include soil, sediments, and weathered rock affecting the ground shaking experienced during an earthquake. Amplification factors are usually proposed with each attenuation relationship; those modify the ground motion parameter appropriately to include the site effects. Mathematical relationships for the amplification have not been implemented in this version of RISK.iitb so far, and the amplification factors can be specified by the user for each soil type, if required, using the interactive input option of the software tool.

The uncertainties associated with each of the above factors may be quantified. However, this has not been taken into account in the present implementation of RISK.iitb, since it is based on deterministic risk assessment. The hazard assessment thus determines the median peak ground acceleration based on the selected earthquake attenuation model.

2. Damage Intensity

The intensity of an earthquake at a place is a measure of the destructive effects of the earthquake on buildings and other structures at that place. Several attempts have been made to correlate earthquake intensity (on intensity scale) to specific physical parameters of ground motion, especially peak ground acceleration (PGA). For the present study, the approximate empirical relationship by Wald et al. (1999) based on data from California has been used to obtain the Modified Mercalli Intensity I_{mm} from the PGA at any location:

$$I_{mm} = 2.20 \log(\text{PGA}) + 1.00 \quad (5)$$

The Indian Standard code (BIS, 2002) specifies damage intensity in terms of the MSK intensity scale, and not the Modified Mercalli Intensity (MMI) scale. Expressions relating MSK and MMI intensity levels have been proposed (for example, ASK, 1977), which show that these levels are similar in the range of interest (i.e., between the intensity levels IV and IX). Since MMI and MSK levels are quite similar in definition and range of expected structural response at each level on considering the uncertainty in assigning damage levels based on visual observation of structural behaviour, MMI values are assumed to be equal to MSK values in the present study. The resulting errors are expected to be smaller than or of similar order to those due to other factors such as error in hazard characterization, data on structural vulnerability, etc. The authors also intend to implement local-damage-intensity-to-PGA relationships, as and when those become available, which can improve the intensity assessment and consequently loss estimation in RISK.iitb by incorporating the local data that considers the effect of parameters, such as ground motion duration, frequency content, etc.

3. Seismic Vulnerability

Seismic vulnerability quantifies the propensity of a building or a type of buildings to be damaged during earthquake ground motions (Karnik et al., 1984). Several methods are available for performing the vulnerability analyses. The type of method chosen depends on the objective of the assessment and the availability of data (Lang, 2002). In the present study, vulnerability of the buildings implied in macro seismic intensity scales has been considered. The method utilizes damage probability matrices (DPMs) that provide the level of damage corresponding to ground motion intensity as a conditional probability factor.

Different buildings vary in their degree of vulnerability as a function of geometrical or qualitative characteristics (such as height, plan dimensions, elevation configurations, age, etc.), and structural characteristics (such as mass, stiffness, quality of construction, strength, intrinsic ductility, state of stress, seismic displacements, non-linear behaviour parameters, and other structural information). Hence, there is a need to classify the structures by their types and uses. In the present study, the types of buildings have been defined on the basis of the material used for construction and are (1) reinforced concrete, (2) steel, (3) masonry, and (4) non-engineered buildings. Each building type is further classified based on whether the building has been designed as per the code, i.e., complying with the earthquake-resistant provisions or without complying with the code provisions. In the present study, five damage states have been defined based on BIS (2002), Sinha and Adarsh (1999), and Musson (2000). Each damage state has been assigned a mean damage probability, indicating the mean loss, corresponding to different earthquake intensities. The percentage of loss in total value corresponding to different damage intensities for each building type is obtained from loss functions, which are based on the data available from previous earthquakes. By using appropriate loss functions one can assess the potential damage loss suffered by a grid for a given scenario earthquake. The vulnerability function, relating the earthquake damage intensity to damage state, used in this study is based on Sinha and Adarsh (1999) and is given in Figure 2.

When using grid-wise simulation, where the region under study is divided into small-square grids, each grid may contain several buildings of different building types. Therefore, the total built area of all buildings of a specified building type in a grid is considered in this study. The vulnerability of a building type is quantified by assigning a damage state based on the MSK intensity at the centroid of the grid.

4. Exposure

Exposure includes property, i.e., the inventory (structural and non-structural) value of the buildings and building contents, and the human population at risk, of being exposed to the damaging earthquake.

The assessment of the consequences of an earthquake on exposure requires the assessment on each component separately as described below.

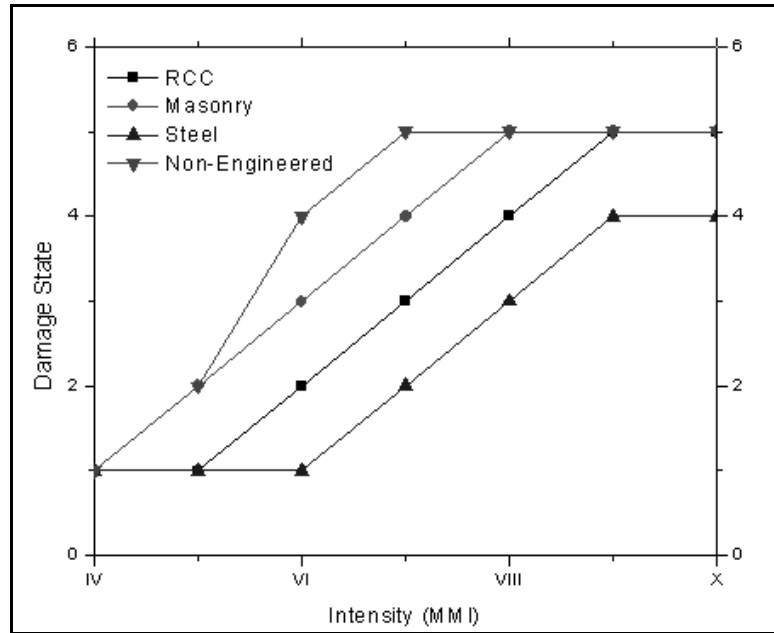


Fig. 2 Vulnerability curves for different building types (Sinha and Adarsh, 1999)

4.1 Population Analysis

A population analysis evaluates the total population of the region exposed to the earthquakes and distributes it to different building types. This evaluation is carried out grid-wise. In this study, the population distribution is done based on the time of scenario earthquake, occupancy classes, model building types, and area of various buildings present in the grid (see Table 1). The temporal occupancy model by Coburn and Spence (2002), which gives the distribution of population during different times of the day, has been used to obtain the population in different buildings at the time of the earthquake as an alternative. This model is based on the data obtained from developed countries. However, it may be noted that the range of commercial activities in Mumbai closely resembles that in major cities of developed countries in terms of typical office timings, presence of operations on 24×7 basis, and typical commuting time. Based on these considerations, and in view of the absence of temporal occupancy models based on Indian data, the temporal occupancy model by Coburn and Spence (2002) has been implemented in RISK.iitb.

The total population in all buildings of a given occupancy type is given by the following relationship:

$$PO = F \times \text{Total Population} \quad (6)$$

where F is the percentage of population residing in a given occupancy type at a particular time. This is specified in Gupta (2006) for the night population and is obtained from Table 1 for the floating population.

Table 1: Distribution of Floating Population in Different Building Types (Gupta, 2006)

Building Type	Population (%)
Residential	0
Commercial	90
Industrial	5
Non-engineered (and mixed occupancy)	5

4.2 Property Analysis

The property analysis in each grid refers to the evaluation of structural and non-structural components and the contents of all buildings in the grid. The value of the structural and non-structural components of a building has been assumed to depend on model building type and the occupancy class of the building. The occupancy classes included in the system are (a) residential, (b) commercial, and (c) industrial (Gupta, 2006).

5. Loss Estimation

Loss estimation refers to the evaluation of social and economic losses that are likely to be experienced during the scenario earthquake. The methodology for the assessment of these losses is described below.

5.1 Social Losses

This process involves the estimation of number of people likely to be injured at different severity levels. This evaluation considers the population in each building of the grid at the time of the earthquake, its model building type, the earthquake intensity, and is obtained using the casualty model. Since building-wise information is not available, the evaluation is carried out for the sum of all buildings of each building type in a grid. The computation uses a series of partial probability factors that are applied to each building or area with buildings. For a particular model building type, the number of injuries at a particular severity level can be expressed as (Coburn and Spence, 2002)

$$K_s = C \times (M1 \times M2 \times M3 \times M4) \tag{7}$$

where C is the percentage of buildings of that type and damaged due to the scenario earthquake. This is obtained from the mean damage factor corresponding to the intensity of damage suffered by the buildings, as explained earlier. The factor $M1$ is the probability of occupancy of the building type, or its occupancy rate, $M2$ is the probability of occupancy at the time of earthquake, or its occupancy factor, $M3$ represents the probability of occupants trapped or otherwise injured in the building, or injury rate, while the factor $M4$ represents the probability of the injuries being fatal, or the fatality rate. The social loss conditional probability factors, $M3$ and $M4$, have been taken from Coburn and Spence (2002), who determined these factors considering a large number of earthquakes from both developing and developed countries. Since India-specific factors are not available to assess the “lethality” of the collapse mechanisms of typical constructions, the use of these factors for $M3$ and $M4$ is considered as a reasonable approximation. It may also be noted that the poor quality of typical construction practices in the urban areas of India is reflected through the Damage Probability Matrix of each construction type and does not require further modification in $M3$ and $M4$. The injury factors are given in Figure 3, and the fatality factor is given in Table 2.

5.2 Economic Losses

Economic losses are estimated by taking into account five types of losses, which include structural building loss (i.e., loss due to structural damage), non-structural building loss (i.e., loss due to non-structural damage), building content loss, loss due to injuries, and loss due to deaths. Those depend on various model building types, occupancy classes, and extent of damage to buildings in the affected grids. The damage factors for structural and non-structural components and contents are given in Figures 4 and 5.

The loss to structural, non-structural, or content value is evaluated using the following equation:

$$\text{Loss}_i = \sum_{j=1}^5 C_{ij} \times V_j \tag{8}$$

where, Loss_i is the loss to the parameter i , viz., structural, non-structural, or content value; C_{ij} is the mean damage ratio of the i th parameter due to the j th damage state or mean damage ratio; and V_j is the total worth of the structural, non-structural, or content value of the buildings of the same building type in

a grid. The worth of structural/non-structural/content value of the buildings has been modelled depending on the size of the building and its occupancy type (Gupta, 2006) and is given in Tables 3 and 4.

The losses due to human injuries or fatalities are evaluated in Rupees per person for each injury category, or for death as per the compensation policy of Government of India (Aditya, 2007).

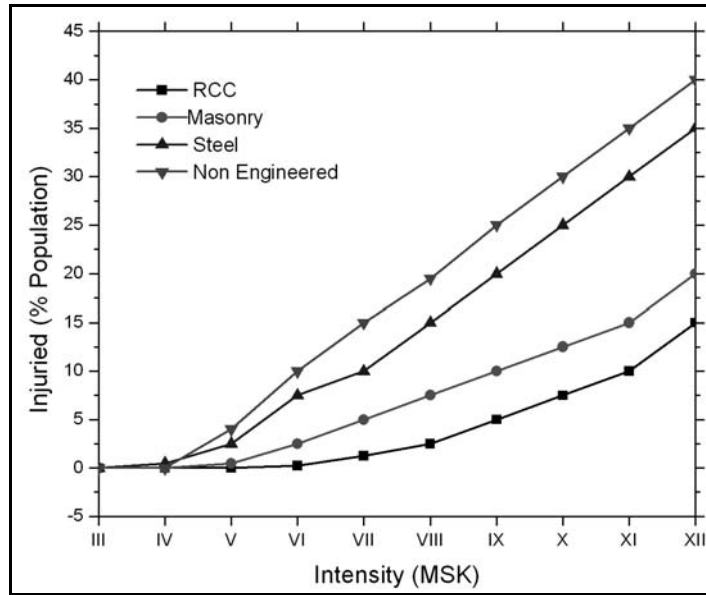


Fig. 3 Percentage of population likely to be injured during different earthquake intensities (Gupta, 2006)

Table 2: Fatalities as a Percentage of Injuries in Different Building Types

Building Type	Deaths (%)
RCC	40
Masonry	20
Steel	50
Non-engineered	10

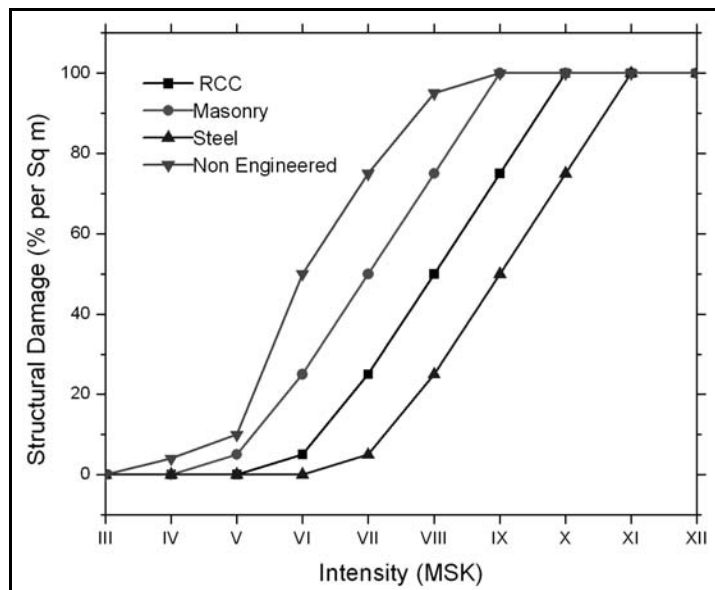


Fig. 4 Extent of likely structural damage during different earthquake intensities (Gupta, 2006)

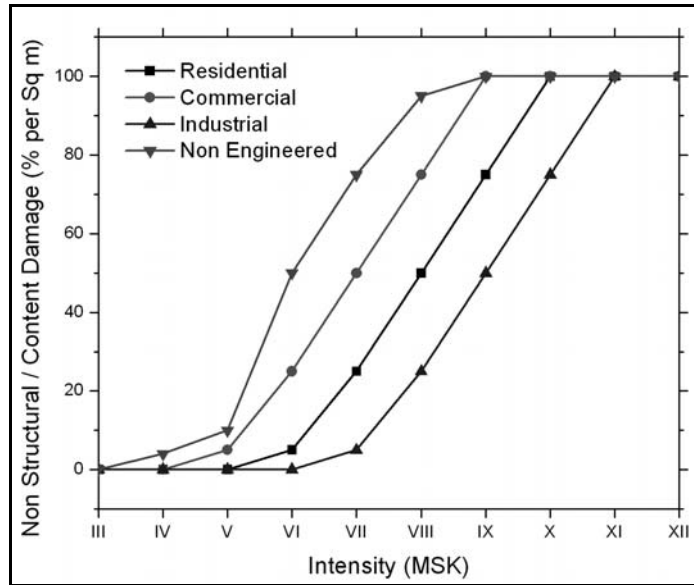


Fig. 5 Extent of likely non-structural and content damage during different earthquake intensities (Gupta, 2006)

Table 3: Structural Worth of a Building in Terms of Replacement Cost of the Built-up Area

Building Type	Structural Worth per m ² (Rs.)
RCC	1000
Masonry	600
Steel	1000
Non-engineered	300

Table 4: Non-structural and Content Worth of a Building in Terms of Replacement Cost of Built-up Area Considered for the Example Simulation

Occupancy Category	Non-structural Worth per m ² (Rs.)	Content Worth per m ² (Rs.)
Residential	1000	150
Commercial	3000	500
Industrial	5000	1000
Non-engineered	1000	150

IMPLEMENTATION ON GIS PLATFORM

The methodology outlined above has been implemented in RISK.iitb on a GIS platform. Due to the immense flexibility in its use, and considering the multi-sectoral requirement of GIS platform for urban governance by municipal authorities, ArcGIS has been used as the GIS platform for implementation (ESRI Developer Network¹, accessed on November 10, 2005). RISK.iitb has been developed using VBA as the programming environment. The software performs various calculations as indicated earlier in the methodology. Since a large number of data values are required for various calculations, the data is stored in database files in .dbf format. The software also allows interactive modifications to the data during risk evaluations. The results for the risk assessment are presented in maps as well as in a table, indicating the total losses under the given scenario earthquake.

When the software is executed, the master user interface is presented to the user as shown in Figure 6. The interface consists of several command buttons which, when clicked, perform the calculations of

¹ Website of ESRI Developer Network, <http://edn.esri.com>

different steps of the methodology. The following steps describe the procedures for carrying out the risk assessment.

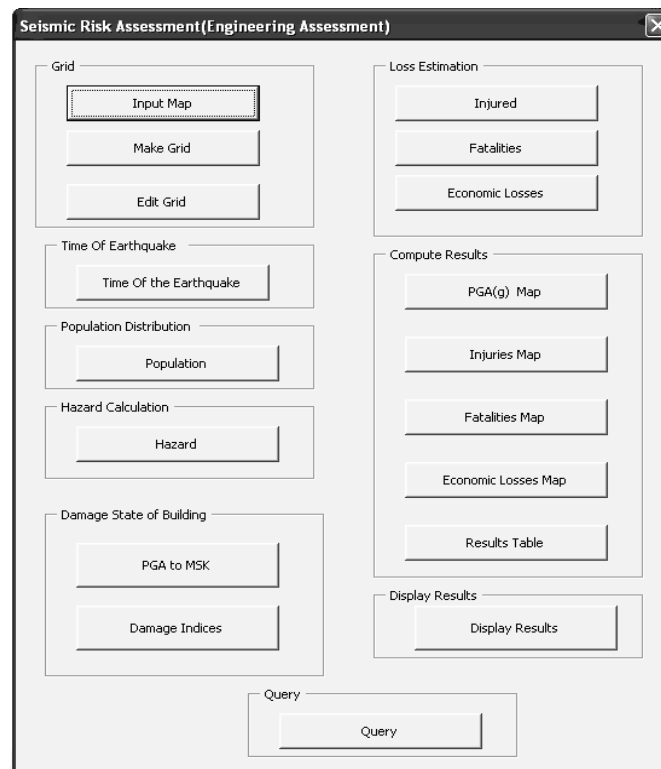


Fig. 6 User interface for starting seismic risk assessment using RISK.iitb

1. Basic Inputs and Evaluation Details

The first step is to input the data required to perform the risk assessment of the area under study. This information can be collected from the target area or city for the earthquake scenario simulation. Following steps are performed for the seismic risk assessment using RISK.iitb:

- a) Input a geo-referenced image of the area under study. The map may be a scanned map of the urban area under study in case grid-wise assessment is to be carried out. If the same is already available as a GIS map, it can also be used after converting to a geo-referenced image format. GIS maps in ArcGIS compatible file format can be directly read by the software. RISK.iitb uses the geo-referenced image to create a layer of grids, of the grid-size specified by the user, to overlay the map.
- b) Edit the grid map, to exclude the grids that do not lie within the urban area under study.
- c) Input the grid weight for each grid. The available grid-weight classifications are given in Table 5. For each grid, the weight chosen depends on the land area in that grid. For grids that include major water bodies, the grid weight is suitably reduced.
- d) Input soil type information for each grid.
- e) Specify zone classification and population weight for each grid. The various occupancy classes have been described earlier. The default values are given in Tables 6 and 7.
- f) Specify the proportion of total built-up area in each grid that belongs to different building types and occupancy classes. The buildings are classified into four model building types and three occupancy types in the example study presented herein. However, the tool has the ability to accommodate fifteen model building types and fifteen occupancy classes. The use of additional building types requires the user to update the database files accordingly.
- g) If the basic data described above is available from other studies or previous simulations, then that database file may be optionally provided wherein the grid data in the area under study can be directly added to the attribute table of the grid map. Steps b–f are not required under this situation.
- h) Input the total built-up area of the buildings in the area under study. This is the total area of all the buildings of each type, and is distributed grid-wise based on the zone classification and population weight.
- i) Specify the time at which the scenario earthquake takes place.

j) Input the total population (i.e., night and floating population) of the region under study. Alternately, the base population can be specified and occupancy estimated as described earlier. All these inputs are required during the different stages of seismic risk assessment. It may be noted that most of the basic geographical and physical data would also be required for the assessment of risk to other hazards, and RISK.iitb has been developed considering the possibility of extending it to other hazards in a seamless manner.

Table 5: Grid Weight Classification for the Computation of Land Area

Area Class	Grid Weight
Class 1	0.01
Class 2	0.1
Class 3	0.25
Class 4	0.5
Class 5	1

Table 6: Zone Classification Based on the Usage of Constructed Area

	Residential (%)	Commercial (%)	Industrial (%)
Zone 1	5	15	80
Zone 2	45	45	10
Zone 3	45	45	10

Table 7: Population Weight of Each Zone Based on the Land Usage

	Population Weight
Zone 1	1
Zone 2	1
Zone 3 (No-Development Zone)	0.01

2. Seismic Hazard

RISK.iitb allows the user to define a deterministic scenario event. Following two methods are available to estimate the peak ground acceleration (PGA):

- i) The predefined earthquake option gives the user the option of selecting a historical earthquake and an attenuation relationship. The software tool allows the user to choose from a few major earthquakes, which had occurred in peninsular India in the past.
- ii) The user-defined earthquake option asks the user to define the parameters for the scenario earthquake, like latitude and longitude of the epicentre of the earthquake, moment magnitude of the earthquake, and the hypocentral depth of the earthquake, and to select an appropriate attenuation relationship. An alternative option for the specification of earthquake on the basis of epicentre, orientation of fault plane, and rupture length is also available.

The GIS platform allows direct calculation of the source-site distance from the grid map, for use in the attenuation relationships. The PGA is calculated at the centroid of each square representing a grid.

If soil map is present or soil data is defined, the PGA at each centroidal point is modified to take into account the amplification due to soil characteristics at the site.

These inputs are used to evaluate the PGA at the centroid of each grid. These results are saved in the attribute table in the database in .dbf format.

3. Earthquake Intensity and Damage Levels

Based on the PGA, the damage intensity for different types of building is determined for each grid. The damage probability matrix (DPM) that specifies the relationship between damage intensity, seismic hazard, MSK, and damage levels, is based on the Indian data from Sinha and Adarsh (1999) and Gupta (2006) and is shown in Figure 2. These values can be interactively modified by the user, if required, to account for any special characteristics of the area under study or other special simulation requirement.

In order to evaluate losses, population distribution in different building types in each grid is required. RISK.iitb provides the user with two options for distributing the total population to each grid depending on the zone class and grid weight. This step evaluates the number of people in each building at the time of earthquake and adds it to the attribute table of the building map. Several factors that are needed for the population distribution are kept in the database files. These values can be interactively modified by the user to account for any special characteristics of the area under study or other special simulation requirements.

Following calculations are made during the evaluation. Built-up area of a grid, AG , is calculated as

$$AG = \frac{A}{N} \times GW \times ZP \quad (9)$$

where, A is the total built-up area; N is the total number of grids; GW is the grid weight (see Table 5); and ZP is the zone population weight (see Table 7). For each occupancy type in a grid, the built-up area AGO is determined from the following expression:

$$AGO = AG \times ZOP \quad (10)$$

where ZOP is the percentage of a specified occupancy class in a zone (see Table 6). The total built-up area for each occupancy class, AO , is then determined from all grids as

$$AO = \sum_{\text{All Grids}} AGO \quad (11)$$

It may be noted that Zone 3 has a ZP of 0.01, because of which the total built-up area will be reduced. The difference is added to Zone 2 equally among all the grids.

The population per occupancy class, PGO , is estimated for each grid as

$$PGO = \frac{PO \times AGO}{AO} \quad (12)$$

It may be noted that buildings of different construction types can have the same occupancy class (see Table 8). The population in every occupancy type is distributed among different construction types. The summation of this population over all occupancies gives the total population in a construction type in a grid as

$$AGB = \sum_{\text{All Occupancies}} AGO \times FB \quad (13)$$

$$PGB = \sum_{\text{All Occupancies}} PGO \times FB \quad (14)$$

where, AGB is the built-up area of each building type in a grid; PGB is the population of each building type in a grid; and FB is the percentage building type in a given occupancy class and is obtained from Table 8.

Table 8: Distribution of Building Types for Each Occupancy Class

	RCC (%)	Masonry (%)	Steel (%)	Non-engineered (%)
Residential	80	10	9	1
Commercial	80	10	9	1
Industrial	80	10	9	1

4. Loss Estimation

In this step, the number of people injured and the number of fatalities are evaluated, and this data is added as new fields to the attribute table of the grid map. For estimating the economic losses, the software evaluates the cost of structural components, non-structural components, and the cost of contents of each grid. The data values, which give cost per unit area of each component and contents, are stored in the

database files. Using the cost of structural, non-structural components, contents, and the damage level, this step evaluates the economic losses, and a new field is added to the attribute table of the grid map. The models (based on the Indian data) relating seismic intensity with different types of losses are used in the analysis and are described in Aditya (2007). The values obtained from these models are stored in the database files. Values in the database files can be interactively modified by the user depending upon the region of study and to provide other loss models as additional features.

The details of various calculations carried out for the exposure analysis are described below. If the total number of persons injured and the total number of fatalities in a grid are denoted as Inj and D , respectively, these quantities can be determined as

$$Inj = \sum_{\text{All Building Types}} PGB \times FI \quad (15)$$

$$D = Inj \times FD \quad (16)$$

where FI is the percentage of population injured due to a particular damage intensity and is obtained from Figure 3, and FD is the percentage of injured population that results in fatalities. The total number of injuries and fatalities is determined from the summations of Equations (15) and (16) over all grids. For the monetary value of loss calculations, the losses in rupees per person injured and per death are taken as Rs. 50,000 and Rs. 2,00,000, respectively, based on the recent data of compensation following some natural disasters in the country.

If SL is the loss due to damage to structural members in a grid, NSL is the loss due to damage to non-structural members in a grid, and CL is the loss of content due to structural damage in a grid, these losses have been evaluated using the following expressions:

$$SL = AGB \times F1 \times SW \quad (17)$$

$$NSL = AGO \times F2 \times NSW \quad (18)$$

$$CL = AGO \times F3 \times CW \quad (19)$$

where $F1$, $F2$, and $F3$ are percentage structural, non-structural, and content damages, respectively, at a given earthquake intensity, and are obtained from Figures 4 and 5. SW , NSW , and CW are the replacement costs for structural, non-structural, and content components, respectively, per square meter for a given building type and occupancy type, and are obtained from Tables 3 and 4. The total economic loss is estimated as the sum of all losses.

5. Generation of Result Maps and Table

The risk assessment as described above results in the addition of new fields (or layers) containing the values of PGA , MSK , and losses to each grid on the grid map of the city. Colour coded maps with the results are automatically generated by the software. A colour code is assigned for each range of injuries, fatalities, and economic losses, which help to quickly spot the heavily damaged areas. The generated maps include PGA contour maps, damage intensity maps, injuries maps, fatalities maps, and economic losses maps. Besides generating the above maps, a table of results is also generated. This table is stored as a database file, and it contains three columns indicating the values of total number of injuries, total number of fatalities, and total economic losses suffered in the area under study due to the given scenario. These values are computed by the summation of the injuries, fatalities, and economic losses associated with each building type in each grid on the grid map. The results are stored as an output data file in the output directory.

6. Query Results

RISK.iitb allows the user to perform complex queries on the results computed. The user has the option of single-condition query or multi-condition query. When a query is performed, the grids satisfying the query criterion, as defined by the query expression, are highlighted and the map is stored as a layer file in the output directory.

EXAMPLE SCENARIO DEVELOPMENT AND LOSS ESTIMATION FOR MUMBAI

The risk assessment of an example area has been performed using RISK.iitb. The city of Mumbai (within its municipal limits), which is India's most populous city and has an area of approximately 470 km², has been selected to illustrate the use of RISK.iitb. The closest significant active fault is considered to be the Panvel flexure that runs to the east of the city across Thane creek and is oriented approximately in the N-S direction (see Figure 7). A preliminary seismic risk assessment of Mumbai was carried out earlier by Sinha and Adarsh (1999), and the basic data regarding the structural vulnerability of different construction types has been considered in this study. Various parameters and inputs used for the loss estimation are given below:

- i) The geo-referenced map of Mumbai city has been extracted from the scanned image of the master plan of Mumbai Metropolitan Region and is shown in Figure 8.
- ii) The risk assessment has been carried out using three different grid sizes, viz., 2.0, 1.0, and 0.5 km. Detailed results are shown only for the grid size of 0.5 km, while the economic losses and the table of final results are shown for all grid sizes to illustrate the robustness of the procedure and convergence of results.
- iii) The grid weight and zone classification are used as per the data available from the master plan of Mumbai Metropolitan Region. In the absence of reliable data on soil properties, soil amplification has not been considered in the simulations, i.e., soil amplification factor has been taken as unity for all grids.
- iv) The occurrence time of the scenario earthquake has been considered as 3:00 p.m.
- v) Total night (or resident) population in the example area has been taken as 13 million based on the census data and more recent estimates. The floating population of people from outside the city limits during the daytime is taken as 15% of the night population, i.e., 1.95 million based on the recent estimates.
- vi) A user-defined earthquake is considered. The parameters for the earthquake are taken as given below (with the epicentre on Panvel flexure):
 - a) latitude of hypocentre: 19°7'57''N;
 - b) longitude of hypocentre: 73°6'48''E;
 - c) moment magnitude: 6.0; and
 - d) focal depth: 10.0 km.
 Since Mumbai is located in the seismic zone III as per the Indian Standard code (BIS, 2002), representing moderate seismic hazard, the earthquake moment magnitude $M = 6.0$ has been selected for this simulation to represent a typical moderate earthquake. The focal depth of 10 km has been chosen assuming the earthquake to be shallow. The epicentre has been taken on Panvel flexure, which is considered to be the closest significant active fault near Mumbai (Dessai and Bertrand, 1995). The resulting rupture length is 7.8 km, with the epicentre taken at its mid-length.
- vii) The attenuation relationship by Iyengar and Raghukanth (2004), which has been estimated using the local data for the Bhuj earthquake of 2001, has been chosen for the estimation of seismic hazard.

The remaining inputs, which pertain to the physical data of the example area, have been described in Aditya (2007). The results from loss estimation of the example area are shown in Tables 9 and 10. It can be seen that the total area under the grids increases as the grid size becomes larger (or the grid becomes coarser). This is expected since larger grids have greater error due to the inclusion of the entire area of the boundary grids. However, the actual physical area does not change significantly due to the software feature of defining grid weight based on the grid class that considers the land area in each grid (see Table 5).

The physical and economic losses for the above scenario assessment, which have been generated in RISK.iitb, are shown in Table 10. The results are of similar order as those presented in Sinha and Adarsh (1999), thus clearly demonstrating the accuracy of the results for a preliminary assessment of seismic risk. It can be also seen that the results of loss estimation are convergent as the grid size is reduced. This indicates that a grid size of 2×2 km is adequate for carrying out the risk assessment of an area of the size of Mumbai. However, smaller grid sizes give more refined local distributions of the losses, which are of immense importance in developing disaster management strategies and for evaluating spatial variation of risk in the city.

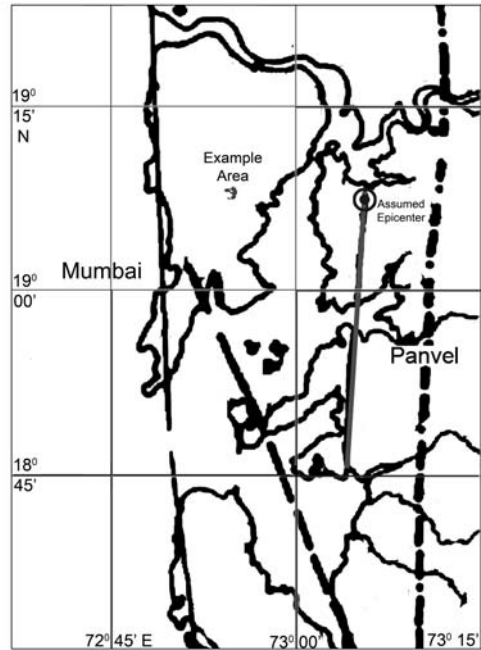


Fig. 7 Fault trace map showing the example area (of Mumbai) considered for scenario development and the lineament under consideration (Dessai and Bertrand, 1995)

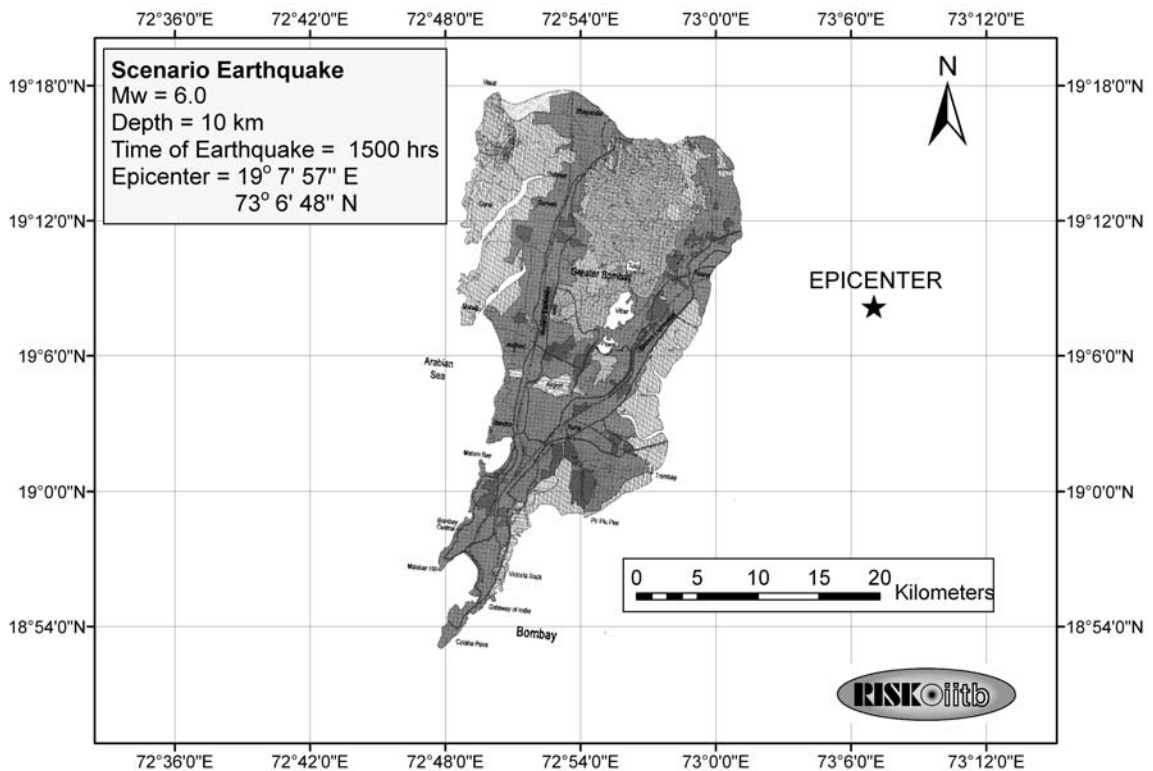


Fig. 8 Geo-referenced map of Mumbai used for the seismic risk assessment

Table 9: Land Area under Different Damage Intensity (on MSK Scale) for the Scenario Earthquake

Grid Size (km)	Area (km ²)		
	MSK VI	MSK VII	MSK VIII
0.5×0.5	331.50	237.75	0.00
1.0×1.0	356.00	249.00	0.00
2.0×2.0	392.00	272.00	0.00

Table 10: Estimated Physical and Economic Losses for the Scenario Earthquake

Grid Size (km)	Number of Injuries	Number of Deaths	Economic Losses (Million Rs.)
0.5×0.5	128825	15212	87230
1.0×1.0	129617	15331	87800
2.0×2.0	130860	15416	88210

Following maps are generated after the analysis:

- Grid maps (2×2, 1×1, and 0.5×0.5 km); the grid map for 0.5×0.5 km grid is shown in Figure 9.
- Grid weight map; the grid weight map for 0.5×0.5 km grid is shown in Figure 10.
- Occupancy zone classification map; the occupancy zone classification map for 0.5×0.5 km grid is shown in Figure 11.
- Soil grid map.
- PGA grid map.
- Damage intensity grid map; the damage intensity map for 0.5×0.5 km grid is shown in Figure 12.
- Injury map (grid-wise or total); the grid-wise injury map for 0.5×0.5 km grid is shown in Figure 13.
- Fatality map (grid-wise or total); the grid-wise fatality map for 0.5×0.5 km grid is shown in Figure 14.
- Economic loss map (grid-wise or total); the grid-wise economic loss maps for all three grid sizes are shown in Figures 15–17.

It is evident that the thematic display of inputs of the analysis and maps of the results, as shown in Figures 8–17, can be easily understood even by the non-technical stakeholders. These maps illustrate the unique advantage of developing a seismic risk assessment system on the GIS-based platform, since the results retain the accuracy of a typical scientific endeavour, while also providing the ability to communicate with various stakeholders in a simple yet accurate manner. Since several major urban areas in India are in the process of updating their records on a GIS-based platform, RISK.iitb provides an opportunity to interface with the municipal database to directly extract the relevant input information from the municipal records as and when it becomes available.

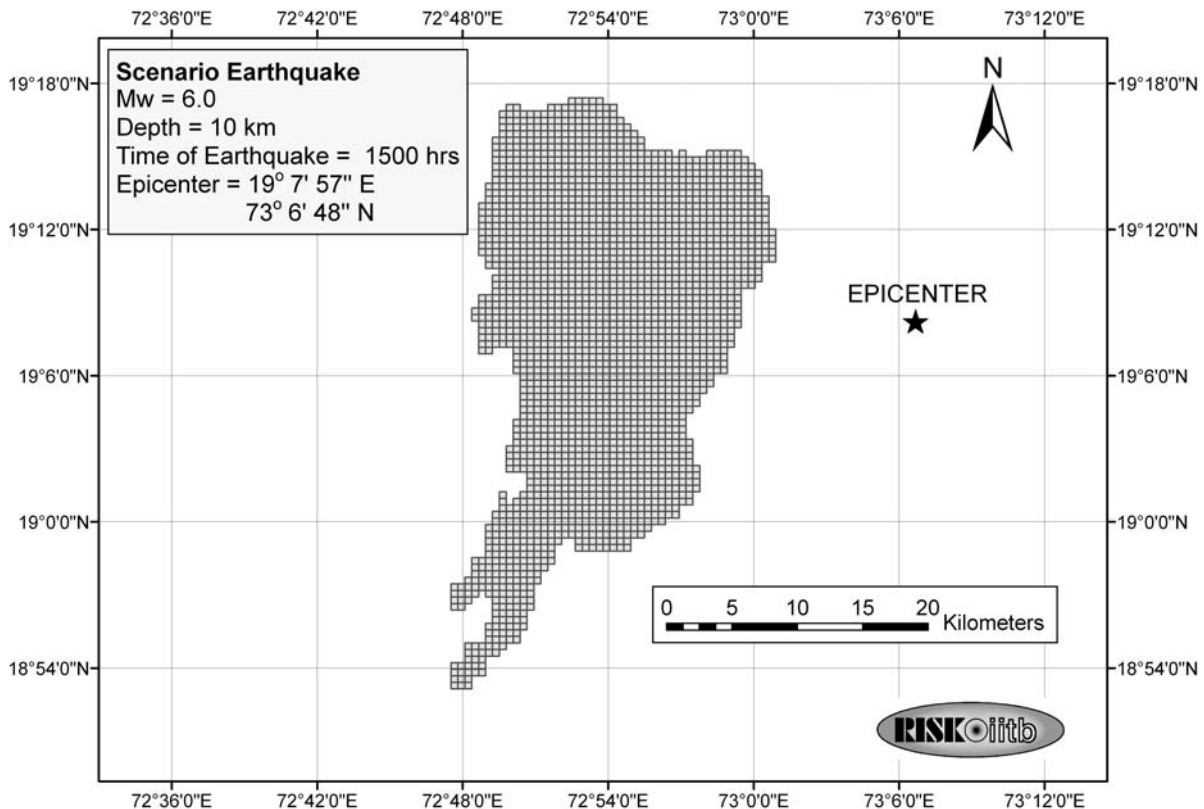


Fig. 9 Grid map of Mumbai with 0.5×0.5 km resolution

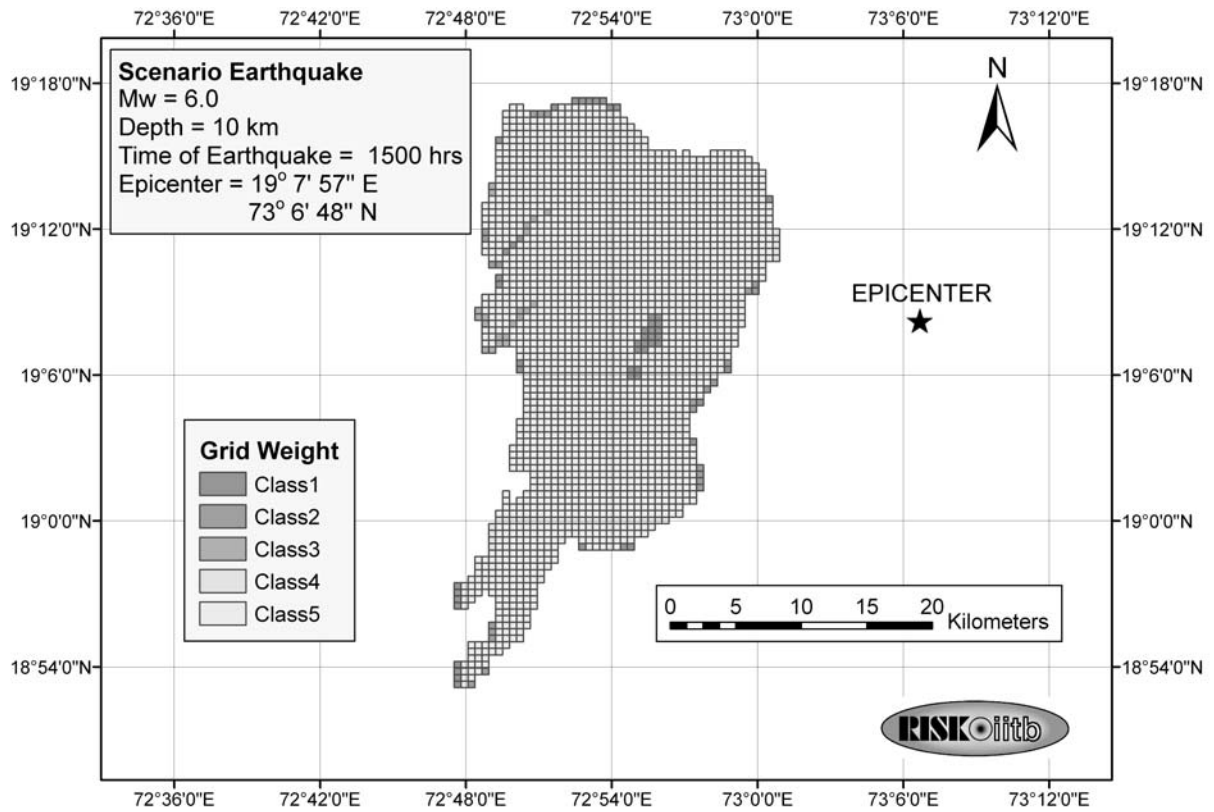


Fig. 10 Grid weight map of Mumbai with 0.5x0.5 km resolution

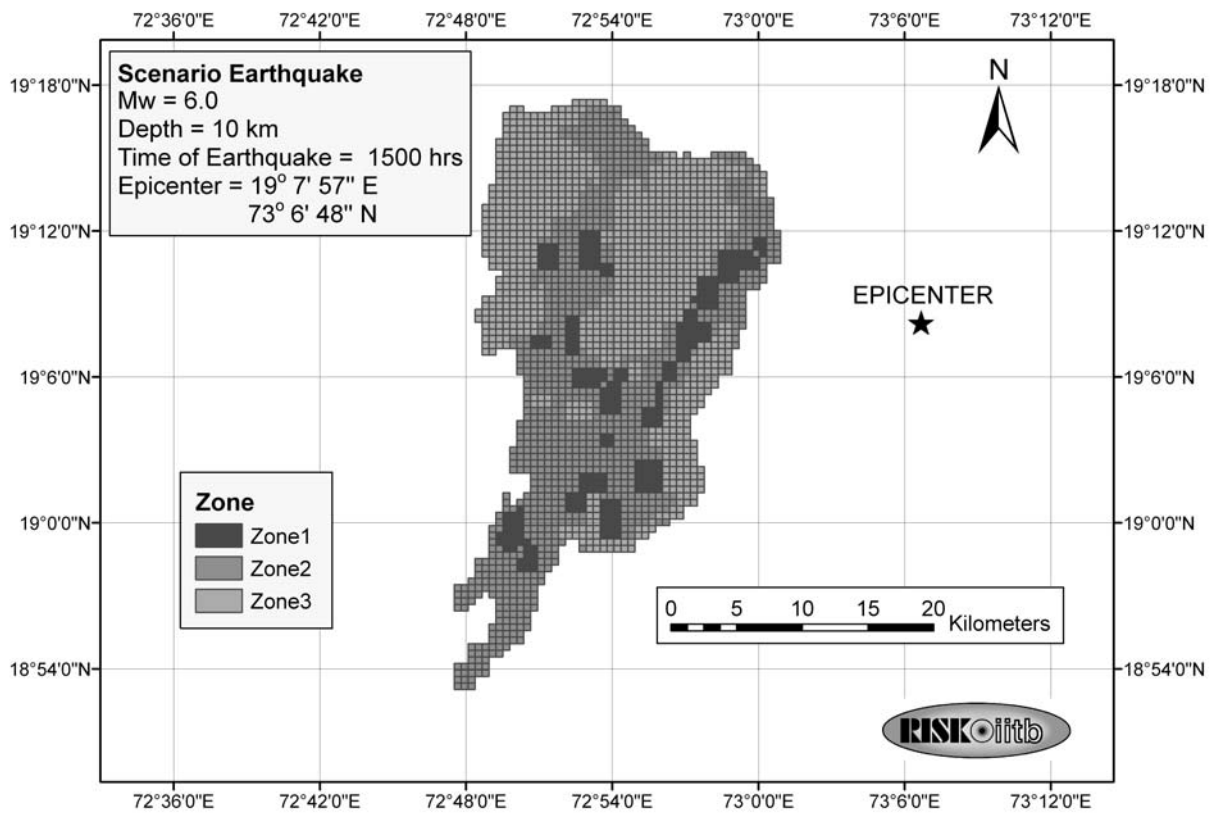


Fig. 11 Occupancy zone map of Mumbai with 0.5x0.5 km resolution

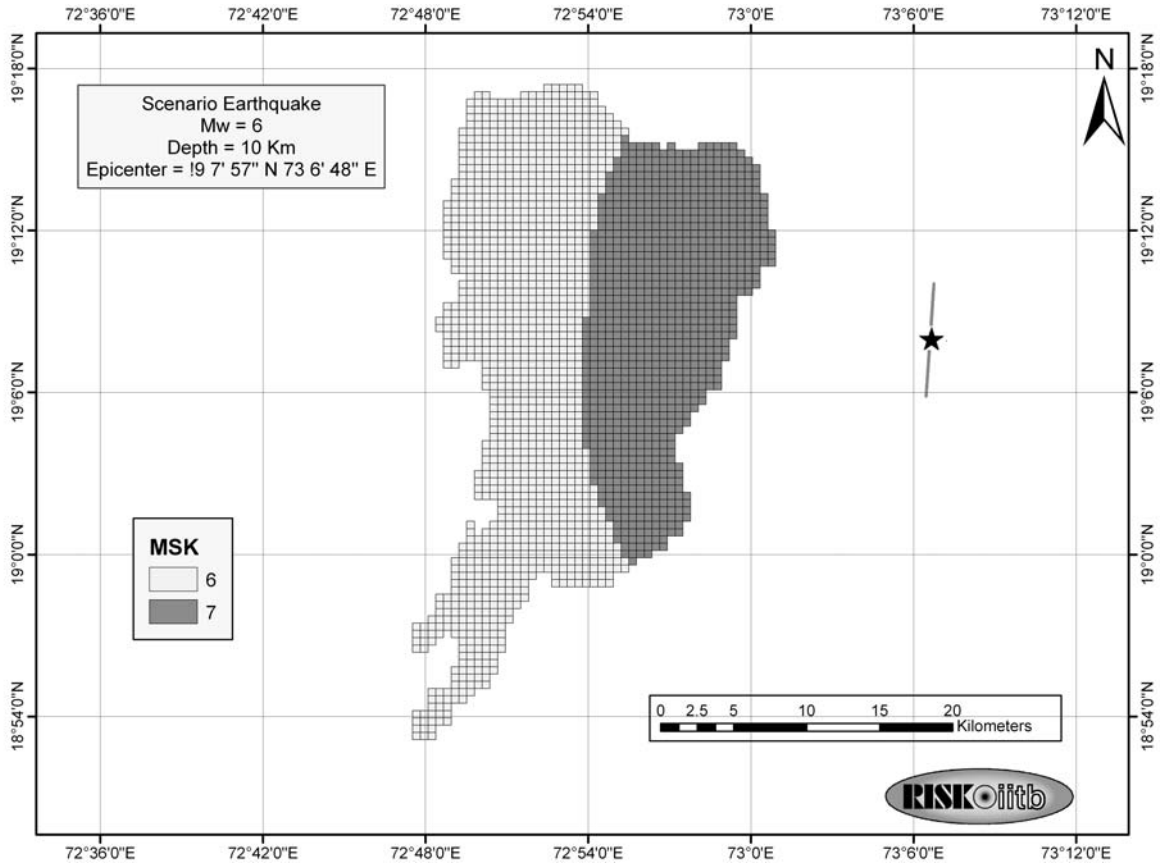


Fig. 12 Damage intensity map of Mumbai with 0.5x0.5 km resolution

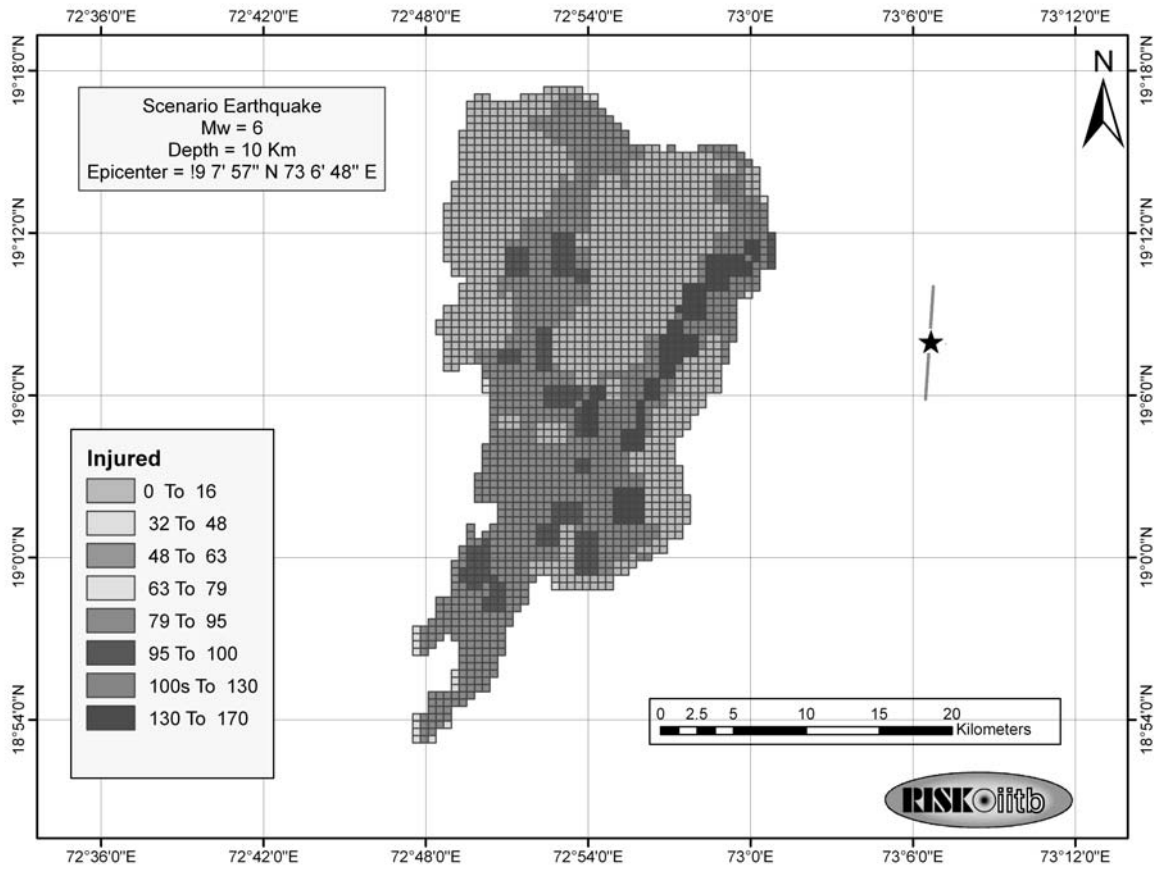


Fig. 13 Injury intensity map of Mumbai with 0.5x0.5 km resolution

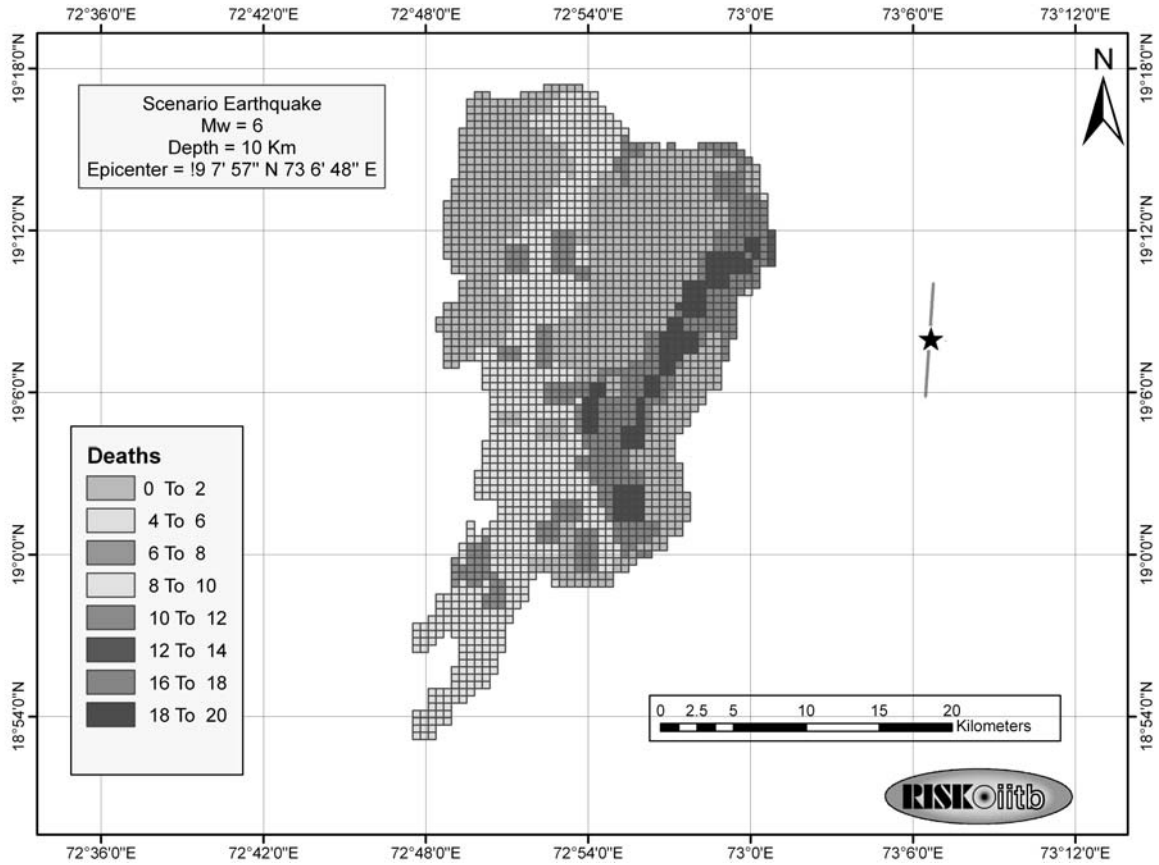


Fig. 14 Fatality intensity map of Mumbai with 0.5x0.5 km resolution

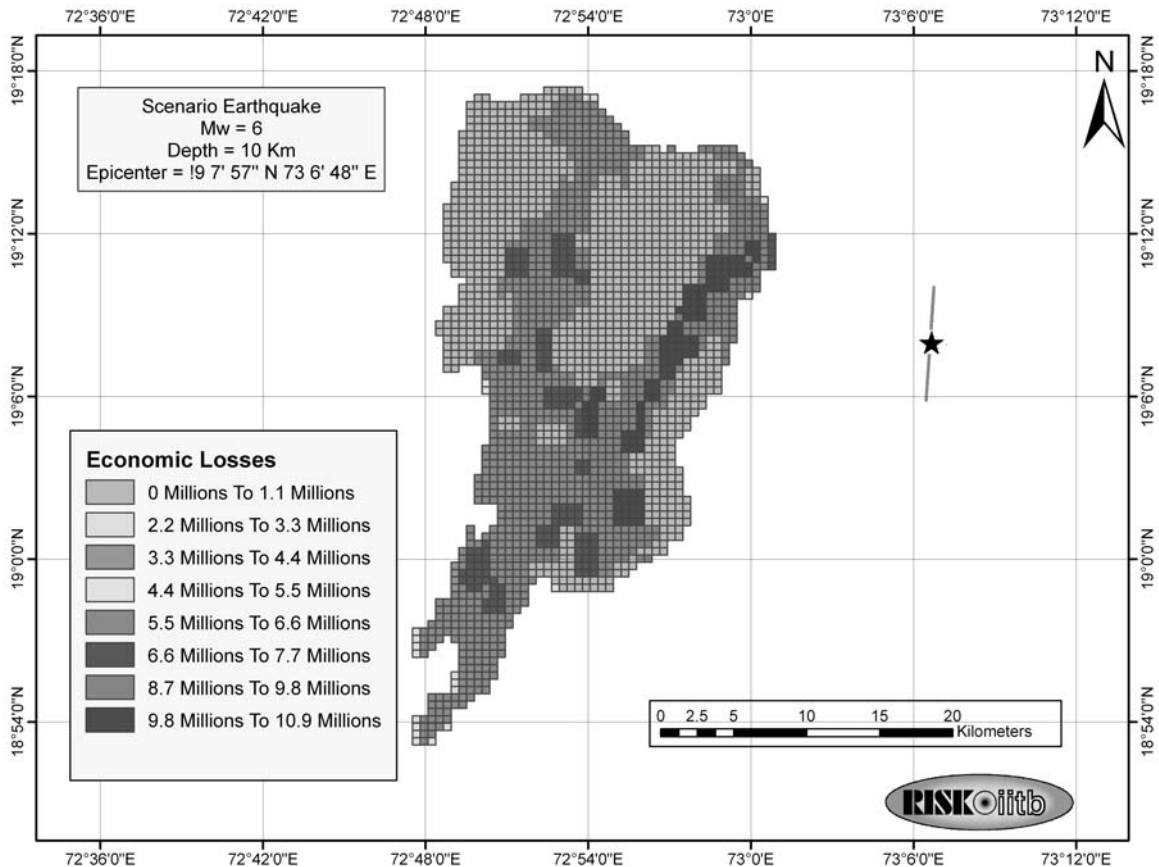


Fig. 15 Economic loss intensity map of Mumbai with 0.5x0.5 km resolution

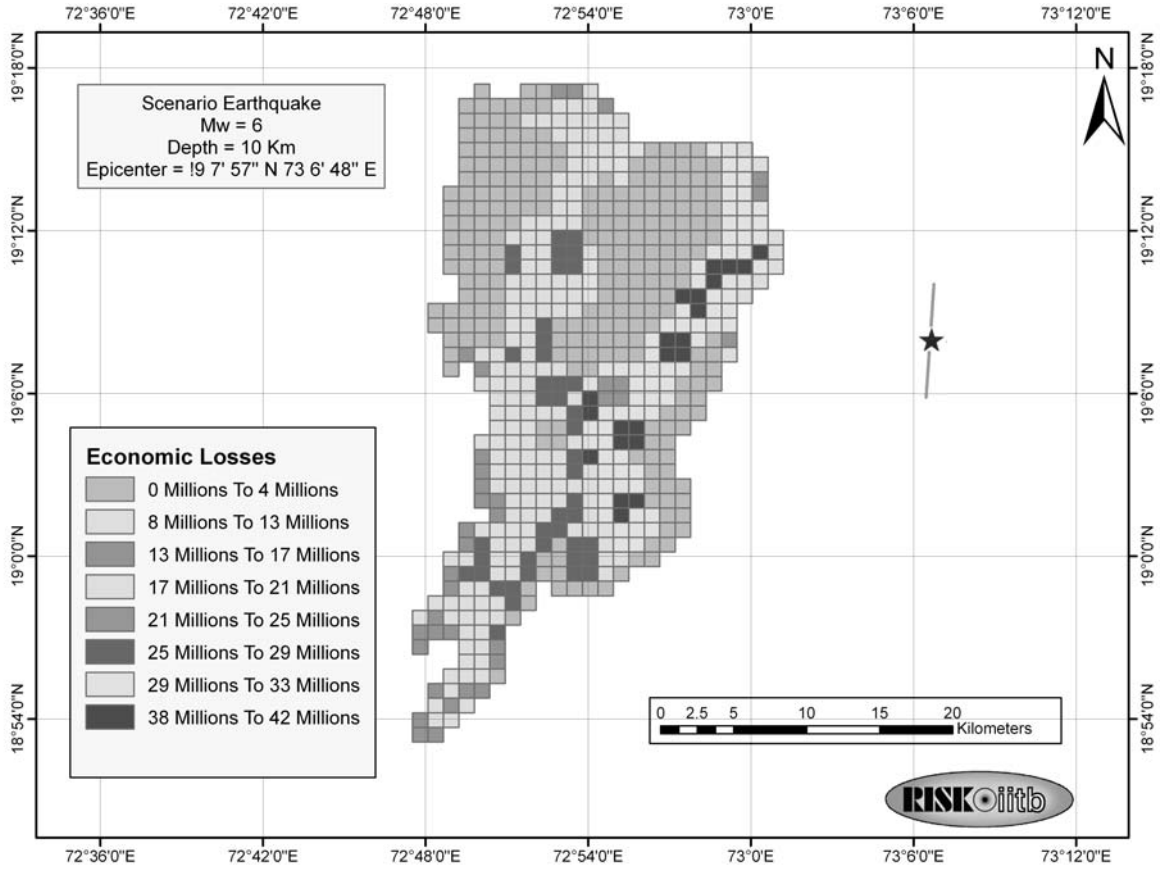


Fig. 16 Economic loss intensity map of Mumbai with 1.0x1.0 km resolution

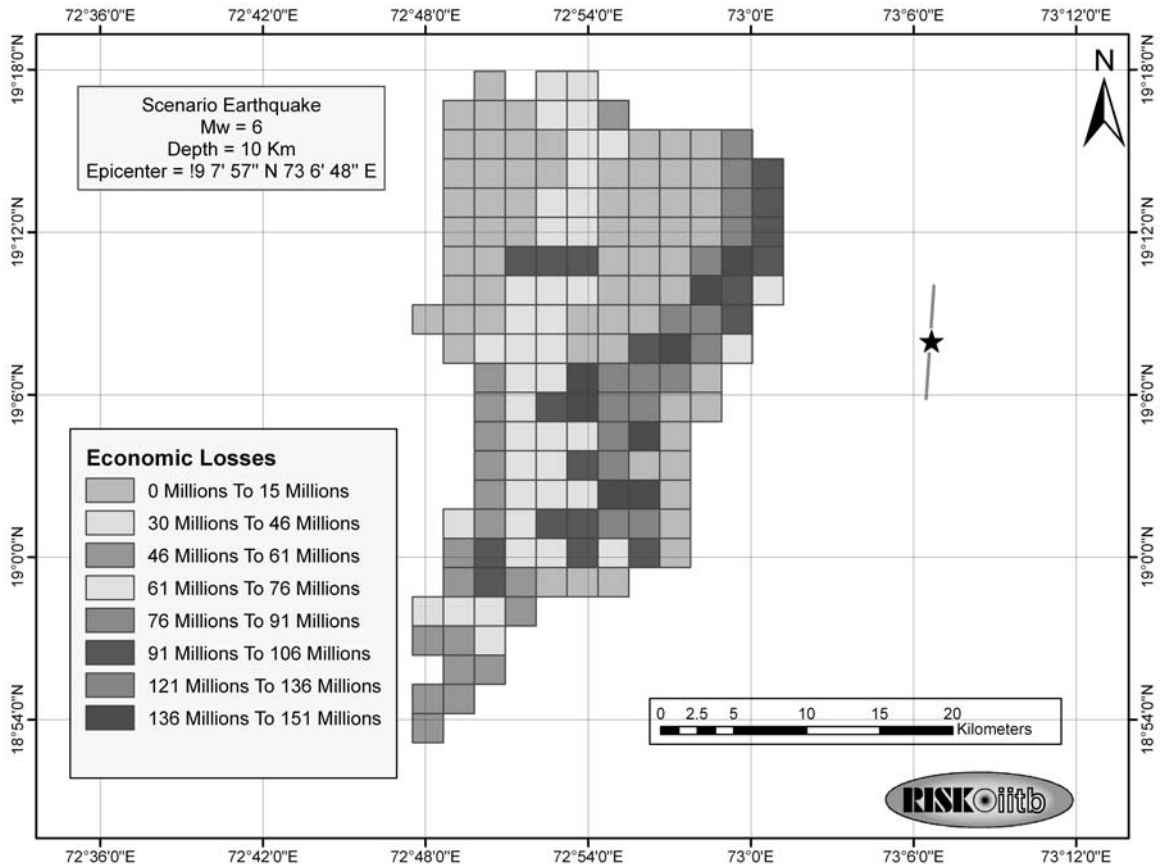


Fig. 17 Economic loss intensity map of Mumbai with 2.0x2.0 km resolution

The results of damage and loss estimation presented in the example assessment above can be considered as preliminary due to the number of assumptions made on account of the non-availability of data. These results can be further refined when such information as the soil classification map for amplification assessment, and more refined building data, becomes available. However, it should be noted that these results are adequately detailed for developing initial disaster management plans for the city of Mumbai, and for assessing the scale of likely losses due to the scenario earthquake disaster. Such results and their presentation through tables and thematic maps are, therefore, invaluable for policy-making and for communicating with the non-technical stakeholders.

SUMMARY AND CONCLUSIONS

This paper presents a methodology for carrying out an assessment of the consequences of future earthquake events in urban areas. The risk assessment procedure needs to be scientifically rigorous, while the results should be easy to understand by the various stakeholders. The use of GIS platform for developing seismic risk assessment tools has provided the opportunity to integrate the two requirements. A GIS-based risk assessment tool, RISK.iitb, has been developed considering the Indian conditions. The tool has the capability to carry out seismic risk assessment considering a large number of options regarding hazard and vulnerability. The results are generated in the form of tables and colour-coded maps for parameters such as injury, fatality, and economic loss in the region of interest. The GIS platform facilitates generation and display of various thematic maps.

RISK.iitb can be used for carrying out the risk assessment of urban areas to sensitize the policy-makers and public of the role of different contributors, such as seismic hazard and vulnerability of different categories of buildings, to the seismic risk. Since the assessment results, such as the extent of damaged buildings and also the number of injuries and casualties, are generated for each grid, those can be used in identifying areas with potentially heavy damage in the case of an earthquake, so that the disaster management plans in those areas can be suitably strengthened.

The results of risk assessment depend on the inventory data available. It is shown that the basic level assessment can be carried out using the urban data already available from a variety of sources. However, a more accurate assessment requires detailed data that is not available or is difficult to compile. Since most major urban areas are expected to update their records on an IT platform in future, and several are also expected to migrate to GIS-based platforms, the development of RISK.iitb provides the opportunity to various urban authorities to compile the most important data for carrying out the seismic risk assessment. This will enable a more accurate seismic risk assessment in a larger number of urban areas and will be invaluable in developing their disaster management plans.

An example seismic risk assessment for the city of Mumbai has been carried out to demonstrate the main features of the system. It is seen that consistent and convergent results are obtained for the grid-size between 2.0 and 0.5 km. It is also seen that there is an insignificant difference between the results obtained for the 2.0×2.0 km and 0.5×0.5 km grid sizes. Based on this example, it can be concluded that a grid resolution of 2.0×2.0 km is adequate for an urban area of the size of Mumbai, and further assessment can be carried out for other earthquake scenarios using a larger grid size. However, the spatial variation of risk has much better resolution when smaller grid sizes are used, and thus provides a basis for choosing the grid density.

RISK.iitb is undergoing continuing improvements to improve its capability and modelling. For example, besides specifying the earthquake hazard in terms of its epicentral parameters, faults can also be specified and the earthquake magnitude estimated from the type of faulting and the rupture length. Several other enhancements are also currently in progress.

It may also be noted that the results presented in the paper can be considered as a postulated scenario and are intended to demonstrate the most useful features of RISK.iitb for communicating the complex issues of seismic risk to the non-technical stakeholders.

REFERENCES

1. Aditya, K.S.P. (2007). "Seismic Risk Assessment of Urban Areas Using GIS", M.Tech. Thesis, Department of Civil Engineering, Indian Institute of Technology Bombay, Mumbai.

2. Aditya, K.S.P. and Sinha, R. (2006). "Influence of Fault-Plane Orientation on Earthquake Scenario Development", Proceedings of the 14th Symposium on Earthquake Engineering, Roorkee, Paper No. 121 (on CD).
3. ASK (1977). "Erdbebenrisikokarten der Schweiz", Technical Report, Abteilung für die Sicherheit der Kernanlagen, Würenlingen, Switzerland (in German).
4. Atkinson, G.M. and Boore, D.M. (1995). "Ground Motion Relations for Eastern North America", Bulletin of the Seismological Society of America, Vol. 85, No. 1, pp. 17–30.
5. Bendimerad, F. (2001). "Loss Estimation: A Powerful Tool for Risk Assessment and Mitigation", Soil Dynamics and Earthquake Engineering, Vol. 21, No. 5, pp. 467–472.
6. BIS (2002). "IS 1893 (Part 1)-2002: Indian Standard Criteria for Earthquake Resistant Design of Structures, Part 1—General Provisions and Buildings (Fifth Revision)", Bureau of Indian Standards, New Delhi.
7. Chen, Q.-F., Chen, Y., Liu, J. and Chen, L. (1997). "Quick and Approximate Estimation of Earthquake Loss Based on Macroscopic Index of Exposure and Population Distribution", Natural Hazards, Vol. 15, No. 2-3, pp. 215–229.
8. Coburn, A.W. and Spence, R.J. (2002). "Earthquake Protection", John Wiley, Chichester, U.K.
9. Dessai, A.G. and Bertrand, H. (1995). "The 'Panvel Flexure' along the Western Indian Continental Margin: An Extensional Fault Structure Related to Deccan Magmatism", Tectonophysics, Vol. 241, No. 1-2, pp. 165–178.
10. Erdik, M., Rashidov, T., Safak, E. and Turdukulov, A. (2005). "Assessment of Seismic Risk in Tashkent, Uzbekistan and Bishkek, Kyrgyz Republic", Soil Dynamics and Earthquake Engineering, Vol. 25, No. 7-10, pp. 473–486.
11. Gupta, A. (2006). "A GIS-Based Seismic Risk Assessment System", M.Tech. Thesis, Department of Civil Engineering, Indian Institute of Technology Bombay, Mumbai.
12. Gupta, A. and Sinha, R. (2006). "RISK.iitb—A GIS-Based Seismic Risk Assessment System", Proceedings of the 14th Symposium on Earthquake Engineering, Roorkee, Paper No. 75 (on CD).
13. Iyengar, R.N. and Raghukanth, S.T.G. (2004). "Attenuation of Strong Ground Motion in Peninsular India", Seismological Research Letters, Vol. 75, No. 4, pp. 530–540.
14. Karnik, V., Schonkova, Z. and Schenk, V. (1984). "Vulnerability and the MSK Scale", Engineering Geology, Vol. 20, No. 1-2, pp. 161–168.
15. Klügel, J.-U., Mualchin, L. and Panza, G.F. (2006). "A Scenario-Based Procedure for Seismic Risk Assessment", Engineering Geology, Vol. 88, No. 1-2, pp. 1–22.
16. Kramer, S.L. (1996). "Geotechnical Earthquake Engineering", Prentice Hall, Upper Saddle River, U.S.A.
17. Lang, K. (2002). "Seismic Vulnerability of Existing Buildings", IBK Report No. 273, Swiss Federal Institute of Technology (ETH), Zurich, Switzerland.
18. Musson, R.M.W. (2000). "Intensity-Based Seismic Risk Assessment", Soil Dynamics and Earthquake Engineering, Vol. 20, No. 5-8, pp. 353–360.
19. NIBS (1999). "Earthquake Loss Estimation Methodology HAZUS: Technical Manual", Report prepared for the Federal Emergency Management Agency, National Institute of Building Sciences, Washington, DC, U.S.A.
20. IDNDRS (1999). "RADIUS: Risk Assessment Tools for Diagnosis of Urban Areas against Seismic Disasters", Technical Report, International Decade for Natural Disasters Reduction Secretariat, United Nations Office for the Coordination of Humanitarian Affairs, Geneva, Switzerland.
21. RMS (1995). "What if the 1906 Earthquake Strikes Again?—A San Francisco Bay Area Scenario", Topical Issues Series, Risk Management Solutions, Newark, U.S.A.
22. Sinha, R. and Adarsh, N. (1999). "A Postulated Earthquake Damage Scenario for Mumbai", ISET Journal of Earthquake Technology, Vol. 36, No. 2-4, pp. 169–183.
23. Sinha, R., Goyal, A., Shaw, R., Arai, H., Saita, J., Pribadi, K., Chaudhari, M. and Jaiswal, K. (2001). "The Great Bhuj Earthquake of January 26th 2001, Consequences and Future Challenges", Joint

- Technical Report, Indian Institute of Technology Bombay, Mumbai and Earthquake Disaster Mitigation Research Center, Kobe, Japan.
24. Spence, R. and Le Brun, B. (2006). "Preface", *Bulletin of Earthquake Engineering*, Vol. 4, No. 4, pp. 319–321.
 25. Toro, G.R., Abrahamson, N.A. and Schneider, J.F. (1997). "Model of Strong Ground Motions for Earthquakes in Central and Eastern North America: Best Estimates and Uncertainties", *Seismological Research Letters*, Vol. 68, No. 1, pp. 41–57.
 26. Wald, D.J., Quitoriano, V., Heaton, T.H. and Kanamori, H. (1999). "Relationships between Peak Ground Acceleration, Peak Ground Velocity, and Modified Mercalli Intensity in California", *Earthquake Spectra*, Vol. 15, No. 3, pp. 557–564.
 27. Wells, D.L. and Coppersmith, K.J. (1994). "New Empirical Relationships among Magnitude, Rupture Length, Rupture Width, Rupture Area, and Surface Displacement", *Bulletin of the Seismological Society of America*, Vol. 84, No. 4, pp. 974–1002.
 28. Yeh, C.-H., Loh, C.-H. and Tsai, K.-C. (2006). "Overview of Taiwan Earthquake Loss Estimation System", *Natural Hazards*, Vol. 37, No. 1-2, pp. 23–37.

GROUND VIBRATION FROM RIGID FOUNDATION BY BEM-TLM

Badreddine Sbartai* and Ahmed Boumekik**

*Department of Civil Engineering
University of Skikda, 21000 Skikda, Algeria

**Department of Civil Engineering
University of Constantine, 25000 Constantine, Algeria

ABSTRACT

This study investigates a prediction model for free-field response in the vicinity of a vibrating foundation. The model is based on a mathematical description of physical phenomena that occur when the massless machine foundation system is excited by a harmonic vertical force. The foundation has a square and rigid shape and is assumed to be placed on the surface of visco-elastic soil overlying the bedrock. Vertical displacements of both the foundation and the surrounding soil are obtained by solving the wave's equation, while considering the conditions of the dynamic soil-foundation interaction. The solution of this equation is formulated in the frequency-domain Boundary Element Method (BEM). In this paper the Thin Layer Method (TLM) is used to calculate the Green's functions for each element. By this approach, the amplitudes of the soil in the vicinity of a vibrating foundation may be obtained under the effect of various parameters.

KEYWORDS: Wave Propagation, BEM, TLM, Soil-Structure Interaction

INTRODUCTION

The major problem that must be addressed during the construction of particular types of structures, such as conventional and nuclear power plants, chemical factories, liquid natural gas tanks, etc., concerns the rigorous safety conditions that must be established to avoid damage caused by various types of excitations to which these structures can be subjected. The strong interest in this problem is not only because of the constant increase in the quality and stability requirements of the constructions in the vicinity of these structures but also because of the need to protect sensitive material. The analysis of the response of these structures and that of the neighbouring soil is a wave-propagation problem that leads to consideration of the soil-structure interaction. To face these challenges, research in this field has been oriented toward numerical methods because the classical analytical methods, which are generally based on restrictive assumptions about the geometry of the foundation and the elastic properties of the soil, are not adapted to treat the problems of such great complexity. Also, the study of soil-structure interaction remains important and justifies the particular interest that many researchers have shown in it up to the present day.

Many studies have been performed in earthquake engineering with regard to wave propagation in ground. In a pioneering work, Lamb (1904) investigated the response of an isotropic, homogeneous, elastic half-space to various loads and established models for two- and three-dimensional wave propagation. Among the many analytical-numerical and numerical works on wave propagation in layered media, with constant material properties in every layer, one can mention the classic text of Reissner (1936) as well as the works of Ewing et al. (1957), Thomson (1950), Haskell (1953), Gupta (1966), and Richart et al. (1970). Later, Takahashi (1985, 1986) studied the response of a structure on visco-elastic half-space to ground-transmitted vibrations caused by a harmonic line source on the surface of the half-space.

The finite-element method (FEM) has been adopted to solve wave-propagation problems with a wide range of soil properties. This method, although attractive, is computationally expensive, because it requires the discretization of both the infinite medium and the foundation. Because of this, its use is limited to two-dimensional problems, such as those addressed by Waas (1972), and Chang-Liang (1974). Using this method, Kausel et al. (1975) analyzed the behaviour of rigid foundations resting on or embedded in a stratum over bedrock. However, Lysmer and Kuhlemeyer (1969) analyzed the behaviour of foundations resting on or embedded in semi-infinite soil by using an absorbing boundary.

More recently, very efficient methods have been developed to treat wave-propagation or diffraction problems, most notably the boundary-element method (BEM). In this approach, field displacement has been formulated by Beskos (1987) as an integral equation in terms of Green's functions. Also, using this method in conjunction with a constant element and Green's function for half-space, Apsel and Luco (1987) calculated the impedance functions for foundations embedded in layered media, and Dominguez (1978) studied the case of a rigid rectangular foundation placed on or embedded in semi-infinite soil. However, Ahmad and Rupani (1999) studied the horizontal impedance of square foundations resting on or embedded in two-layer soil deposits using isoparametric boundary element. In contrast, Beskos et al. (1986) studied the problem of structural isolation from ground-transmitted vibrations by open or infilled orthogonal trenches under the condition of plane strain.

Wong and Luco (1985) developed a method that permits the evaluation of impedance functions for square rigid foundations resting on a visco-elastic layer overlying a visco-elastic half-space. This method is based on dividing the contact area between the foundation and the soil into a number of sub-regions and on assuming that the contact tractions within each area are uniform but of unknown amplitudes.

In addition, Waas (1972) developed a semi-discrete analytical method to model the far field with homogenous boundary conditions for two-dimensional and axi-symmetric problems. With the aid of the thin-layer theory, Kausel and Peek (1982) obtained Green's functions for multi-layered soils. This semi-discrete analytical model has been then combined with the BEM of the near field to solve the soil-structure interaction problems in layered media. Using this approach, Boumekik (1985) and Boumekik et al. (1984) studied the 3-D problem of embedded foundations on layered substrata.

Recently, Wolf (2002) developed the novel scaled-boundary, finite-element method, which combines the advantages of the BEM and the FEM to calculate the dynamic stiffness of the embedded foundation and the displacements in the neighbouring soil.

The principal aim of this article is the calculation of the displacements of a foundation, and the soil that surrounds it, at a certain distance caused by a vibrating machine, using a coupled numerical method (BEM, and the thin-layer method or TLM) in the frequency domain in conjunction with the Kausel-Peek Green's function (Kausel and Peek, 1982) for a layered stratum and constant element. The vertical displacement of the foundation is obtained by the determination of its vertical impedance function, for which only the soil-foundation interface is discretized, and the results are validated via comparison with the results of Dominguez (1978), Wong and Luco (1978, 1985), and Mylonakis et al. (2006). However, calculation of the vertical soil displacements near the foundation is carried out by means of a mathematical model developed in this study by the combination of BEM and TLM. This model represents the product of compatible tractions at the soil-foundation interface and the flexibility matrix of the neighbouring soil. The principal advantage of this model is that it allows the calculation of the attenuation of vertical displacements near the foundation for several types of soils and foundations.

MODELS AND EQUATIONS

1. Physical Model and Basic Equations

The source of vibrations is assumed to be a square, massless foundation (see Figure 1), with length B_x and width B_y , and subjected to a unit vertical harmonic force $P_z e^{i\omega t}$. The foundation is placed on a surface of visco-elastic soil characterized by its shear modulus G_1 , shear wave velocity C_{s1} , mass density ρ_1 , Poisson's ratio ν_1 , and hysteretic damping coefficient β_1 . This soil layer of depth H is limited by a bedrock characterized by its shear modulus G_2 , shear wave velocity C_{s2} , mass density ρ_2 , Poisson's ratio ν_2 , and hysteretic damping coefficient β_2 . In the following equations, the term $e^{i\omega t}$ will be implicit for displacements and forces.

The (complex) displacement of point A at the free surface, defined by its abscissa $x = d/2B_x$ from the foundation edge, is obtained from the wave equation

$$(C_p^2 - C_s^2)u_{j,ij} + C_s^2 u_{i,ji} + \omega^2 u_i = 0 \quad (1)$$

where u_i is the x -component of the harmonic displacement amplitude vector; $u_{j,ij}$ is the partial derivative of u_j with respect to x - and y -axes; $u_{i,ij}$ is the second partial derivative of u_i with respect to y -axis; C_s and C_p are the shear (S)- and compression (P)-wave velocities; and ω is the angular frequency of excitation.

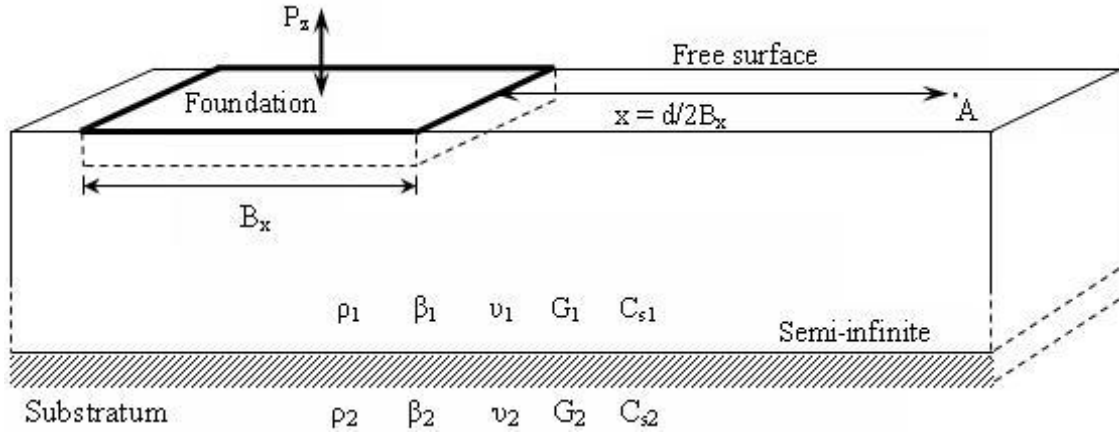


Fig. 1 The geometry of the model

The solution of Equation (1) can be obtained in form of the following boundary integral equation in frequency domain:

$$u_j(x, \omega) = \int_s G_{ij}(x, \xi, \omega) t_i(\xi, \omega) ds(\xi) \tag{2}$$

Here, G_{ij} represents the Green's function tensor, and t_j the surface traction.

Equation (2) remains difficult to solve as long as the domain is a continuum. However, if the domain is discretized in an appropriate form, Equation (2) can be algebraically evaluated for each element. In this approach, the discretization principle of the soil mass is represented in Figure 2. It is based on two types of discretization, one horizontal and other vertical. The horizontal discretization consists of subdividing any horizontal section of the soil mass into square elements. The average displacement of the element is replaced by its centre displacement, for which the distribution of the constraints is supposed to be uniform.

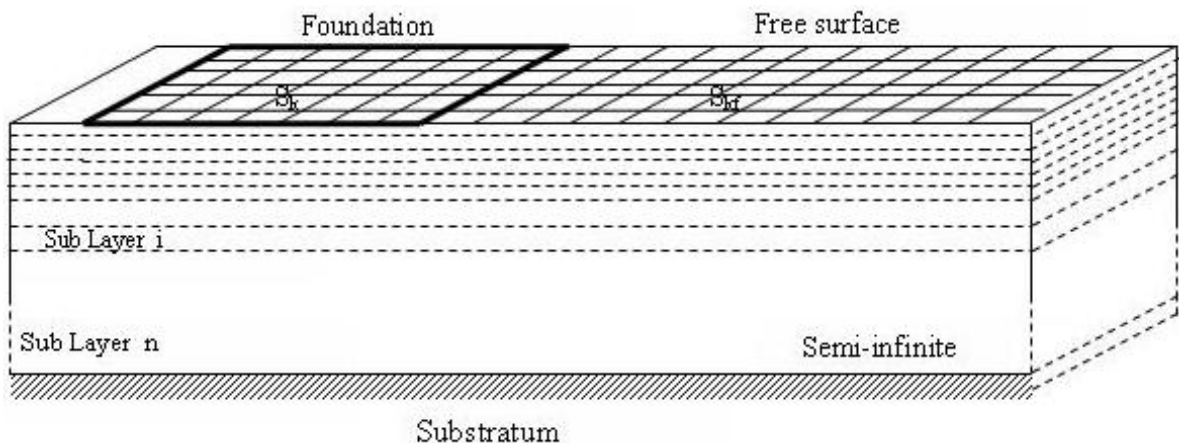


Fig. 2 The discretization of the model

The vertical discretization consists of subdividing the soil mass into sub-layers, which have a rather low thickness compared with the Rayleigh wavelength ($= \lambda/10$), in order to linearize the displacement from one sub-layer to the next. The interface of soil and foundation is horizontally subdivided into N_f

quadrilateral elements, on which uniform forces are applied. The free surface where the displacements are investigated is subdivided into N_h quadrilateral elements.

In the discretized model, Equation (2) is expressed in the algebraic form as follows:

$$u_j = \sum_{i=1}^{\text{NRT}} \int_s G_{ij} t_i ds \quad (3)$$

Here, NRT represents the total number of elements, which discretize the free surface and the interface between the soil and the foundation.

2. Determination of Green's Functions by TLM

In this work, body B is a layered stratum resting on a substratum base with n horizontal layer interfaces defined by $z = z_1, z_2, \dots, z_N$ and with layer j defined by $z_n < z < z_{n+1}$, as shown in Figure 3. The medium of each n th layer of h_n thickness is assumed to be homogeneous, isotropic, and linearly elastic. For this body, the Green's function in frequency domain is obtained with the aid of the Thin Layer Method (TLM).

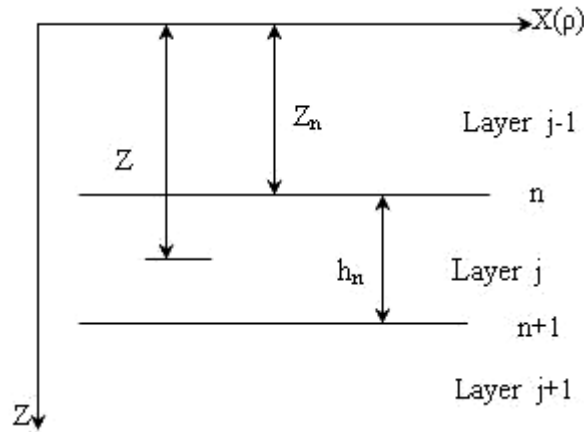


Fig. 3 Geometry of layered stratum B

Actually, the Green's function for a layered stratum is obtained by an inversion of the thin-layer stiffness matrix through the spectral decomposition procedure of Kausel and Peek (1982). The advantage of the thin-layer stiffness matrix technique over the classical Haskell-Thomson transfer matrix technique for finite layers (Haskell, 1953; Thomson, 1950) and the finite-layer stiffness matrix technique of Kausel and Roesset (1981) is that the transcendental functions in the layered stiffness matrix are linearized. According to the thin-layer theory of Lysmer and Waas (1972) and Lysmer et al. (1981), the thickness of each layer is chosen to be sufficiently small (less than 1/10 of the Rayleigh wavelength), such that the displacements in this layer can be assumed to vary linearly with depth and then remain continuous in the x -direction. Thus the Fourier transform of the displacements with respect to the x -domain can be represented by a linear interpolation of the discrete nodal displacements at the n th-layer interfaces as

$$\begin{aligned} U^{(n)}(z) &= (1-\eta)U^n + \eta U^{n+1} \\ V^{(n)}(z) &= (1-\eta)V^n + \eta V^{n+1} \\ W^{(n)}(z) &= (1-\eta)W^n + \eta W^{n+1} \end{aligned} \quad (4)$$

where $\eta = (z - z_n)/h_n$ with $0 \leq \eta \leq 1$, and $U^{(n)}$, $V^{(n)}$, and $W^{(n)}$ are the transformed displacements along the x -, y -, and z -directions as functions of z in the layer j , and U^n , V^n , and W^n are their nodal values at the layer interface $z = z_n$.

Thus, the Green's frequency-domain displacement tensor, after inversion of the Fourier transform, can finally take the form of Kausel and Peek (1982):

$$G_{ij}^{mn} = \sum_{l=1}^{2N} \frac{a_{\alpha\beta} \phi_i^{ml} \phi_j^{nl}}{k^2 - k_l^2} \quad (5)$$

where $a_{\alpha\beta} = 1$ if $\alpha = \beta$, and $a_{\alpha\beta} = k / k_l$ if $\alpha \neq \beta$; indices i and j refer to the x -, y -, and z -axes; k and k_l are wave numbers; m represents the interface where the load is applied; n represents the interface where the Green's functions are calculated; ϕ_i^{ml} denotes the eigenvector component in the i th direction at the m th layer interface of the l th wave mode; and ϕ_j^{nl} denotes the eigenvector component in the j th direction at the n th layer interface of the l th wave mode.

The Green's functions thus obtained are complex and constitute the starting point for the determination of the flexibility matrix of an arbitrary soil volume. However, taking into account the geometry of the foundation, we adopt a system of Cartesian coordinates. The Green's functions thus obtained, in fact, constitute the terms of the flexibility matrix of the soil, $[F_s]$. The determination of this flexibility matrix allows us, in turn, to obtain the impedance functions of one or several foundations. For more details about the computation of the above Green's functions, the reader may refer to the works of Boumekik (1985) and Kausel and Peek (1982).

Visco-elastic soil behavior can be easily introduced in the present formulation by simply replacing the elastic constants λ and G with their complex values,

$$\lambda^* = \lambda(1 + 2i\beta) \quad (6)$$

$$G^* = G(1 + 2i\beta) \quad (7)$$

where β is the constant hysteretic damping coefficient.

3. Mathematical Model

The knowledge of Green's functions allows obtaining harmonic displacements resulting from the discretized domain by successive application of unit forces on all the interface elements, and thus flexibility matrix is constructed. In the particular case of a symmetric foundation (i.e., rectangular, square, ...), it is possible to uncouple the flexibility matrix along the two principal axes (x and y) to reduce its dimension. This matrix is essential to calculate the displacements of the soil. In this work, we look for the vertical displacements through the following relation:

$$\{u_z\} = [F_s] \{t_z\} \quad (8)$$

where $[F_s] = \{G_{ij}^{mn}\}$ represents the flexibility matrix of the discretized domain, which includes the terms of Green's functions; $\{u_z\}$ represents the vertical harmonic displacements; and $\{t_z\}$ represents the surface tractions. In fact, this relation constitutes the formulated solution, in terms of the displacements of Equation (2) that essentially requires a discretized domain. If u_{zf} and u_{zh} are respectively the harmonic displacements under the foundation and in its neighbourhood, Equation (8) can be explicitly written as

$$\begin{Bmatrix} u_{zf} \\ u_{zh} \end{Bmatrix} = \begin{bmatrix} F_f \\ F_h \end{bmatrix} \{t_z\} \quad (9)$$

This expression permits us to obtain displacement forces under the foundation,

$$\{u_{zf}\} = [F_f] \{t_z\} \quad (10)$$

and displacement forces in the vicinity of the foundation,

$$\{u_{zh}\} = [F_h] \{t_z\} \quad (11)$$

with $[F_f]$ denoting the complex flexibility matrix of discretized soil under the foundation; $[F_h]$ denoting the complex flexibility matrix outside the foundation; $\{u_{zf}\}$ denoting the soil displacement vector under the foundation; $\{u_{zh}\}$ denoting the soil displacements outside the foundation; and $\{t_z\}$ denoting the traction forces on any element at the soil-foundation interface.

When the foundation is in place, all elements must move as a rigid body. This condition is expressed by

$$\{u_{z_f}\} = [R]\{D_z\} \quad (12)$$

where $\{D_z\}$ denotes the vertical displacements of the foundation; and $[R]$ represents the transformation matrix of size $N_f \times 1$.

The dynamic equilibrium between the traction forces on each element and the exterior force is expressed by

$$\{P_z\} = [R]^T \{t_z\} \quad (13)$$

where $\{P_z\}$ is the vertical exterior force.

From Equations (10) and (12), the compatible forces to apply on the elements are

$$\{t_z\} = [F_f]^{-1} [R]\{D_z\} \quad (14)$$

Combining Equations (11)–(14), the displacements of the foundation and on the free surface are obtained as

$$\{D_z\} = [K_z(\omega)]\{P_z\} \quad (15)$$

where

$$[K_z(\omega)] = [R]^T [F_f]^{-1} \{R\} \quad (16)$$

is the vertical impedance function of the foundation. It is customary to introduce the dimensionless frequency $a_0 = \omega B_x / C_s$ at the soil-foundation interface, to scale $K_z(\omega)$ with static-stiffness coefficient K_{st} ($= K_z(\omega = 0)$), and to apply the following decomposition:

$$[K_z(\omega)] = [K_{st}(k(a_0) + ia_0c(a_0))](1 + 2i\beta) \quad (17)$$

with $k(a_0)$ denoting the dimensionless spring coefficient; c denoting the dimensionless damping coefficient; β denoting the constant hysteretic damping coefficient; and

$$\{u_{z_h}\} = [F_h][F_f]^{-1}\{R\}\{D_z\} \quad (18)$$

In the following, this relation is used to analyze the surface vibration in the vicinity of the harmonic machine foundation load.

RESULTS

The accuracy of the above-described BEM-TLM formulation for the computation of the ground vibration due to a machine foundation is tested in this section through comparisons with other methods.

Let us consider initially the comparison involving the method of Dominguez (1978), relating to a rectangular surface and an embedded foundation, and then that of Wong and Luco (1978) relating only to a surface foundation. The foundation, which is rigid, massless, and rectangular with sides $2B_x$ and $2B_y$, is placed on a semi-infinite soil with Poisson's ratio $\nu = 1/3$ (see Figure 4). Figures 5(a) and 5(b) show the real part K_z/K_{st} and imaginary part C_z/K_{st} of the vertical impedances as functions of the dimensionless frequency $a_0 = \omega B_x / C_s$. It may be observed that the results of this study, for both surface and embedded cases, match those of Dominguez (1978), with the differences being negligible. Figure 5(c) shows the real part K_z and imaginary part C_z/a_0 of the vertical impedances as functions of the dimensionless frequency. It may be observed that the results of this study have an excellent agreement with those of Wong and Luco (1978).

The second comparison concerns the case of a square foundation resting on a visco-elastic layer overlying a visco-elastic semi-infinite soil. In Figure 6, the effect of the relative ratio of layer thickness is

examined for a given frequency, with H/B_x taken as 1 and 2. The soil is characterised by wave velocities ratio $C_{s1}/C_{s2} = 0.8$ and Poisson's ratios $\nu_1 = \nu_2 = 0.33$; the density ratio ρ_2/ρ_1 is taken as 1.13; and the material damping constants in the layer and the semi-infinite soil are taken to be as $\beta_1 = 0.05$ and $\beta_2 = 0.03$. It may be observed that the results of this study have an excellent agreement with those of Wong and Luco (1985).

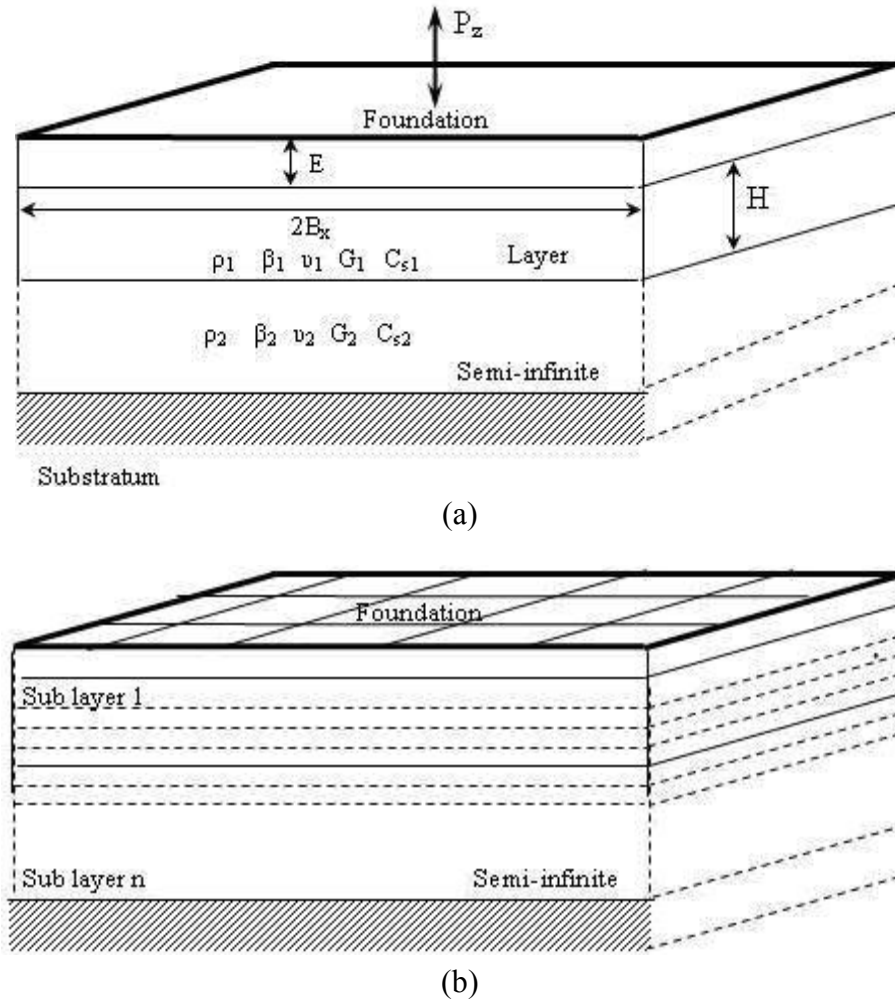


Fig. 4 Model for validation: (a) geometry, (b) discretization

The third comparison concerns the case of a rectangular foundation placed on homogeneous soil layer overlying the bedrock. In Figure 7(a), the effect of the relative length of the foundation is examined for a given frequency, with B_x/B_y taken as 1 and 2. The soil is characterised by the relative depth $H/b = 4$ and Poisson's ratio $\nu = 0.3$. In Figure 7(b), the effect of the relative depth of soil is examined for a square foundation (i.e., $B_x/B_y = 1$) resting on a soil layer with Poisson's ratio $\nu = 0.3$, with H/B_x taken as 2 and 4. For the two cases, it may be observed that these results have an excellent agreement with those of Mylonakis et al. (2006).

Figure 8 shows the comparison between the displacements of free surface in the vicinity of a surface machine foundation for the static case and those obtained by the analytical Boussinesq-Cerruti method that has been generalised for a dynamic case by Lamb (1904). In this method the vertical displacement due to unit vertical contact pressure uniformly distributed over a rectangular area is given by the following equation:

$$u_z = \frac{(1-\nu^2)F}{\pi EB_x} \tag{19}$$

where ν denotes Poisson's ratio; E denotes Young's modulus; and F is a coefficient that varies only with the ratio d/B_x and foundation dimensions, and is given by the Król table (Król, 1971; Cheng, 1977).

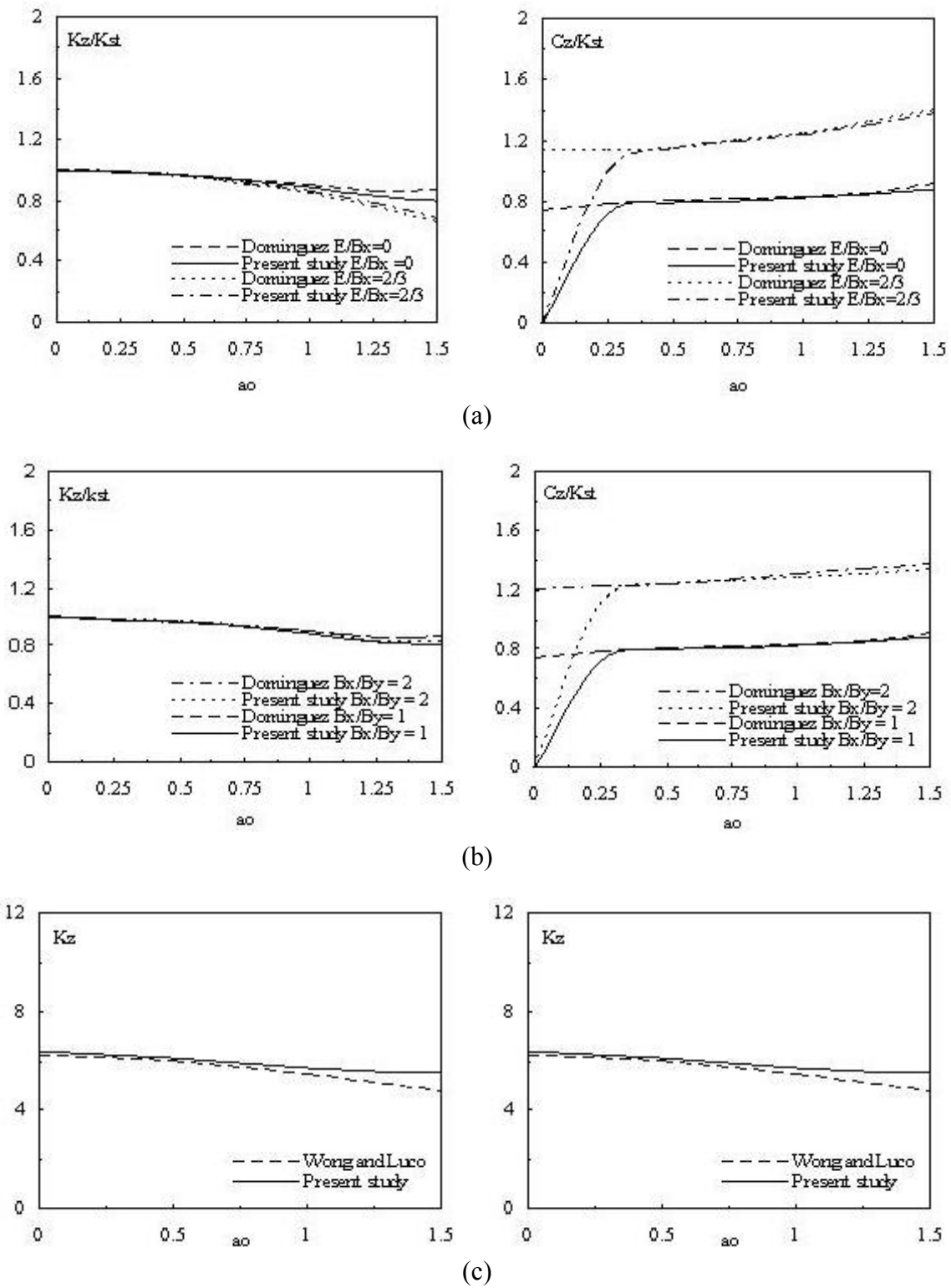


Fig. 5 Validation of vertical impedance functions of rigid foundation on semi-infinite soil: (a) square surface and embedded foundation; (b) square and rectangular foundation; (c) square surface foundation

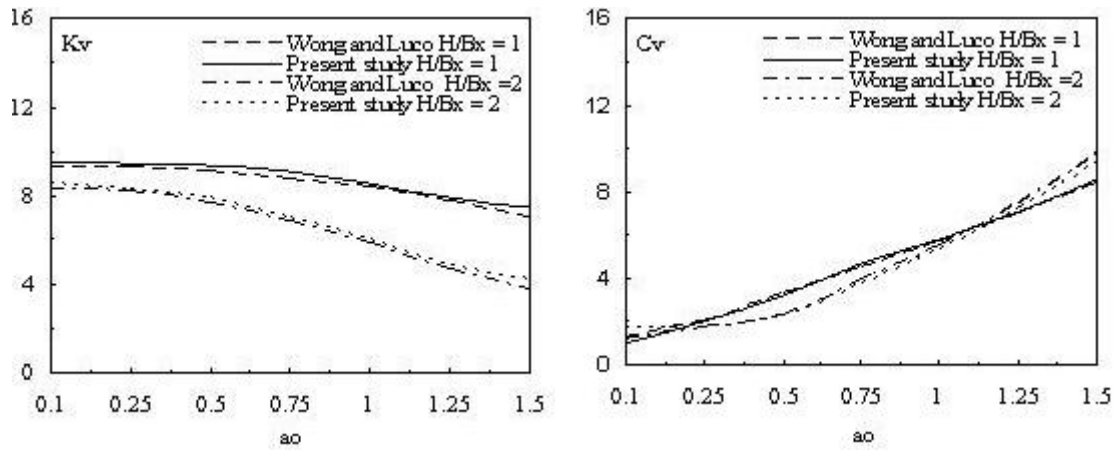


Fig. 6 Validation of vertical impedance function of square rigid foundation resting on layer overlying semi-infinite soil for varying relative ratio of layer thickness ($H/B_x = 1, 2$), with $C_{s1}/C_{s2} = 0.8$ and $\rho_2/\rho_1 = 1.13$ (uniform layer case)

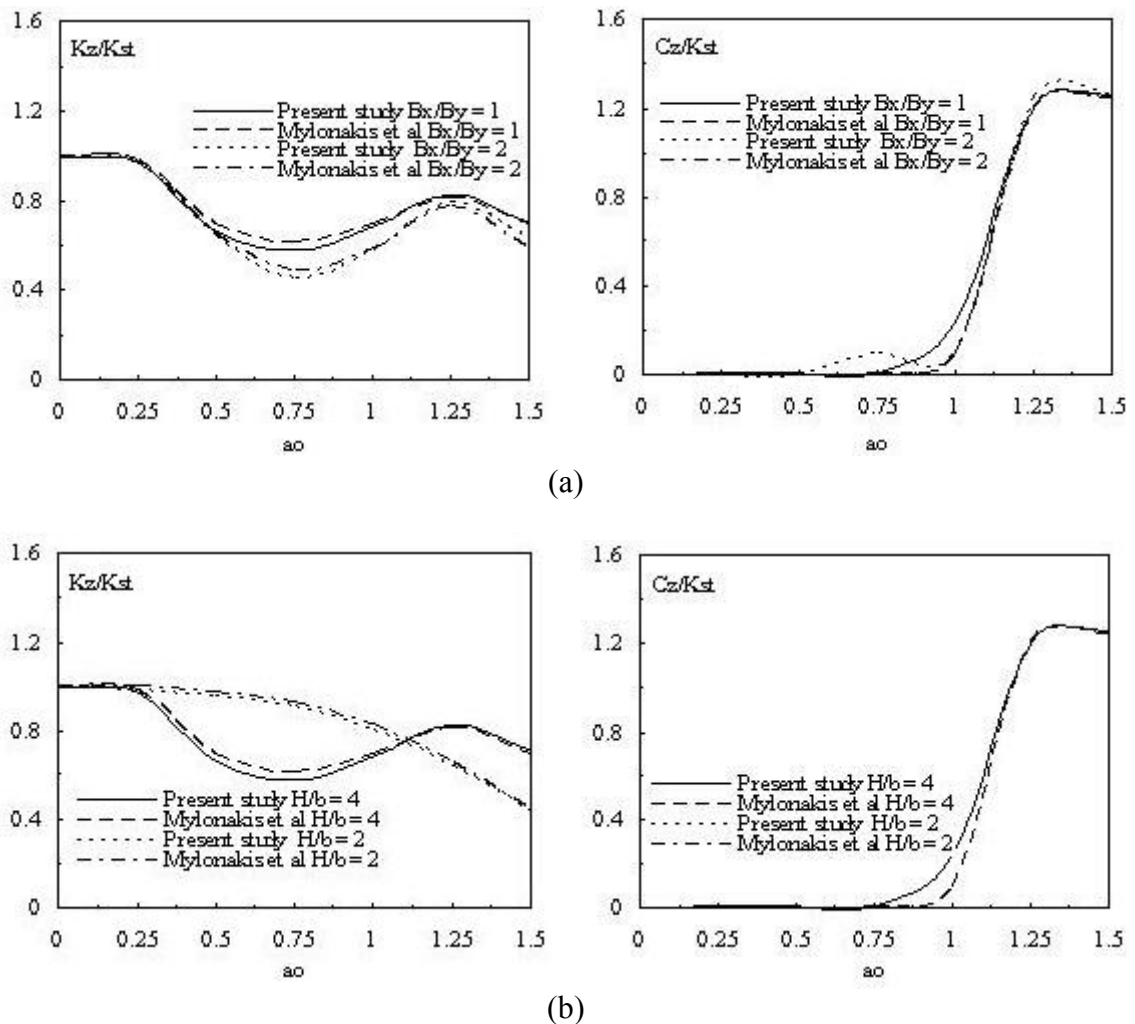


Fig. 7 Validation of vertical impedance function of rigid foundation on soil layer over bedrock: (a) rectangular surface foundation for varying relative length, with $H/B_x = 4$; (b) square surface foundation for varying depths of the substratum

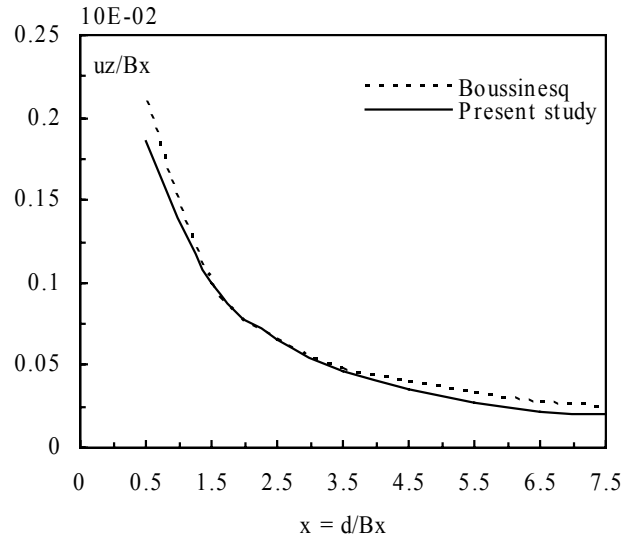


Fig. 8 Validation for static vertical displacement along the free surface

Figure 8 provides the dimensionless, vertical surface amplitude u_z / B_x as a function of the relative distance d / B_x , where B_x is the width of the foundation, and $\rho = 1$, $G = 1$, $E = 1.37$ and $\nu = 0.333$ are the properties of the soil. The comparison of these results with the analytical results clearly shows very good agreement between the two methods.

The dimensionless vertical displacement near the foundation (i.e., $Re u_z / 2B_x$ and $Im u_z / 2B_x$) is studied for different cases of the dimensionless frequency (i.e., $a_0 = 0, 1, 2, 3, 4$) at a relative distance of $x = d / 2B_x = 9.25$. In this application, the analysis concerns the case of a square foundation placed at the surface of a visco-elastic, semi-infinite soil, and the considered foundation is subjected to unit vertical force (i.e., $P_z = 1$) for different values of dimensionless frequency $a_0 = \omega B_x / 2C_s$. The free surface and the soil-foundation interface are discretized into 20 quadrilateral constant elements, and the soil is characterised by $\rho = 1$, $G = 1$, $\nu = 0.333$, and $\beta = 0.05$. By varying the excitation frequency, following observations are made for the real displacements (see Figure 9):

1. There is an important variation in the magnitude of the displacement at close distances ($x \leq 3$). The real vertical displacement decreases, when the excitation frequency is increased.
2. The real vertical displacement decreases, when the relative distance is increased.
3. There is a remarkable shift in the resonant frequencies toward the lower frequencies.
4. There is a variation in the resonance peaks governed by the Rayleigh wave.

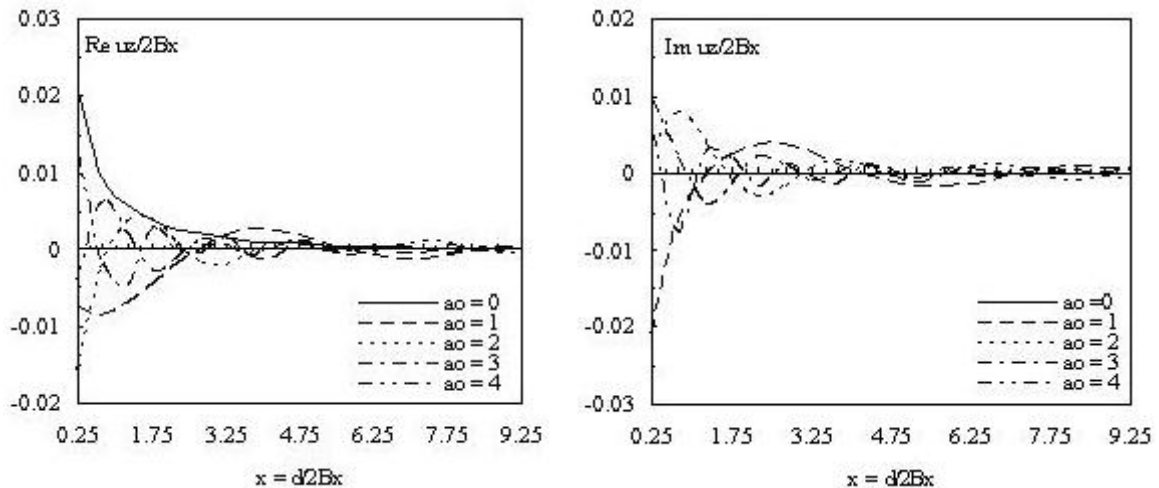


Fig. 9 Amplitude of vertical displacement along the free surface

The behaviour of the imaginary displacements is similar to that described above for the real displacements.

Figure 10 shows the effect of the relative depth of the substratum, for a relative distance along the free surface, with $H/2B_x$ taken as 2, 4, and that for the semi-infinite case, respectively for $a_0 = 0, 1, 2, 3,$ and 4. The soil and the substratum are characterised, respectively, by $\rho_1 = 1, G_1 = 1, C_1 = 1, \nu_1 = 0.333, \beta_1 = 0.05,$ and $\rho_2 = 1, G_2 = 1, C_2 = 1, \nu_2 = 0.333, \beta_2 = 0.01.$ While varying the substratum depth, it may be noted that the variation in the vertical direction is governed by the Rayleigh wave velocity $C_R,$ with $C_R/C_S = 0.94$ for $\nu = 0.333.$ This is clearly visible in Figure 10. The resulting wavelength $\lambda (= C_R/(a_0/2\pi))$ is equal to 2.95, 1.476, 0.8, 0.74 for $a_0 = 1, 2, 3, 4,$ respectively.

For both the low frequencies and the static case (i.e., $a_0 = 0$), a quick decreasing of the soil displacement without oscillations may be noted when the substratum approaches the free surface. We also note that the vertical displacement decreases when the relative distance is increased.

In Figure 11, the effect of the wave-velocity ratio of a semi-infinite soil versus relative distance is examined, for a given frequency, with C_{s1}/C_{s2} taken as 0.2, 0.4, and 1. In varying the wave-velocity ratio, following observations may be made:

1. There is a clear amplification of the vertical displacements, when the wave-velocity ratio is decreased. This can be explained by the fact that the surface waves are imprisoned in the soft layer (i.e., $C_{s1}/C_{s2} = 0.2$).
2. The vertical displacement decreases when the relative distance is increased.

CONCLUSIONS

In this study, the vertical displacements transmitted at the free surface by a vibrating rigid foundation, resting on homogeneous visco-elastic soil and subjected to vertical harmonic external excitation, have been calculated (the case of heterogeneous soil will be treated in the second part of this study). The solution has been formulated by employing the frequency-domain boundary-element method (BEM) in conjunction with the Kausel-Peek Green's function for a layered stratum, along with a quadrilateral constant element determined using the thin-layer method (TLM). The study shows well the great importance of the wave-propagation problem in the vicinity of a machine foundation, which proves to be more complicated than the static case of the Boussinesq problem. On the basis of the results presented in this paper, the following conclusions can be stated:

1. The proposed BEM-TLM formulation provides a very good tool for studying wave propagation and soil-structure interaction problems in multilayered soils.
2. The problem of soil-structure interaction has been treated in a highly accurate and efficient way by calculating the vertical impedance function of a rigid foundation resting on a semi-infinite soil or soil layer. The case of an embedded and arbitrary-geometry foundation has also been treated.
3. Parametric studies have been conducted to assess the effects of the various substratum depths, frequencies, and wave-velocity ratios on the ground-vibration response and to provide some design guidelines to the engineers.
4. The vertical ground vibration is governed by the Rayleigh wave velocity.
5. The effect of the low frequencies on the vertical displacements is more pronounced than that of the higher frequencies for a semi-infinite soil case.
6. For a substratum with little depth, the attenuation of the ground vibrations is more important in the low frequencies than in the high ones (for the propagation of waves without oscillations).
7. A higher variation has been observed in the vertical ground displacements for the soft, semi-infinite soils than for the stiff ones.
8. The soil vibrations are less pronounced, when the relative distance increases (for a visco-elastic soil). It is thus recommended to take into account all of these phenomena in the study of any structure placed in the vicinity of a machine foundation because the transmitted waves represent a critical factor that influences the behaviour of the structure and the amount of damage that can be caused to it.

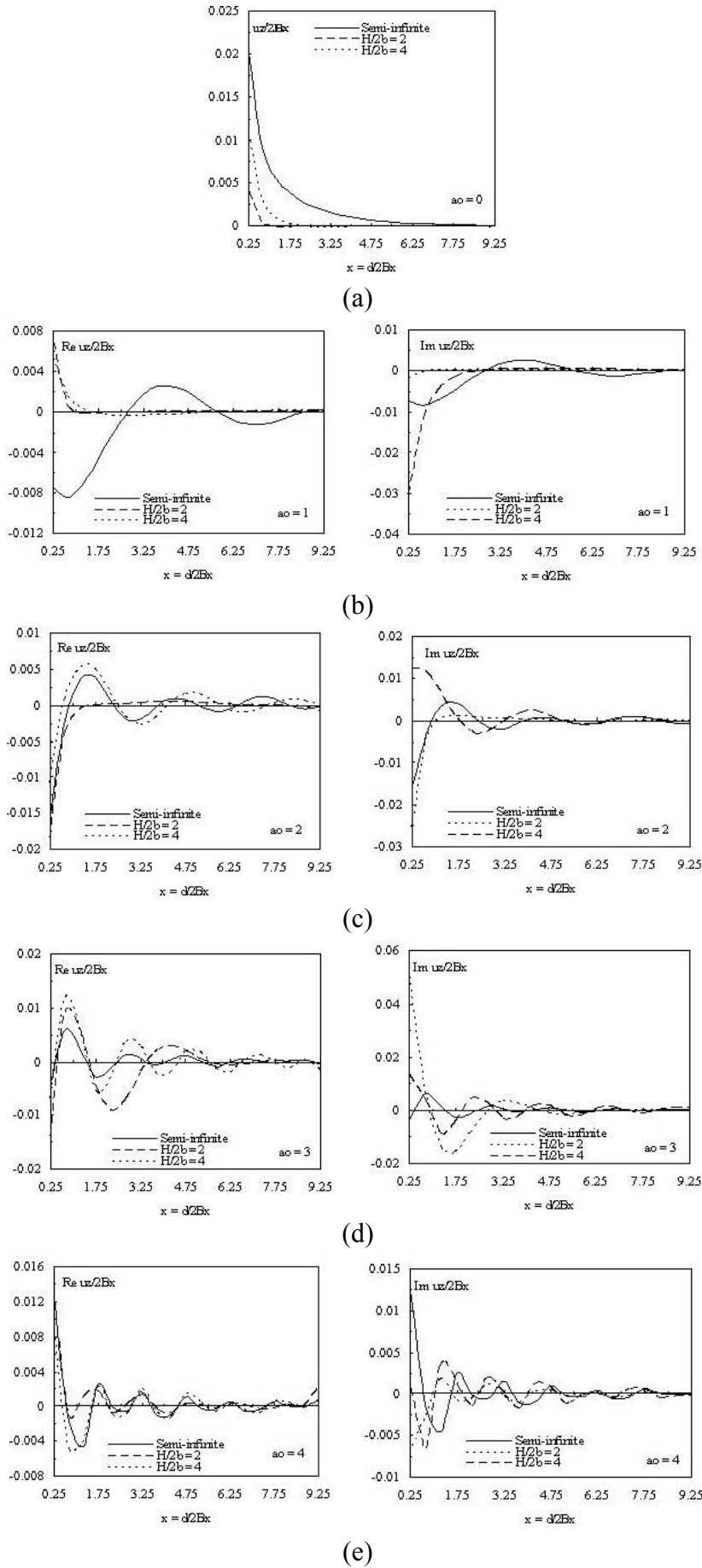


Fig. 10 Amplitude of vertical displacement along free surface for varying depths of the substratum and frequency a_0 equal to (a) 0, (b) 1, (c) 2, (d) 3, (e) 4

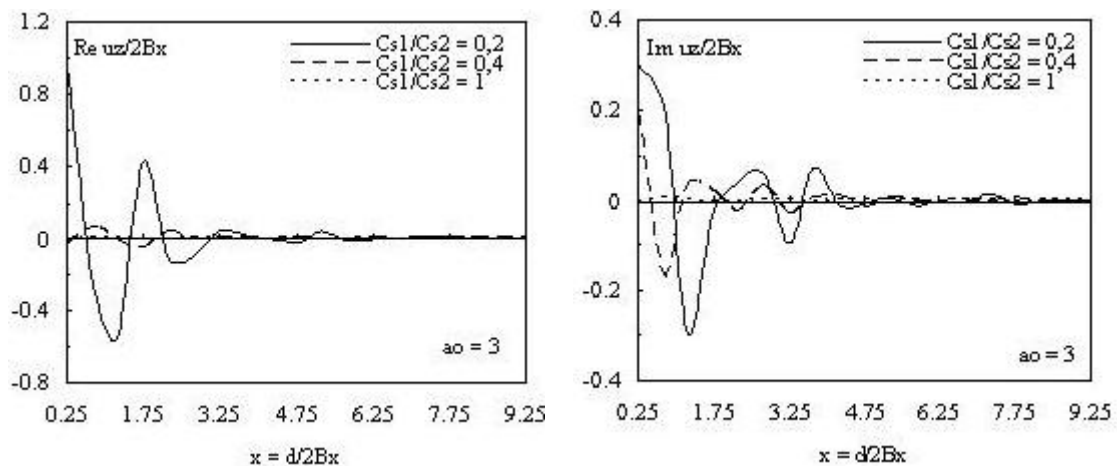


Fig. 11 Amplitude of vertical displacement along free surface for varying shear wave velocity ratio of the soil layer

ACKNOWLEDGEMENTS

The authors are grateful to the Ministry of Higher Education and Scientific Research for supporting this work under grant No. J2501/04/02/05. The calculation program developed during this work represents a continuity of the FONDVIB program worked out within the Soil Mechanics Laboratory of the Free Brussels University of Belgium by the coauthor, Professor A. Boumekik, in collaboration with Professors J. Nuyens and I.C. Constantopoulos.

REFERENCES

1. Ahmad, S. and Rupani, A.K. (1999). "Horizontal Impedance of Square Foundation in Layered Soil", *Soil Dynamics and Earthquake Engineering*, Vol. 18, No. 1, pp. 59–69.
2. Apsel, R.J. and Luco, J.E. (1987). "Impedance Functions for Foundations Embedded in a Layered Medium: An Integral Equation Approach", *Earthquake Engineering & Structural Dynamics*, Vol. 15, No. 2, pp. 213–231.
3. Beskos, D.E. (1987). "Boundary Element Methods in Dynamic Analysis", *Applied Mechanics Reviews*, Vol. 40, No. 1, pp. 1–23.
4. Beskos, D.E., Dasgupta, B. and Vardoulakis, I.G. (1986). "Vibration Isolation Using Open or Filled Trenches", *Computational Mechanics*, Vol. 1, No. 1, pp. 43–63.
5. Boumekik, A. (1985). "Fonctions Impédances d'une Fondation Vibrante en Surface ou Partiellement Encastrée dans un Sol Multicouche", Ph.D. Thesis, Université Libre de Bruxelles, Brussels, Belgium (in French).
6. Boumekik, A., Nuyens, J. and Constantopoulos, I.C. (1984). "Soil-Structure Interaction Effect on Noncircular Structure Embedded in Multilayered Soil", *Annales des Travaux Publics de Belgique*, Vol. 6, No. 3, pp. 563–592.
7. Chang-Liang, V. (1974). "Dynamic Response of Structures in Layered Soils", Ph.D. Thesis, Massachusetts Institute of Technology, Cambridge, U.S.A.
8. Cheng, Y.K. (1977). "Beams, Slabs, and Pavements" in "Numerical Methods in Geotechnical Engineering (edited by C.S. Desai and J.T. Christian)", McGraw-Hill, New York, U.S.A.
9. Dominguez, J. (1978). "Dynamic Stiffness of Rectangular Foundations", Report R78-20, Department of Civil Engineering, Massachusetts Institute of Technology, Cambridge, U.S.A.
10. Ewing, W.M., Jardetzky, W.S. and Press, F. (1957). "Elastic Waves in Layered Media", McGraw-Hill, New York, U.S.A.
11. Gupta, R.N. (1966). "Reflection of Elastic Waves from a Linear Transition Layer", *Bulletin of the Seismological Society of America*, Vol. 56, No. 2, pp. 511–526.

12. Haskell, N.A. (1953). "The Dispersion of Surface Waves on Multilayered Media", *Bulletin of the Seismological Society of America*, Vol. 43, No. 1, pp. 17–34.
13. Kausel, E. and Peek, R. (1982). "Dynamic Loads in the Interior of a Layered Stratum: An Explicit Solution", *Bulletin of the Seismological Society of America*, Vol. 72, No. 5, pp. 1459–1481.
14. Kausel, E. and Roesset, J.M. (1981). "Stiffness Matrices for Layered Soils", *Bulletin of the Seismological Society of America*, Vol. 71, No. 6, pp. 1743–1761.
15. Kausel, E., Roesset, J.M. and Waas, G. (1975). "Dynamic Analysis of Footings on Layered Media", *Journal of the Engineering Mechanics Division, Proceedings of ASCE*, Vol. 101, No. EM5, pp. 679–693.
16. Król, W. (1971). "Statique des Fondations en Béton Armé, Compte Tenue de la Rigidité de la Superstructure", *Dunod Éditeur, Paris, France* (in French).
17. Lamb, H. (1904). "On the Propagation of Tremors over the Surface of an Elastic Solid", *Philosophical Transactions of the Royal Society of London—Series A*, Vol. 203, No. 359–371, pp. 1–42.
18. Lysmer, J. and Kuhlemeyer, R.L. (1969). "Finite Dynamic Model for Infinite Media", *Journal of the Engineering Mechanics Division, Proceedings of ASCE*, Vol. 95, No. EM4, pp. 859–877.
19. Lysmer, J. and Waas, G. (1972). "Shear Waves in Plane Infinite Structures", *Journal of the Engineering Mechanics Division, Proceedings of ASCE*, Vol. 98, No. EM1, pp. 85–105.
20. Lysmer, J., Tabatabaie-Raissi, M., Tajirian, F., Vahdani, S. and Ostadan, F. (1981). "SASSI: A System for Analysis of Soil Structure Interaction", *Report UCB/GT-81/02, University of California, Berkeley, U.S.A.*
21. Mylonakis, G., Nikolaou, S. and Gazetas, G. (2006). "Footings under Seismic Loading: Analysis and Design Issues with Emphasis on Bridge Foundations", *Soil Dynamics and Earthquake Engineering*, Vol. 26, No. 9, pp. 824–853.
22. Reissner, E. (1936). "Stationäre, Axialsymmetrische, durch eine Schüttelnde Masse Erregte Schwingungen eines Homogenen Elastischen Halbraumes", *Ingenieur-Archiv*, Vol. 7, No. 6, pp. 381–396 (in German).
23. Richart Jr., F.E., Hall Jr., J.R. and Woods, R.D. (1970). "Vibrations of Soils and Foundations", *Prentice-Hall, Englewood Cliffs, U.S.A.*
24. Takahashi, D. (1985). "Wave Propagation in Ground-Structure Systems with Line Contact", *Journal of Sound and Vibration*, Vol. 101, No. 4, pp. 523–537.
25. Takahashi, D. (1986). "Wave Propagation in Ground-Structure Systems, Part I: Analysis of the Model with Surface Contact", *Journal of Sound and Vibration*, Vol. 105, No. 1, pp. 27–36.
26. Thomson, W.T. (1950). "Transmission of Elastic Waves through a Stratified Soil Medium", *Journal of Applied Physics*, Vol. 21, No. 2, pp. 89–93.
27. Waas, G. (1972). "Linear Two-Dimensional Analysis of Soil Dynamics Problems in Semi-infinite Layered Media", *Ph.D. Thesis, University of California, Berkeley, U.S.A.*
28. Wolf, J.P. (2002). "Response of Unbounded Soil in Scaled Boundary Finite-Element Method", *Earthquake Engineering & Structural Dynamics*, Vol. 31, No. 1, pp. 15–32.
29. Wong, H.L. and Luco, J.E. (1978). "Tables of Impedance Functions and Input Motions for Rectangular Foundations", *Report CE 78-15, University of Southern California, Los Angeles, U.S.A.*
30. Wong, H.L. and Luco, J.E. (1985). "Tables of Impedance Functions for Square Foundations on Layered Media", *Soil Dynamics and Earthquake Engineering*, Vol. 4, No. 2, pp. 64–81.

A MODAL COMBINATION RULE FOR ORDERED PEAK RESPONSE UNDER MULTI-COMPONENT GROUND MOTION

Ayan Sadhu and Vinay K. Gupta
Department of Civil Engineering
Indian Institute of Technology Kanpur
Kanpur-208016

ABSTRACT

The traditional earthquake-resistant design philosophy involves estimation of the peak elastic response for the specified seismic hazard, which in turn requires a modal combination rule for the multi-degree-of-freedom systems. The typically used rules estimate just the largest response peaks, while the second largest, third largest, ... peaks are assumed to be of no significance. Considering the possibility that structural damage in the post-yield regime can be correlated with these higher-order peaks, a new modal combination rule is developed for the ordered peak response of multistoried buildings excited by the multi-component ground motions. The proposed rule is formulated by using the stationary random vibration theory and by making suitable approximations regarding the peak factors and nonstationarity factors. A numerical study shows that the proposed rule performs better than the CQC3 rule when the building is stiffer to the ground motion and that the level of accuracy for the higher-order peaks up to the 10th largest peak is comparable to that for the largest peak.

KEYWORDS: Multi-Degree-of-Freedom Systems, Multi-component Ground Motions, Higher-Order Peaks, Order Statistics, Modal Combination Rule

INTRODUCTION

The present practice of designing multistoried buildings for seismic resistance involves the use of design (response) spectra as specified for the site under consideration. Design spectra typically specify the maximum elastic response of the single-degree-of-freedom (SDOF) oscillators of different periods and damping ratios under the perceived seismic hazard. Structural response estimated from these spectra is reduced via specified reduction factors in order to take advantage of the energy dissipation during the inelastic response of ductile structural systems. Estimating the (elastic) peak structural response in the case of a multi-degree-of-freedom (MDOF) system involves the use of a modal combination rule, unless the system can be assumed to vibrate as a SDOF system under the earthquake excitation. One can possibly generate time-histories consistent with the design spectra and estimate the peak structural response via numerical integration due to the easy availability of inexpensive and fast computational power. However, practicing engineers find it more convenient to estimate the peak response directly from the response spectra. Furthermore, seismic codes rely on simple and direct procedures, like modal combination rules, wherever possible.

Several researchers (e.g., Goodman et al., 1953; Rosenblueth and Elorduy, 1969; Der Kiureghian, 1981; Wilson et al., 1981; Singh and Mehta, 1983; Der Kiureghian and Nakamura, 1993) have worked on the estimation of the largest peak response in a MDOF system from a prescribed design spectrum and have proposed simple rules of modal combination for different situations. The most popular of these rules, i.e., the SRSS (Square-Root-of-Sum-of-Squares) rule by Goodman et al. (1953), is meant for the structures with well-separated dominant modes and for the ground motions acting like white noise over those modes. Rosenblueth and Elorduy (1969) made the first attempt to account for the correlation in different modes, while Der Kiureghian (1981) and Wilson et al. (1981) proposed the popular CQC (Complete Quadratic Combination) rule without requiring the use of the duration of earthquake excitation. However, both rules are however based on the use of white noise idealization of the excitation and are therefore inappropriate for application when the dominant frequencies of the system are outside the frequency-band of significant energy in the excitation. Singh and Mehta (1983), Der Kiureghian and Nakamura (1993), and Gupta (1994) later proposed more generalized modal combination rules that could account for the narrow-band seismic inputs and effects of high-frequency modes. None of the past efforts,

except that by Gupta (1994), could however be used to estimate the higher-order (second largest, third largest, ...) response peak amplitudes. This is perhaps because higher-order peaks in the linear response were never recognized to constitute an important data for the earthquake-resistant design, even though Amini and Trifunac (1985), Gupta and Trifunac (1987a), and Gupta and Trifunac (1989) made significant attempts to estimate the ordered peak amplitudes in the response of MDOF systems. Recently, Sadhu (2007) showed that higher-order peaks in the linear response may be useful in a simple estimation of a damage measure during the inelastic response. Gupta (1994) developed a modal combination rule that proposed an improvement over the existing rules in a simple manner and also provided for the estimation of the higher-order peaks.

The modal combination rules as mentioned above were proposed for the specific situation of translational ground motion acting along one of the structure axes. However, as shown by Penzien and Watabe (1975), it is important to consider all three translational components of the ground motion acting simultaneously in estimating the structural response. They showed that there exists a set of principal directions along which the ground motion components are uncorrelated. They also observed that these directions remain stable with time during the strong motion phase of the ground motion and that the major principal axis remains horizontal and directed from the epicenter to the site while the minor principal axis is kept vertical.

Development of combination rules for the multi-component ground motions was first attempted by O'Hara and Cunniff (1963). They suggested the NRLS (Naval Research Laboratory Sum) method, in which the resultant response is defined as the maximum of the three components plus the SRSS of the other two. Chu et al. (1972) proposed the use of SRSS method for finding the resultant response. This was later accepted by USNRC (1976). Among the percentage rules, Newmark (1975) suggested the (Max + 40%) rule wherein the maximum of the three components is added to 40% of the other two. In a slightly modified form, Rosenblueth and Contreras (1977) proposed the (Max + 30%) rule, which was later incorporated in the ATC-3 provisions (ATC, 1978). Anagnostopoulos (1981) made a comparative study of different rules and showed that neither of the existing rules properly accounted for the cross-correlation between the ground motion components. Smeby and Der Kiureghian (1985) and Menun and Der Kiureghian (1998) generalized the CQC rule to the CQC3 (Complete Quadratic Combination with three components) rule for application to multi-component excitations, based on the Penzine-Watabe characterization of ground motions and thus accounting for the cross-correlation between the different ground motion components. Hernandez and Lopez (2002) developed a more versatile combination rule, GCQC3 (Generalised Complete Quadratic Combination with three components) that takes into account the quasi-horizontal and quasi-vertical principal components. None of these rules is however meant to estimate the higher-order response peak amplitudes. Further, these rules are developed specifically for those situations when the input ground motion can be assumed to be white noise over the dominant structural frequencies. The response spectrum-based formulation by Gupta and Trifunac (1987b) is the only effort in the direction of estimating the higher-order peaks under multi-component excitations. However, this formulation is for the situation when the structural axes are aligned with the principal axes of the ground motion, and further this does not provide the convenience of a modal combination rule.

Based on the above, there exists a clear need to develop a simple and more versatile modal combination rule that can estimate not just the largest peak but also the second largest, third largest, ... peaks in the response of a multi-storied building under the excitation of multi-component ground motion with arbitrary characteristics. The present study aims to develop such a rule for a fixed-base, MDOF system excited by a multi-component ground motion. The proposed rule is developed by broadly following the procedure adopted by Gupta (1994) under the framework of stationary random vibration theory. Performance of the proposed rule is evaluated through a numerical study based on six recorded ground motions with wide variety in their characteristics and for a 5-story building with seven different sets of floor mass and story stiffness properties.

FORMULATION OF THE PROPOSED RULE

1. PSDF of a Typical Response

Let us consider a linear, classically damped, lumped-mass system having n degrees of freedom (DOFs). The system is fixed-base and is subjected to three translational ground accelerations at its base:

$\ddot{u}_{g1}(t)$ and $\ddot{u}_{g2}(t)$ along two mutually perpendicular horizontal directions (X_s and Y_s) aligned with the structure axes, and $\ddot{u}_{g3}(t)$ along the vertical direction. On expanding the response of the system in terms of the normal coordinates and undamped mode shapes of the system, let ω_j and ζ_j respectively denote the natural frequency and damping ratio in the j th mode. Further, let $\gamma_1^{(j)}$, $\gamma_2^{(j)}$, and $\gamma_3^{(j)}$ respectively denote the participation factors with respect to $\ddot{u}_{g1}(t)$, $\ddot{u}_{g2}(t)$, and $\ddot{u}_{g3}(t)$ in the j th mode.

On assuming stationarity in the excitation and in the response, PSDF of the response $r(t)$ of the system may be expressed as (Sadhu, 2007)

$$S_r(\omega) = \sum_{k=1}^3 \sum_{l=1}^3 S_z^{kl}(\omega) \sum_{j=1}^n \sum_{q=1}^n r_j r_q \gamma_k^{(j)} \gamma_l^{(q)} \text{Re}(H_j(\omega) H_q^*(\omega)) \quad (1)$$

where $S_z^{kl}(\omega)$ is the cross-PSDF of the k th and l th components of the base acceleration for $k \neq l$, and is the PSDF of the k th component for $k = l$; r_j is the normalized amplitude of the response $r(t)$ in the j th mode of vibration and is expressed as a linear combination of the elements of the j th mode shape (e.g., it is equal to the i th element of the j th mode shape for the displacement response at the i th DOF); and

$$H_j(\omega) = \frac{-1}{\omega_j^2 - \omega^2 + 2i\zeta_j \omega_j \omega} \quad (2)$$

(with $i = \sqrt{-1}$) is the transfer function relating the relative displacement of the equivalent SDOF oscillator in the j th mode to the input base acceleration.

On using the partial fractions for $\text{Re}(H_j(\omega) H_q^*(\omega))$ as in Gupta and Trifunac (1990), Equation (1) leads to

$$S_r(\omega) = \sum_{k=1}^3 \sum_{l=1}^3 S_z^{kl}(\omega) \sum_{j=1}^n \sum_{q=1}^n \left\{ r_j r_q \gamma_k^{(j)} \gamma_l^{(q)} (C_{jq} + D_{jq}) |H_j(\omega)|^2 - r_j r_q \gamma_k^{(j)} \gamma_l^{(q)} D_{jq} \frac{|\omega H_j(\omega)|^2}{\omega_j^2} \right\} \quad (3)$$

where C_{jq} and D_{jq} are the coefficients given in terms of ζ_j , ζ_q , and $\varrho = \omega_q/\omega_j$ as

$$C_{jq} = \frac{1}{B_{jq}} \left[8\zeta_j (\zeta_j + \zeta_q \varrho) \{ (1 - \varrho^2)^2 - 4\varrho (\zeta_j - \zeta_q \varrho) (\zeta_q - \zeta_j \varrho) \} \right] \quad (4)$$

$$D_{jq} = \frac{1}{B_{jq}} \left[2(1 - \varrho^2) \{ 4\varrho (\zeta_j - \zeta_q \varrho) (\zeta_q - \zeta_j \varrho) - (1 - \varrho^2)^2 \} \right] \quad (5)$$

with

$$B_{jq} = 8\varrho^2 \left[(\zeta_j^2 + \zeta_q^2)(1 - \varrho^2)^2 - 2(\zeta_q^2 - \zeta_j^2 \varrho^2)(\zeta_j^2 - \zeta_q^2 \varrho^2) \right] + (1 - \varrho^2)^4 \quad (6)$$

C_{jq} becomes maximum at $\varrho = 1$, while D_{jq} becomes maximum near $\varrho = 1$ (it is equal to zero at $\varrho = 1$). Both sharply fall off to small values as $\varrho \ll 1$ and $\varrho \gg 1$.

In general, the translational components $\ddot{u}_{g1}(t)$, $\ddot{u}_{g2}(t)$, and $\ddot{u}_{g3}(t)$ are correlated processes. However, Penzien and Watabe (1975) have shown that there exists a set of (orthogonal) principal directions, along which the components of ground acceleration are uncorrelated. The orientation of these axes remains approximately constant with time during the strong motion phase of the ground motion. During this phase, the major principal axis is horizontal and directed from the epicenter to the site, the intermediate principal axis is horizontal and perpendicular to the major axis, and the minor principal axis is nearly vertical. Since the axes X_s and Y_s of a structure in plan may not always align with the major and intermediate principal axes, X_p and Y_p , as shown in Figure 1, components of the motion along the axes of the structure are usually correlated. The degree of this correlation depends on the relative orientation of the structure axes with respect to the principal directions of the excitation.

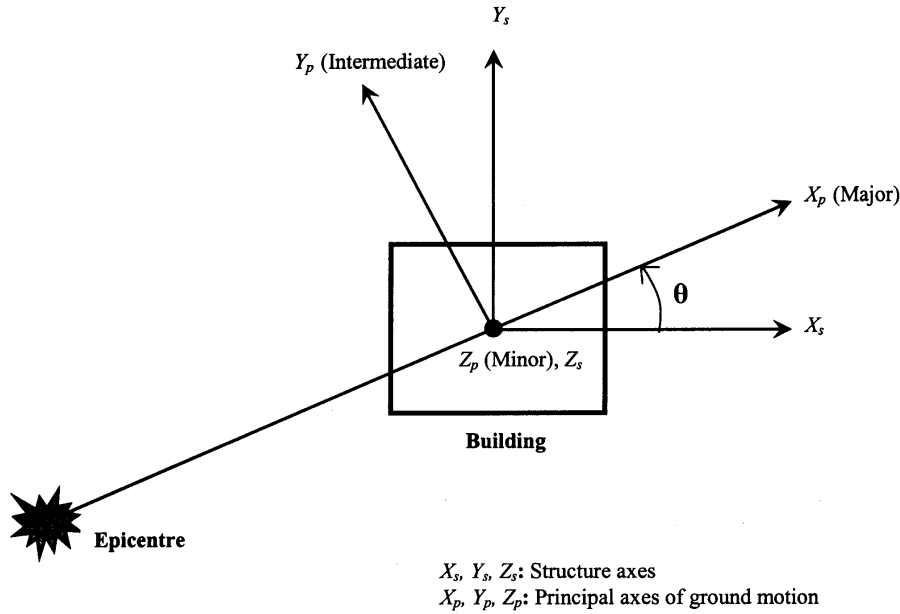


Fig. 1 Illustration of structure axes and principal axes of ground motion

It is possible to express the PSDF matrix $[S_z(\omega)]$ of the ground acceleration vector $\{\ddot{u}_g(t)\}$ along the structure axes in terms of the PSDF matrix $[S_z^p(\omega)]$ of the acceleration vector $\{\ddot{u}_g^p(t)\}$ along the principal directions as (Smeby and Der Kiureghian, 1985)

$$[S_z(\omega)] = [R]^T [S_z^p(\omega)] [R] \quad (7)$$

where $[R]$ is the transformation matrix given by

$$[R] = \begin{bmatrix} \cos \theta & \sin \theta & 0 \\ -\sin \theta & \cos \theta & 0 \\ 0 & 0 & 1 \end{bmatrix} \quad (8)$$

in terms of the relative orientation θ of the major principal axis X_p with respect to the structure axis X_s (see Figure 1). The off-diagonal elements of $[S_z(\omega)]$ and $[S_z^p(\omega)]$ denote the cross-PSDFs of the corresponding ground acceleration components. Since the off-diagonal elements of $[S_z^p(\omega)]$ are zero, i.e., $S_z^{kl,p} = 0$ for $k \neq l$, the off-diagonal elements of $[S_z(\omega)]$ are real quantities. Also, the cross-PSDFs of the vertical component ($\ddot{u}_{g_3}(t)$) with the two horizontal components ($\ddot{u}_{g_1}(t)$ and $\ddot{u}_{g_2}(t)$) are zero.

On substituting the expressions of PSDFs and cross-PSDFs of the accelerations along the structure axes from Equation (7), Equation (3) becomes

$$\begin{aligned}
 S_r(\omega) = \sum_{j=1}^n \sum_{q=1}^n r_j r_q \left\{ (C_{jq} + D_{jq}) |H_j(\omega)|^2 - D_{jq} \frac{|\omega H_j(\omega)|^2}{\omega_j^2} \right\} \times \\
 \left[\sum_{k=1}^3 \gamma_k^{(j)} \gamma_k^{(q)} S_z^{kk,p}(\omega) - \sum_{k=1}^2 \sum_{l=1}^2 (-1)^{k+l} \gamma_l^{(j)} \gamma_l^{(q)} S_z^{kk,p}(\omega) \sin^2 \theta \right. \\
 \left. - \sum_{k=1}^2 (-1)^k (\gamma_1^{(j)} \gamma_2^{(q)} + \gamma_2^{(j)} \gamma_1^{(q)}) S_z^{kk,p}(\omega) \sin \theta \cos \theta \right] \quad (9)
 \end{aligned}$$

This expression can be used to obtain the response PSDF of the system from the (three) PSDFs of principal ground accelerations and orientation of X_p with respect to X_s (instead of PSDFs and cross-PSDFs for the ground accelerations along the structure axes).

2. Ordered Peak Response Amplitudes

In stationary random vibration theory, ordered peak amplitudes of any response are estimated by computing moments of the PSDF of the response process and by multiplying the peak factor computed from these moments with the root-mean-square (r.m.s.) value of the process. This procedure is followed in this section to formulate the expression for an ordered peak of a typical response $r(t)$.

On taking the p th moment of $S_r(\omega)$ about the origin,

$$\lambda_p^r = \int_0^\infty \omega^p S_r(\omega) d\omega \quad (10)$$

Equation (9) leads to

$$\lambda_p^r = \sum_{j=1}^n \sum_{q=1}^n r_j r_q \left[\sum_{k=1}^3 \gamma_k^{(j)} \gamma_k^{(q)} \delta_{p,jq}^k \lambda_{p,j}^{D,k} - \sum_{k=1}^2 \sum_{l=1}^2 (-1)^{k+l} \gamma_l^{(j)} \gamma_l^{(q)} \delta_{p,jq}^k \lambda_{p,j}^{D,k} \sin^2 \theta - \sum_{k=1}^2 (-1)^k (\gamma_1^{(j)} \gamma_2^{(q)} + \gamma_2^{(j)} \gamma_1^{(q)}) \delta_{p,jq}^k \lambda_{p,j}^{D,k} \sin \theta \cos \theta \right] \quad (11)$$

where,

$$\delta_{p,jq}^k = C_{jq} + D_{jq} v_{p,j}^k \quad (12)$$

with

$$v_{p,j}^k = 1 - \frac{\lambda_{p,j}^{V,k}}{\omega_j^2 \lambda_{p,j}^{D,k}} \quad (13)$$

is the term determining the extent of cross-correlation of the j th and q th modes in the p th moment during the excitation by the k th principal component of the ground acceleration. Further, in Equations (11) and (13),

$$\lambda_{p,j}^{D,k} = \int_0^\infty \omega^p |H_j(\omega)|^2 S_z^{kk,p}(\omega) d\omega \quad (14)$$

is the p th moment of the PSDF of the relative displacement response of a SDOF oscillator with ω_j frequency and ζ_j damping ratio, and subjected to the base acceleration $\ddot{u}_{gk}^p(t)$, and

$$\lambda_{p,j}^{V,k} = \int_0^\infty \omega^p |\omega H_j(\omega)|^2 S_z^{kk,p}(\omega) d\omega \quad (15)$$

is the p th moment of the PSDF of the relative velocity response of this oscillator. It may be mentioned that for $p = 0$, $v_{p,j}^k$ is a measure of the deviation of the rate of zero crossings of the displacement response of the same SDOF oscillator from that in the case of an ideal white noise excitation (Gupta, 2002). This factor decreases with the increasing natural period and becomes zero near the dominant period of the ground motion. Further, $v_{p,j}^k$ together with D_{jk} becomes an important component of cross-correlation when ω_j is not close to the dominant frequency of the ground motion and therefore may be ignored when the excitation acts like white noise over the frequencies of interest.

Equation (11) may be used to calculate the moments, λ_0^r , λ_2^r , and λ_4^r , of the response PSDF by taking $p = 0, 2, 4$, respectively. The r.m.s. value of the response process may be estimated by taking the square-root of λ_0^r , and the peak factor (for the desired order and level of confidence) may be estimated by using all three moments along with the strong motion duration of excitation (Gupta, 2002). On multiplication of the r.m.s. value with the peak factors for different orders, estimates of the largest, second largest, third largest, ... peaks may be obtained. In order to include the effects of inherent nonstationarity in response, the (stationary) r.m.s. value may be modified by multiplying it with a nonstationarity factor. We assume that this factor is known. It is further assumed that the peak factors would remain affected due to the nonstationarity, as those depend on the ratios of the moments of response PSDF, not on the moments *per se*. The nonstationarity factor may be close to unity provided the excitation PSDF $S_z^{kk,p}(\omega)$

is compatible with a response spectrum (for the k th principal component of the ground acceleration) and thus includes the effects of nonstationarity indirectly (see, for example, Kaul, 1978; Unruh and Kana, 1981; Christian, 1989).

In view of the above discussion, the s th ordered peak amplitude of the response process may be expressed as

$$r_{\text{peak}}^{(s)} = \eta_r^{(s)} \beta_r^{(s)} \left[\sum_{j=1}^n \sum_{q=1}^n r_j r_q \left\{ \sum_{k=1}^3 \gamma_k^{(j)} \gamma_k^{(q)} \delta_{0,jq}^k \lambda_{0,j}^{D,k} - \sum_{k=1}^2 \sum_{l=1}^2 (-1)^{k+l} \gamma_l^{(j)} \gamma_l^{(q)} \delta_{0,jq}^k \lambda_{0,j}^{D,k} \sin^2 \theta - \sum_{k=1}^2 (-1)^k (\gamma_1^{(j)} \gamma_2^{(q)} + \gamma_2^{(j)} \gamma_1^{(q)}) \delta_{0,jq}^k \lambda_{0,j}^{D,k} \sin \theta \cos \theta \right\} \right]^{1/2} \quad (16)$$

where $\eta_r^{(s)}$ is the corresponding peak factor and $\beta_r^{(s)}$ is the nonstationarity factor.

Continuing with the logic of relating the ordered peak response with the r.m.s. response via nonstationarity factor and peak factor, $\lambda_{0,j}^{D,k}$ may be expressed as $(SD_j^k / \eta_{j,(1)}^{D,k} \beta_j^{D,k})^2$, where SD_j^k is the largest peak amplitude of the relative displacement response of the SDOF oscillator with ω_j frequency and ζ_j damping ratio in response to the base acceleration, $\ddot{u}_{gk}^p(t)$, for the same level of confidence to which $\eta_r^{(s)}$ corresponds; $\eta_{j,(1)}^{D,k}$ is the corresponding peak factor; and $\beta_j^{D,k}$ is the nonstationarity factor associated with the response process. In the same way, $\lambda_{0,j}^{V,k}$ may be expressed as $(SV_j^k / \eta_{j,(1)}^{V,k} \beta_j^{V,k})^2$, where SV_j^k is the largest peak amplitude of the relative velocity response; $\eta_{j,(1)}^{V,k}$ is the corresponding peak factor; and $\beta_j^{V,k}$ is the nonstationarity factor. Equation (16) may thus be expressed as

$$r_{\text{peak}}^{(s)} = \left[\sum_{j=1}^n \sum_{q=1}^n r_j r_q \left\{ \sum_{k=1}^3 \gamma_k^{(j)} \gamma_k^{(q)} \delta_{0,jq}^k \left(\frac{SD_j^k}{\bar{\eta}_{j,(1)}^{D,k} \bar{\beta}_j^{D,k}} \right)^2 - \sum_{k=1}^2 \sum_{l=1}^2 (-1)^{k+l} \gamma_l^{(j)} \gamma_l^{(q)} \delta_{0,jq}^k \left(\frac{SD_j^k}{\bar{\eta}_{j,(1)}^{D,k} \bar{\beta}_j^{D,k}} \right)^2 \sin^2 \theta - \sum_{k=1}^2 (-1)^k (\gamma_1^{(j)} \gamma_2^{(q)} + \gamma_2^{(j)} \gamma_1^{(q)}) \delta_{0,jq}^k \left(\frac{SD_j^k}{\bar{\eta}_{j,(1)}^{D,k} \bar{\beta}_j^{D,k}} \right)^2 \sin \theta \cos \theta \right\} \right]^{1/2} \quad (17)$$

where, $\bar{\eta}_{j,(1)}^{D,k}$ is the peak factor $\eta_{j,(1)}^{D,k}$ normalized by $\eta_r^{(s)}$ and $\bar{\beta}_j^{D,k}$ is the nonstationarity factor $\beta_j^{D,k}$ normalized by $\beta_r^{(s)}$. Further, $\delta_{0,jq}^k$ may be expressed as

$$\delta_{0,jq}^k = C_{jq} + D_{jq} \left[1 - \left(\frac{\eta_{j,(1)}^{D,k}}{\eta_{j,(1)}^{V,k}} \right)^2 \left(\frac{\beta_j^{D,k}}{\beta_j^{V,k}} \right)^2 \left(\frac{SV_j^k}{PSV_j^k} \right)^2 \right] \quad (18)$$

where $PSV_j^k (= \omega_j SD_j^k)$ is the largest peak amplitude of the pseudo-velocity response.

In the next sub-section, suitable approximations will be made to develop a modal combination rule from Equation (17).

3. Approximations for the Proposed Rule

Equation (17) may be used to estimate the ordered response peak amplitudes for the same level of confidence for which SD_j^k and SV_j^k have been estimated. This may also be used to estimate the peak amplitudes consistent with the seismic hazard at a site, which is characterized by certain spectral displacement (SD) and spectral velocity (SV) curves for the three components of the ground motion. There is a need, however, to have reasonable estimates of normalized nonstationarity and peak factors (in Equation (17)) and nonstationarity and peak factors for the displacement and velocity responses (in Equation (18)).

It is proposed to carry out two types of simplifications: one relating to the factors in Equation (17) and another to the factors in Equation (18). The normalized nonstationarity and peak factors refer to how different these factors are in the largest modal response and in a higher-order system response. The normalized nonstationarity factors may be assumed equal to unity provided (i) the system response and the modal response for any order of peak are affected by comparable amounts due to nonstationarity, and (ii) a higher-order response is affected as much by the nonstationarity as the largest response in the modal and system responses. The former is strictly not true as the rate of convergence to the state of stationarity by a modal response depends on the number of cycles per unit time in response (or the modal frequency) whereas this rate in the system response is governed by the natural frequencies of the dominating modes. Due to this, the normalized nonstationarity factor is likely to be less than unity in the case of lower modes, and greater than unity for the higher modes. Similarly, normalized nonstationarity factors may be more in the case of higher-order peaks as nonstationarity affects a higher-order response more than a lower order response (Gupta and Trifunac, 1987a). For simplicity, however, $\bar{\beta}_j^{D,k}$ is uniformly assumed equal to unity. The normalized peak factor $\bar{\eta}_{j,(1)}^{D,k}$ also involves the effects of (i) the peak factors being different for the system response and the modal response (for the same order of peak), and (ii) the peak factors being different for different orders of peaks (for the system or modal response). The effect of the former is negligible due to little sensitivity of the peak factor to the governing statistical parameters (i.e., band-width and number of peaks) within the range anticipated for both system and modal responses. The effect of the order of peak can be approximated by a simple expression proposed by Gupta (1994), and therefore, the normalized peak factor is proposed to be

$$\begin{aligned} \bar{\eta}_{j,(1)}^{D,k} &\equiv \frac{\eta_{j,(1)}^{D,k}}{\eta_r^{(s)}} = 1 && ; \quad s = 1 \\ &= \frac{1}{0.4e^{-0.25s} + 0.67}; && s = 2, 3, \dots \end{aligned} \tag{19}$$

The nonstationarity factor for the modal displacement response in Equation (18) is likely to be greater than that for the modal velocity response due to domination by the longer periods. For simplicity, however, this discrepancy between the two factors is proposed to be neglected. The peak factors for the modal displacement and velocity responses are anyway expected to be very close as both refer to the largest peak.

In view of the above approximations, the proposed modal combination rule may be expressed as

$$\begin{aligned} r_{\text{peak}}^{(s)} &= \left[\sum_{j=1}^n \sum_{q=1}^n r_j r_q \left\{ \sum_{k=1}^3 \gamma_k^{(j)} \gamma_k^{(q)} \delta_{0,jq}^k \left(\frac{SD_j^k}{\bar{\eta}_{j,(1)}^{D,k}} \right)^2 - \sum_{k=1}^2 \sum_{l=1}^2 (-1)^{k+l} \gamma_l^{(j)} \gamma_l^{(q)} \delta_{0,jq}^k \left(\frac{SD_j^k}{\bar{\eta}_{j,(1)}^{D,k}} \right)^2 \sin^2 \theta \right. \right. \\ &\quad \left. \left. - \sum_{k=1}^2 (-1)^k (\gamma_1^{(j)} \gamma_2^{(q)} + \gamma_2^{(j)} \gamma_1^{(q)}) \delta_{0,jq}^k \left(\frac{SD_j^k}{\bar{\eta}_{j,(1)}^{D,k}} \right)^2 \sin \theta \cos \theta \right\} \right]^{1/2} \end{aligned} \tag{20}$$

with

$$\delta_{0,jq}^k = C_{jq} + D_{jq} \left[1 - \left(\frac{SV_j^k}{PSV_j^k} \right)^2 \right] \tag{21}$$

and $\bar{\eta}_{j,(1)}^{D,k}$ as in Equation (19). It may be mentioned that the proposed rule becomes same as the CQC3 rule (Menun and Der Kiureghian, 1998) for $\delta_{0,jq}^k = C_{jq}$ and for $s = 1$. The former condition is effectively obtained by assuming $\nu_{0,j}^k$ as zero, which, as discussed earlier, is strictly true only in the case of white-noise excitations. Further, $\delta_{0,jq}^k$, as in Equation (21), is similar to the cross-correlation term used in the formulation of Singh and Mehta (1983).

NUMERICAL ILLUSTRATION OF THE PROPOSED RULE

1. Example Building and Excitations

In order to illustrate the proposed rule, two horizontal components of six ground motion records as in Table 1 are considered. Vertical component is not considered, and thus $k = 2$ for each of these cases. Principal directions (major and intermediate) for each record are obtained through eigenvalue analysis of the 2×2 (temporal) covariance matrix of the common strong motion phase of the two horizontal components, as identified by the duration definition of Trifunac and Brady (1975). Orientation of the major principal direction with respect to the first component of each example motion in Table 1 (see the 4th column) is given in Table 2. For example, orientation of the major principal axis with respect to the S04E component in the case of the Borrego Mountain motion is 23.5° (clockwise). Using these values of orientation, principal components of the example motions ($\{\ddot{u}_g^p(t)\}$) are obtained as $[R]\{\ddot{u}_g(t)\}$, with θ in Equation (8) taken as the orientation of the major principal direction (from Table 2).

Table 1: Details of the Example Ground Motions

Record No.	Earthquake	Site	Components
1	Borrego Mountain Earthquake, 1968	Engineering Building, Santa Ana, Orange County, California	S04E S86W
2	Imperial Valley Earthquake, 1940	El Centro Site, Imperial Valley Irrigation District, California	S00E S90W
3	Kern County Earthquake, 1952	Taft Lincoln School Tunnel, California	N21E S69E
4	Michoacan Earthquake, 1985	Av. University Centre, Mexico City	N00E N90E
5	Parkfield Earthquake, 1966	Array No. 5, Cholame, Shandon, California	N05W N85E
6	San Fernando Earthquake, 1971	Utilities Building, 215 West Broadway, Long Beach, California	N90E N00E

Table 2: Details of the Principal Components of Example Ground Motions

Earthquake	Orientation of the Major Component (degree)	Characteristics	Major Component	Intermediate Component
Borrego Mountain Earthquake, 1968	-23.5	T_g (s)	5.6	1.9
		PGA (g)	0.014	0.011
Imperial Valley Earthquake, 1940	-21.6	T_g (s)	0.68	0.51
		PGA (g)	0.35	0.19
Kern County Earthquake, 1952	34.4	T_g (s)	0.65	0.42
		PGA (g)	0.21	0.15
Michoacan Earthquake, 1985	26.8	T_g (s)	2.10	2.07
		PGA (g)	0.19	0.08
Parkfield Earthquake, 1966	-18.4	T_g (s)	0.32	0.30
		PGA (g)	0.42	0.39
San Fernando Earthquake, 1971	-8.2	T_g (s)	5.82	4.91
		PGA (g)	0.03	0.02

The Fourier and pseudo spectral acceleration (PSA) spectra of the principal components of the six example motions are shown in Figures 2(a)–2(f) and Figures 3(a)–3(f). Figures 2(a)–2(f) show these spectra for the major principal component of the Borrego Mountain, Imperial Valley, Kern County, Michoacan, Parkfield, and San Fernando motions respectively, while Figures 3(a)–3(f) show these spectra for the intermediate principal component of these motions. In each figure, the two spectra are normalized to their respective maximum values. Table 2 gives the values of dominant period T_g (the period corresponding to the maximum of the Fourier spectrum) and peak ground acceleration (PGA) for both principal components of each of the six example motions. It may be observed that all the six motions cover a wide range of energy distributions, with dominant periods as 5.82 s at one end for the San Fernando motion and 0.3 s on the other for the Parkfield motion. In terms of the band of significant energy, the Michoacan motion is at one extreme with significant energy over a narrow band of 1.8–3 s, while the Kern County motion is at the other with significant energy over a wide band of 0.2–6 s.

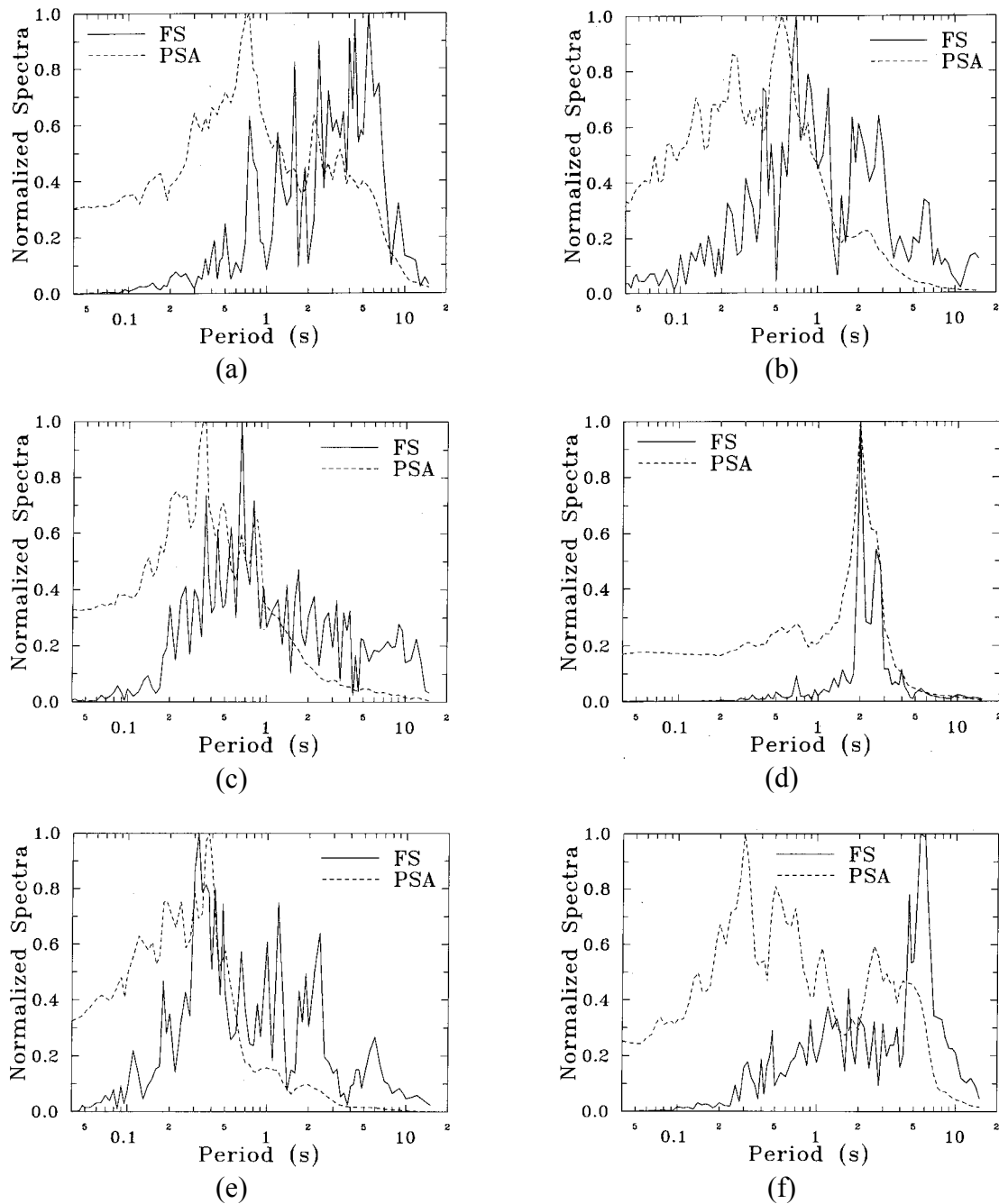


Fig. 2 Normalized Fourier amplitude and PSA spectra for the major principal component of (a) Borrego Mountain, (b) Imperial Valley, (c) Kern County, (d) Michoacan, (e) Parkfield, and (f) San Fernando earthquake motions

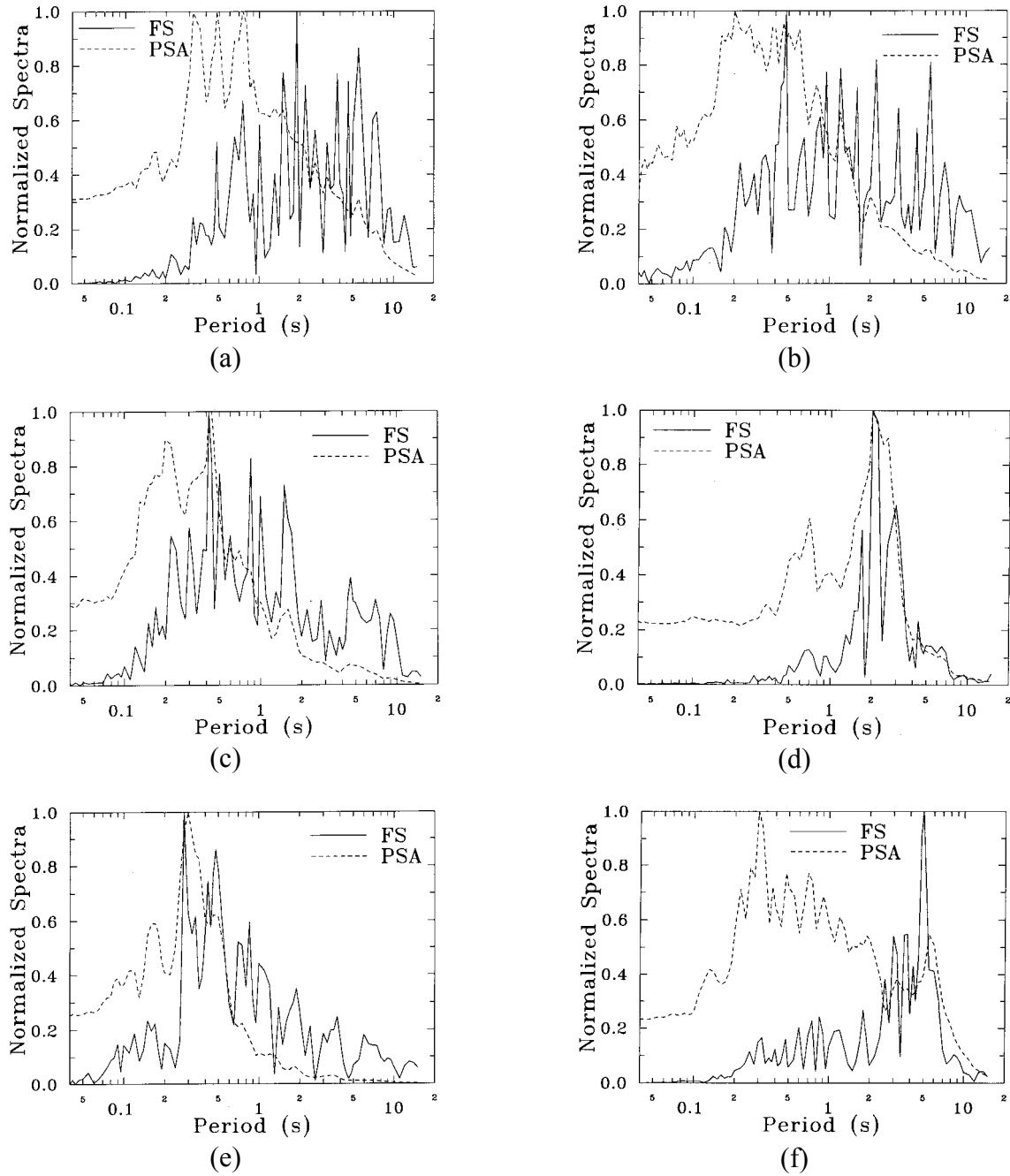


Fig. 3 Normalized Fourier amplitude and PSA spectra for the intermediate principal component of (a) Borrego Mountain, (b) Imperial Valley, (c) Kern County, (d) Michoacan, (e) Parkfield, and (f) San Fernando earthquake motions

A 5-story symmetric building having rigid floor masses supported by massless, inextensible columns is considered for the numerical study. Two translational DOFs are considered at each floor, and therefore, the example building is a 10-DOF system ($n = 10$). Seven different cases of this building involving different proportions in floor masses and story stiffnesses are considered. Table 3 shows the values of the reference floor masses and story stiffnesses (in the X_s - and Y_s -directions), and Table 4 shows seven different sets of factors α and β that are multiplied with the reference masses and stiffnesses, respectively, for the seven example cases of the building. Table 4 also shows the corresponding fundamental periods of the building in the X_s - and Y_s -directions. It may be observed that a wide range of fundamental periods of the multistoried buildings is covered by these example cases (0.03–2.0 s in the X_s -direction). The example building is assumed to be classically damped with modal damping ratio as 0.05. It may be noted that the pairs of the closely spaced modes in the example building are uncoupled,

and therefore, the illustration would not include the contribution of modal cross-correlation due to the closeness of frequencies for a single-component excitation. This is not a serious limitation though, because the proposed rule accounts for this contribution on well-established lines and thus the focus here is indeed not on examining the proposed rule against this contribution.

Table 3: Details of the Reference Floor Masses and Story Stiffnesses

Floor Level from Top	Floor Mass (t)	Story Stiffness in the X_s -Direction (kN/m)	Story Stiffness in the Y_s -Direction (kN/m)
1	800	2212000	1392000
2	800	2696000	2179000
3	800	3100000	2697000
4	800	3424000	3112000
5	1150	4998000	4792000

Table 4: Properties of the Example Building for Different Cases of Mass and Stiffness Properties

Case	α	β	Fundamental Period in the X_s -Direction (s)	Fundamental Period in the Y_s -Direction (s)
I	0.125	16	0.031	0.029
II	0.25	8	0.063	0.058
III	0.5	4	0.125	0.117
IV	1	2	0.254	0.234
V	2	1	0.53	0.467
VI	4	0.5	1.1	0.938
VII	8	0.25	2	1.87

2. Results and Discussion

To illustrate and evaluate the performance of the proposed modal combination rule, the example building is subjected, in all seven cases (of mass and stiffness properties), to each of the six pairs of horizontal principal excitations at its base, and the estimates of the largest base shear in the X_s -direction are obtained from (i) the (exact) time-history analysis, (ii) the proposed rule, and (iii) the CQC3 rule (Menun and Der Kiureghian, 1998). Since the orientation θ of the principal axis X_p of the ground motion (with respect to the structure axis X_s) is an input parameter, the estimates of the largest base shear are obtained for the entire range of θ from 0° to 180° .

Figures 4(a)–4(f) show the comparisons of the largest peaks of base shears in the X_s -direction for the exact, proposed, and CQC3 analyses in the cases of Borrego Mountain, Imperial Valley, Kern County, Michoacan, Parkfield, and San Fernando motions, respectively. Each figure shows the comparisons for the entire range of θ values. For these results, the example building is assumed to have mass and stiffness properties for Case IV, with fundamental periods equal to 0.254 and 0.234 s in the X_s - and Y_s -directions, respectively. All six figures show that the largest base shear in the X_s -direction is symmetric about $\theta = 90^\circ$ in the cases of proposed and CQC3 rules. This is due to the fact that the example building is symmetric and therefore there is no coupling between the modes of the building in the X_s - and Y_s -directions. The curves for the time-history results are however asymmetric, since $\ddot{u}_{g1}^p(t)$ and $\ddot{u}_{g2}^p(t)$ are not exactly uncorrelated (because the orientation of the principal directions has been determined based on

the strong motion segment of the ground acceleration). Due to this, accelerations along the X_s - and Y_s - directions in the case of $\theta = \alpha$ become different from those in the case of $\theta = 180^\circ - \alpha$, in terms of both frequency content and cross-correlation. In the case of this “residual cross-correlation” between the two principal components becoming zero, the two acceleration components (in the X_s - and Y_s -directions) for $\theta = \alpha$ would be different from those for $\theta = 180^\circ - \alpha$ only in the sense of the sign of the cross-PSDF between them, and this will not make any difference in the base-shear results due to symmetry of the structure. It may be observed from Figures 4(a)–4(f) that the estimates of base-shear from both rules (i.e., proposed and CQC3) are in reasonably good agreement with those from the time-history analysis results at all values of θ , except in the case of the Kern County motion. For this motion, both rules lead to large errors at around $\theta = 60^\circ$. This is possibly due to significant “residual correlation” between the two principal components.

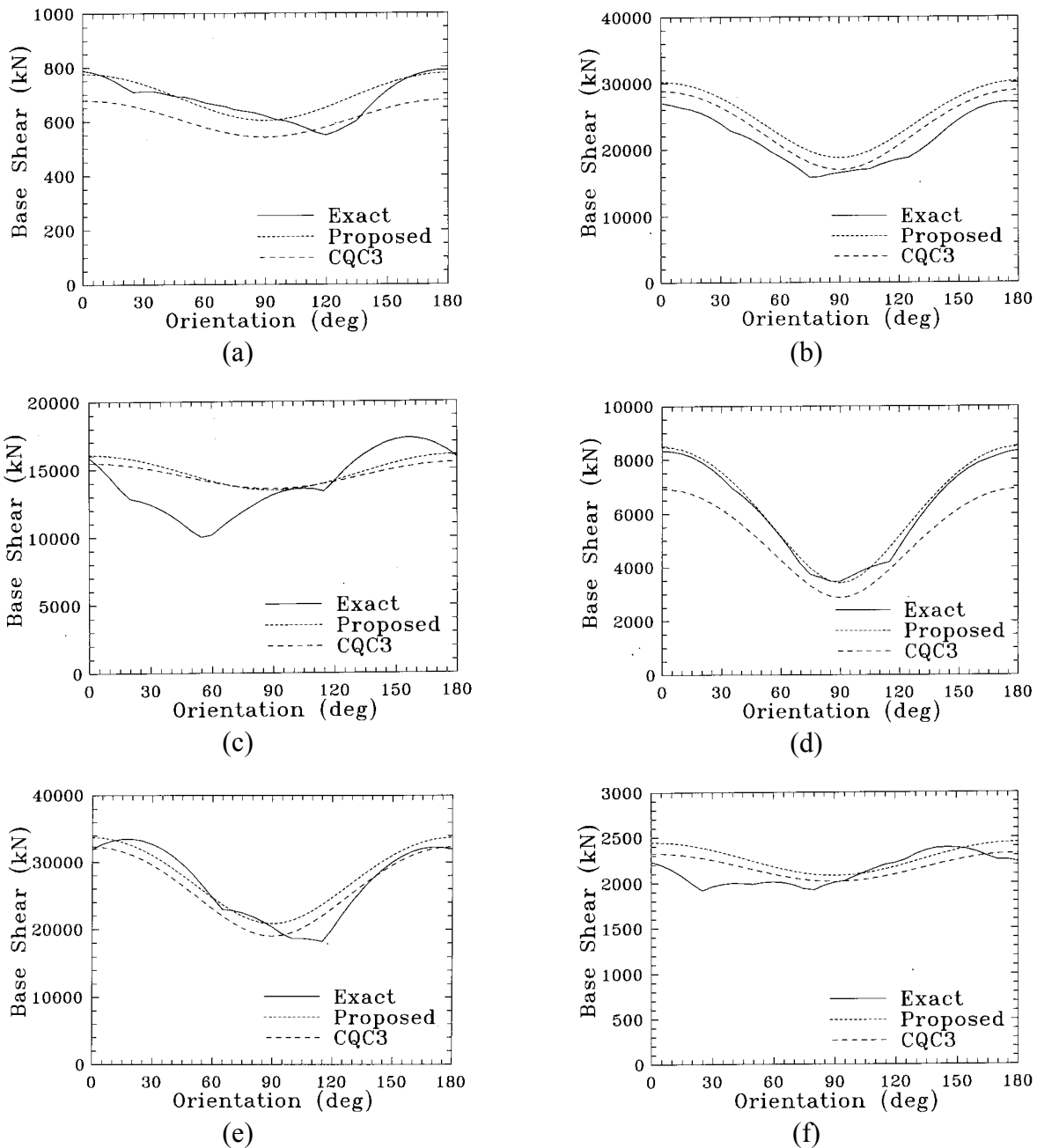


Fig. 4 Variation of largest base shear in the X_s -direction with orientation θ for (exact) time-history analysis, proposed rule, and CQC3 rule in the case of (a) Borrego Mountain, (b) Imperial Valley, (c) Kern County, (d) Michoacan, (e) Parkfield, and (f) San Fernando earthquake motions

For a more direct comparison of the performances of the proposed and CQC3 rules in the case of the base shear in the X_s -direction, absolute error is averaged over the entire range of θ between 0° – 180° and plotted with respect to $T_{g,\text{mean}}/T_{n,\text{mean}}$ for each of the six ground motions. Here, $T_{g,\text{mean}}$ is the average of the dominant periods of the major and intermediate principal components of the ground motion, and $T_{n,\text{mean}}$ is the average of the periods of the example building in the X_s - and Y_s -directions. Since there is not much difference in the periods in the X_s - and Y_s -directions, it is assumed that $T_{g,\text{mean}}/T_{n,\text{mean}}$ would be a good estimate for the mean of the ratios of dominant period to natural period in the two principal directions and thus this parameter would properly describe the extent to which the building is stiff to the ground motion. Higher the ratio, stiffer would be the building relative to the ground motion. Figures 5(a)–5(f) show the plots of absolute error with $T_{g,\text{mean}}/T_{n,\text{mean}}$ for the proposed and CQC3 rules in the cases of the Borrego Mountain, Imperial Valley, Kern County, Michoacan, Parkfield, and San Fernando motions, respectively. It may be observed that the performance of the proposed rule is quite good with the average error remaining within 16% in all the cases considered here. CQC3 rule is associated with greater errors in most of the cases, even though these errors do not exceed 22%. The performance of the proposed rule is significantly better than that of the CQC3 rule, particularly when the building is stiffer relative to the ground motion ($T_{g,\text{mean}}/T_{n,\text{mean}} \gg 1$). In the case of a narrow-band motion like Michoacan motion, this happens for $T_{g,\text{mean}}/T_{n,\text{mean}} > 1$. On the other hand, for a broad-band motion like Kern County motion, there is no clear value of $T_{g,\text{mean}}/T_{n,\text{mean}}$ (in the range of building periods considered) above which the proposed rule performs significantly better than the CQC3 rule. It may also be observed that when the building periods fall within the band-width of the ground motion and $\delta_{0,jq}^k = C_{jq}$, both rules lead to similar errors which are due to the approximations made for the nonstationarity factors.

The performance of the proposed rule is evaluated next in the estimation of the second largest, third largest, ... response peaks. Figure 6 shows the higher-order peak base shear along the X_s -direction, after normalization with respect to the largest value, in the case of the Borrego Mountain motion, with the example building assumed to have mass and stiffness properties for Case VI (with natural period equal to 1.1 s in the X_s -direction) and for $\theta = 75^\circ$. First 20 peaks are considered for this plot and results obtained from the proposed rule are compared with those from the time-history analysis. These results indicate that the ratio of the largest peak to a higher-order peak, as in Equation (19), works well in the example considered. Similar trends have been observed with the other ground motions as well. For a more comprehensive evaluation, absolute error values of the estimated first 20 peaks (from the proposed rule with respect to the time-history results) are averaged over θ (varying between 0° and 180°), and those are compared for the example ground motions in Figure 7 (with mass and stiffness properties remaining same as for Case VI). It is clear from this figure that for the first 10 peaks, the proposed formulation leads to very good estimates, with the absolute average error remaining close to 10%. The error increases for the next 10 peaks due to the effects of nonstationarity being dependent on the order of peak, as discussed earlier. Even for these peaks, the absolute average error remains within 30%, except in the case of Imperial Valley and Parkfield motions. It may be noted that the example building considered for these results is stiff with respect to the Borrego Mountain, Michoacan, and San Fernando motions, and is flexible with respect to the Imperial Valley, Kern County, and Parkfield motions. Thus, the results presented in Figure 7 cover a wide range of relative flexibility of building systems with respect to the ground motions.

It will be useful to also judge the performance of the proposed rule on the basis of algebraic percentage error and to consider this over all 20 peaks in an average sense. With this purpose, the averaging is done now over both θ (varying between 0° and 180°) and the order of peak (for the first 20 peaks), and the average error values are given in Table 5 for all 42 combinations of building periods and example motions. Negative values in this table indicate that the estimates from the proposed rule on average are greater than the time-history results. There is no specific trend available from these results. However, the proposed formulation seems to overestimate the first 20 response peaks much more often than underestimating, and the extent of error typically ranges from 10% to 20%. There are cases like Parkfield motion in which same nonstationarity factor cannot be assumed irrespective of the order of

peak, and therefore there is a need for further improvement in this direction. Nevertheless, it is clear that besides being more accurate than the CQC3 rule (for the largest response peak) in specific situations, the proposed rule provides reasonably accurate estimates for the higher-order response peaks in a simple manner.

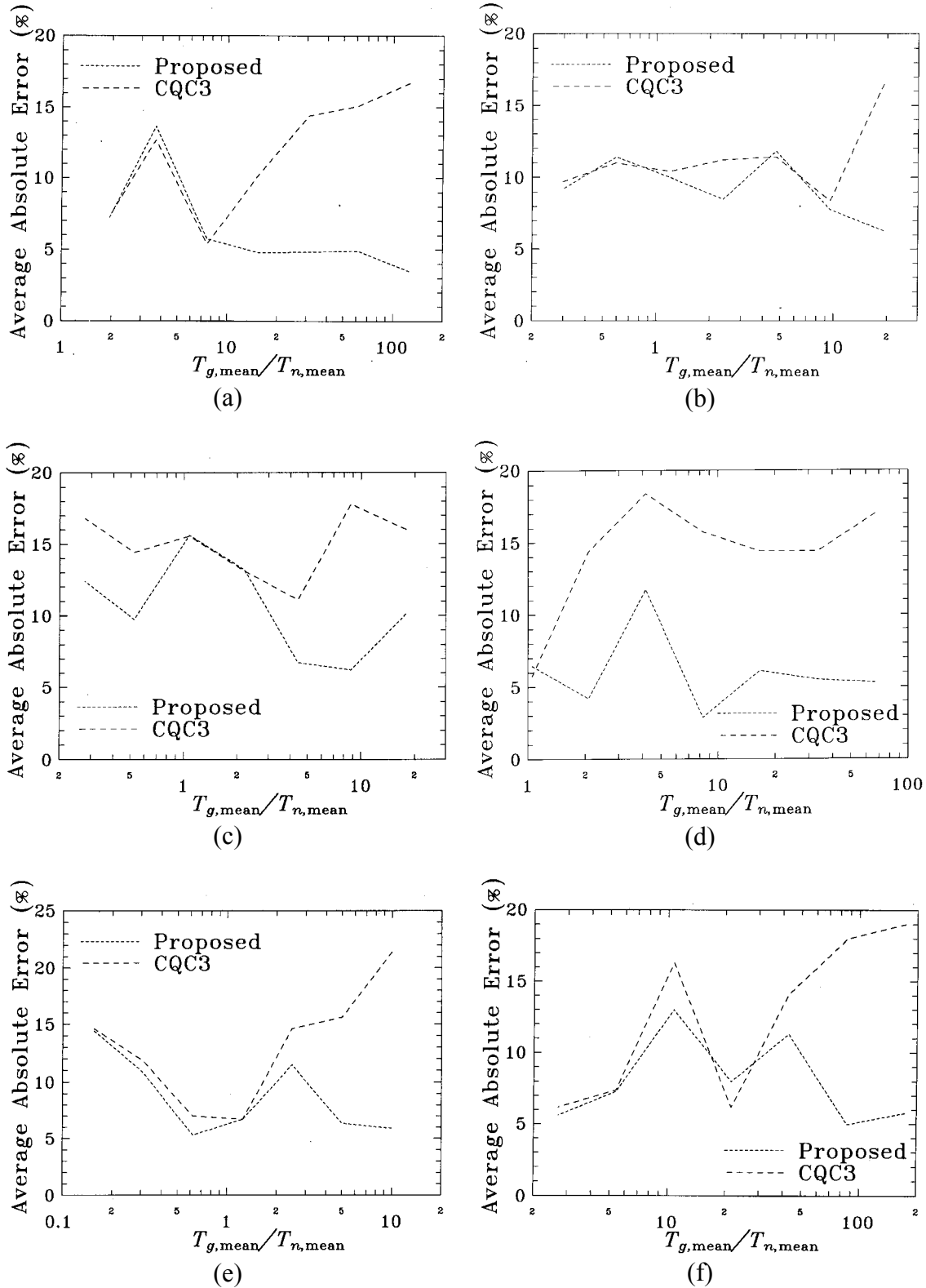


Fig. 5 Variation of absolute error averaged over θ with $T_{g,mean}/T_{n,mean}$ for the proposed and CQC3 rules in the case of (a) Borrego Mountain, (b) Imperial Valley, (c) Kern County, (d) Michoacan, (e) Parkfield, and (f) San Fernando earthquake motions

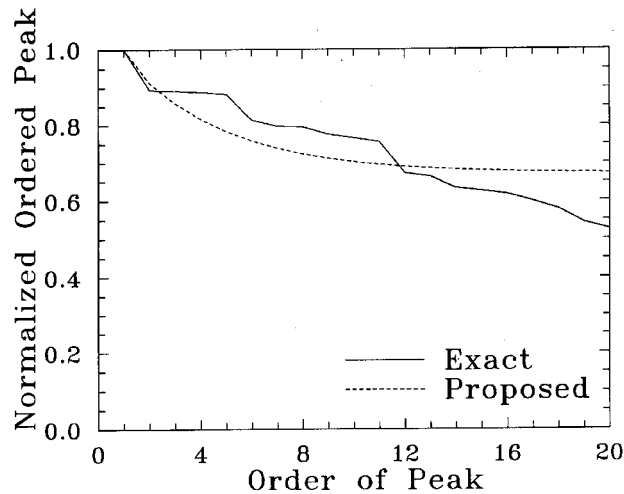


Fig. 6 Comparison of normalized ordered peak base shear in Case VI for $\theta = 75^\circ$ as obtained from the exact (time-history) analysis and the proposed rule in the case of Borrego Mountain motion

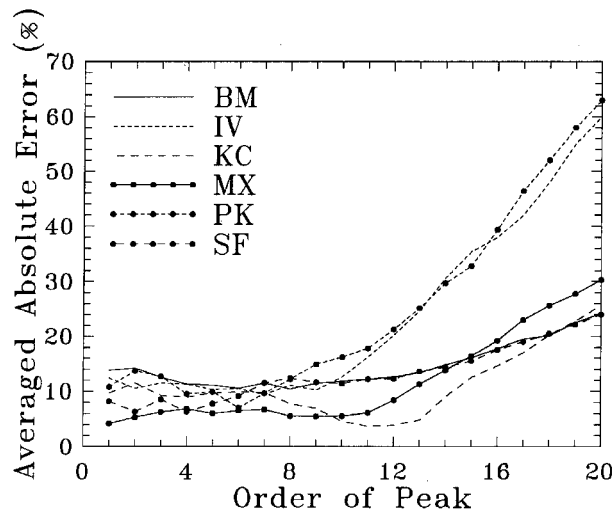


Fig. 7 Variation of the averaged (over θ) absolute error in the ordered peak amplitude with the order of peak for the Borrego Mountain (BM), Imperial Valley (IV), Kern County (KC), Michoacan (MX), Parkfield (PK), and San Fernando (SF) motions

Table 5: Percentage Error with the Proposed Rule as Averaged over Orientation and Order of Peak for Different Cases of Mass and Stiffness Properties and Ground Motions

Example Motion	Case I	Case II	Case III	Case IV	Case V	Case VI	Case VII
Borrego Mountain	-11.6	-8.84	-3.36	-2.58	-14.7	-11.5	1.58
Imperial Valley	-6.7	-7.23	-18.4	-21.9	-13.1	-18.3	-11.6
Kern County	-17.1	-20	-6.1	-9.3	-19.2	-2.83	12.6
Michoacan	21	12.54	8.8	5.1	-24	-9.41	-14.5
Parkfield	-38.8	-36.5	-24.1	-27.6	-25.4	-19.8	-15.6
San Fernando	-1.42	0.26	-7.74	-3.53	-10.9	-10.6	-3.7

The proposed rule requires SV ordinates of the principal components of the input ground motion for the estimation of $\delta_{0,iq}^k$ (see Equation (18)). This may limit the usefulness of the proposed rule because the

characterization of seismic hazard at the site under consideration is not always available in terms of the SV curves. For such situations, we propose to approximate SV ordinates in terms of the pseudo-spectral acceleration (PSA) curves and mean period T_c of the ground motion as (Gupta, 2008)

$$SV_j^k = \begin{cases} \frac{1}{\omega_j} \sqrt{(\text{PSA}_j^k)^2 - (\text{PGA}^k)^2}; & \omega_j > \frac{2\pi}{T_c^k} \\ \frac{1}{\omega_j} \text{PSA}_j^k & ; \omega_j \leq \frac{2\pi}{T_c^k} \end{cases} \quad (22)$$

where $\text{PSA}_j^k (= \omega_j^2 \text{SD}_j^k)$ is the largest peak amplitude of the pseudo-acceleration response (of the SDOF oscillator with ω_j frequency and ζ_j damping ratio), PGA^k is the peak ground acceleration, and T_c^k is the period corresponding to the center of gravity of the undamped PSV curve, for the k th principal component of ground acceleration. It may be observed that for SV_j^k equal to PSA_j^k/ω_j for all natural frequencies of the system, the proposed rule in the case of the largest response peak will become same as the CQC3 rule. It has been observed that by approximating SV ordinates as in Equation (22), the numerical results undergo only minor variations and therefore same observations can be made as before (for example, see Table 6 for the recomputed results of Table 5 on using the SV approximation of Equation (22)).

Table 6: Percentage Error with the Proposed Rule, as Averaged over Orientation and Order of Peak for Different Cases of Mass and Stiffness Properties and Ground Motions, on Using the SV Approximation

Example Motion	Case I	Case II	Case III	Case IV	Case V	Case VI	Case VII
Borrego Mountain	-11.2	-7.5	-2.4	-1.98	-12.1	0.12	3.11
Imperial Valley	-8.2	-7.1	-16.6	-19.1	-17.3	1.3	-13.3
Kern County	-28.1	-21.2	-8.4	-12.7	-33.8	-3.06	-7.0
Michoacan	16.2	12.4	9.63	4.9	-19.2	1.04	-9.4
Parkfield	-32.3	-41.5	-30.3	-29.2	-36.2	-10.2	-39.6
San Fernando	-7.6	0.07	7.3	-3.54	-9.45	-0.04	-31.2

CONCLUSIONS

A new modal combination rule has been formulated for the ordered peak response of a MDOF system subjected to multi-component ground motion. Both, the excitation and the response, have been assumed to be stationary, and the effect of nonstationarity has been included with the help of the response spectrum characterization of the ground motion. Following assumptions have been made in order to arrive at a simple form of the rule. First, the peak factors have been assumed to be same for (i) the largest modal displacement and largest modal velocity responses, and (ii) the system response and modal displacement, for any order of peak. Secondly, the effects of nonstationarity have been assumed to be same for (i) the largest modal displacement and largest modal velocity responses, and (ii) the largest modal displacement and the system response, for any order of peak. It has been also assumed that the ratio of the peak factor for a higher-order peak to that for the largest peak in the modal displacement response is dependent only on the order of the peak, irrespective of the mode. The proposed rule requires (as input) characterization of the seismic hazard in form of the SD and SV spectra for the principal components, and the orientation of the major principal axis of the ground motion with respect to the building. No assumptions have been made regarding the cross-correlation between different modes and regarding the nature of the input excitation.

The proposed combination rule has been illustrated with the help of a 5-story building having seven different sets of floor mass and story stiffness properties and by using six recorded ground motions with

significantly different frequency characteristics. Results show in the case of the largest base shear response that the estimates by the proposed rule follow the (exact) time-history estimates reasonably well for the entire range of the orientation of the major principal axis, and that those are more accurate compared to the estimates from the CQC3 method, particularly when the building is much stiffer to the ground motion. The maximum absolute error averaged over different orientations is about 16% in the case of the proposed rule. Unlike the CQC3 rule, the proposed rule also estimates the higher-order peak amplitudes and in a very simple way. The estimates from the proposed rule for the largest 20 peaks are found to be often larger than the time-history estimates, with the extent of error typically ranging between 10–20%. For the largest 10 peaks, however, the average absolute error remains close to 10%. Considering that only first few orders of peaks are important for the nonlinear response, larger errors for the lower orders of peaks is not a serious limitation. The proposed rule requires additional input data in form of the SV spectra of the principal components, but this requirement can be easily addressed by using the PSA (or PSV) spectra of these components.

REFERENCES

1. Amini, A. and Trifunac, M.D. (1985). “Statistical Extension of Response Spectrum Superposition”, *International Journal of Soil Dynamics and Earthquake Engineering*, Vol. 4, No. 2, pp. 54–63.
2. Anagnostopoulos, S.A. (1981). “Response Spectrum Technique for Three-Component Earthquake Design”, *Earthquake Engineering & Structural Dynamics*, Vol. 9, No. 5, pp. 459–476.
3. ATC (1978). “Tentative Provisions for the Development of Seismic Regulations for Buildings”, Report ATC-3-06, Applied Technology Council, Redwood City, U.S.A.
4. Christian, J.T. (1989). “Generating Seismic Design Power Spectral Density Functions”, *Earthquake Spectra*, Vol. 5, No. 2, pp. 351–368.
5. Chu, S.L., Amin, M. and Singh, S. (1972). “Spectral Treatment of Actions of Three Earthquake Components on Structures”, *Nuclear Engineering and Design*, Vol. 21, No. 1, pp. 126–136.
6. Der Kiureghian, A. (1981). “A Response Spectrum Method for Random Vibration Analysis of MDOF Systems”, *Earthquake Engineering & Structural Dynamics*, Vol. 9, No. 5, pp. 419–435.
7. Der Kiureghian, A. and Nakamura, Y. (1993). “CQC Modal Combination Rule for High-Frequency Modes”, *Earthquake Engineering & Structural Dynamics*, Vol. 22, No. 11, pp. 943–956.
8. Goodman, L.E., Rosenblueth, E. and Newmark, N.M. (1953). “Aseismic Design of Firmly Founded Elastic Structures”, *ASCE Transactions*, Vol. 120, pp. 782–802.
9. Gupta, V.K. (1994). “Higher Order Peaks in the Seismic Response of Multistoried Buildings”, Report 94-03, Department of Civil Engineering, Indian Institute of Technology Kanpur, Kanpur.
10. Gupta, V.K. (2002). “Developments in Response Spectrum-Based Stochastic Response of Structural Systems”, *ISET Journal of Earthquake Technology*, Vol. 39, No. 4, pp. 347–365.
11. Gupta, V.K. (2008). “Short Communication: A New Approximation for Spectral Velocity Ordinates at Short Periods”, *Earthquake Engineering & Structural Dynamics* (in press, DOI: 10.1002/eqe.877).
12. Gupta, I.D. and Trifunac, M.D. (1987a). “Order Statistics of Peaks in Earthquake Response of Multi-Degree-of-Freedom Systems”, *Earthquake Engineering and Engineering Vibration*, Vol. 7, No. 4, pp. 15–50.
13. Gupta, I.D. and Trifunac, M.D. (1987b). “Order Statistics of Peaks of the Response to Multi-Component Seismic Excitation”, *Bulletin of Indian Society of Earthquake Technology*, Vol. 24, No. 3-4, pp. 135–159.
14. Gupta, V.K. and Trifunac, M.D. (1989). “Investigation of Building Response to Translational and Rotational Earthquake Excitations”, Report CE 89-02, University of Southern California, Los Angeles, U.S.A.
15. Gupta, V.K. and Trifunac, M.D. (1990). “Response of Multistoried Buildings to Ground Translation and Rocking during Earthquakes”, *Probabilistic Engineering Mechanics*, Vol. 5, No. 3, pp. 138–145.
16. Hernandez, J.J. and Lopez, O.A. (2002). “Response to Three-Component Seismic Motion of Arbitrary Direction”, *Earthquake Engineering & Structural Dynamics*, Vol. 31, No. 1, pp. 55–77.

17. Kaul, M.K. (1978). "Stochastic Characterization of Earthquake through Their Response Spectrum", *Earthquake Engineering & Structural Dynamics*, Vol. 6, No. 5, pp. 497–509.
18. Menun, C. and Der Kiureghian, A. (1998). "A Replacement for the 30%, 40% and SRSS Rules for Multicomponent Seismic Analysis", *Earthquake Spectra*, Vol. 14, No. 1, pp. 153–163.
19. Newmark, N.M. (1975). "Seismic Design Criteria for Structures and Facilities—Trans-Alaska Pipeline System", *Proceedings of the U.S. National Conference on Earthquake Engineering*, Ann Arbor, U.S.A., pp. 94–103.
20. O'Hara, G.J and Cunnif, P.F. (1963). "Elements of Normal Mode Theory", Report 6002, Naval Research Laboratory, Washington, DC, U.S.A.
21. Penzien, J. and Watabe, M. (1975). "Characteristics of 3-Dimensional Earthquake Ground Motions", *Earthquake Engineering & Structural Dynamics*, Vol. 3, No. 4, pp. 365–373.
22. Rosenblueth, E. and Contreras, H. (1977). "Approximate Design for Multicomponent Earthquakes", *Journal of the Engineering Mechanics Division, Proceedings of ASCE*, Vol. 103, No. EM5, pp. 881–893.
23. Rosenblueth, E. and Elorduy, J. (1969). "Response of Linear Systems to Certain Transient Disturbances", *Proceedings of the Fourth World Conference on Earthquake Engineering*, Santiago, Chile, Vol. 1, Part A-1, pp. 185–196.
24. Sadhu, A. (2007). "Ordered Peak Response under Multi-Component Ground Motion via Modal Combination Rule and Its Correlation with Nonlinear Response", M.Tech. Thesis, Department of Civil Engineering, Indian Institute of Technology Kanpur, Kanpur.
25. Singh, M.P. and Mehta, K.B. (1983). "Seismic Design Response by an Alternative SRSS Rule", *Earthquake Engineering & Structural Dynamics*, Vol. 11, No. 6, pp. 771–783.
26. Smeby, W. and Der Kiureghian, A. (1985). "Modal Combination Rules for Multicomponent Earthquake Excitation", *Earthquake Engineering & Structural Dynamics*, Vol. 13, No. 1, pp. 1–12.
27. Trifunac, M.D. and Brady, A.G. (1975). "A Study on the Duration of Strong Earthquake Ground Motion", *Bulletin of the Seismological Society of America*, Vol. 65, No. 3, pp. 581–626.
28. Unruh, J.F. and Kana, D.D. (1981). "An Iterative Procedure for the Generation of Consistent Power/Response Spectrum", *Nuclear Engineering and Design*, Vol. 66, No. 3, pp. 427–435.
29. USNRC (1976). "Combining Modal Responses and Spatial Components in Seismic Response Analysis", *Regulatory Guide 1.92, Revision 1*, U.S. Nuclear Regulatory Commission, Washington, DC, U.S.A.
30. Wilson, E.L., Der Kiureghian, A. and Bayo, E.P. (1981). "A Replacement for the SRSS Method in Seismic Analysis", *Earthquake Engineering & Structural Dynamics*, Vol. 9, No. 2, pp. 187–194.

MODE-BASED PROCEDURE TO INTERPOLATE STRONG MOTION RECORDS OF INSTRUMENTED BUILDINGS

Rakesh K. Goel

Department of Civil & Environmental Engineering
California Polytechnic State University
San Luis Obispo, CA 93407-0353, U.S.A.

ABSTRACT

This paper examines the accuracy of a commonly used piece-wise cubic polynomial interpolation (PWCPI) procedure to estimate the motions of non-instrumented floors in buildings with significant stiffness discontinuities. It is shown that results from the PWCPI procedure may depend on the locations of instrumented floors. While the PWCPI procedure may provide good estimates of floor displacements, this procedure may not accurately predict story drifts and floor accelerations. Therefore, a mode-based interpolation (MBI) procedure is presented as an enhancement to the PWCPI procedure. The MBI procedure is shown to provide accurate estimates of the floor displacements, story drifts, and floor accelerations. Furthermore, results from the MBI procedure are shown to be much less dependent on the locations of instrumented floors. The mode shapes needed in the MBI procedure may be computed from the eigenanalysis of the building, estimated from the system identification of recorded motions, or computed from the approximate formulas for mode shapes.

KEYWORDS: Acceleration, Buildings, Earthquake Response Interpolation, Modal Analysis, Structural Dynamics

INTRODUCTION

Recorded motions of buildings during strong shaking provide a unique opportunity to evaluate the current analytical procedures—nonlinear static analysis and nonlinear response history analysis—and to develop improved procedures. Needed for this purpose are the height-wise variations of displacement demands—floor displacements and story drifts—as well as the variations of acceleration demands during the ground shaking. Since buildings are typically instrumented at a limited number of floors, motions of the remaining (or non-instrumented) floors are estimated by an interpolation procedure. Typically, a piece-wise cubic polynomial interpolation (PWCPI) procedure is used for the conventional buildings (Naeim, 1997; De la Llera and Chopra, 1997; Goel, 2005, 2007; Limongelli, 2003, 2005), and a combination of cubic-linear interpolation is recommended for the base-isolated buildings (Naeim et al., 2004). It is generally believed that the PWCPI procedure provides reasonable estimates of motions at non-instrumented floors (Naeim, 1997; Naeim et al., 2004; De la Llera and Chopra, 1997). However, previous investigations on the accuracy of the PWCPI procedure have been limited to the estimation of floor displacements and floor accelerations in buildings without significant stiffness discontinuities. Many real buildings contain significant stiffness discontinuities over the building height, such as stiff shear walls in the basement and flexible moment-resisting frames in the upper stories, or soft-story condition. The accuracy of the PWCPI procedure has not been verified for such buildings.

The objective of this investigation is to re-examine the accuracy of the PWCPI procedure in providing accurate estimates of the floor displacements, story drifts, and floor accelerations for buildings with significant stiffness discontinuities. Since the PWCPI procedure is found not to be always accurate, a mode-based interpolation (MBI) procedure is presented as an enhancement to the PWCPI procedure. It is demonstrated that the MBI procedure provides very good estimates of the motions at non-instrumented floors and is much less sensitive, compared to the PWCPI procedure, to the locations of instrumented floors.

THEORETICAL BACKGROUND

Let an N -story building be instrumented at J locations with sensors at the base and roof levels. Also, let r_j be the response—displacement or acceleration—recorded by the j th sensor located at height h_j from the building base, and let r be the desired response at height h (or at a non-instrumented location) of the building. The response r is to be computed by interpolation of the recorded responses r_j . Following is the theoretical background of the commonly used PWCPI procedure and the proposed MBI procedure.

1. Piece-Wise Cubic Polynomial Interpolation (PWCPI) Procedure

For a building with sensors at J locations and sub-divided into $J - 1$ sub-intervals, the response r at height h , within the j th sub-interval, is given by

$$r(h) = a_j (h - h_j)^3 + b_j (h - h_j)^2 + c_j (h - h_j) + d_j \quad (1)$$

in which a_j , b_j , c_j , and d_j are the constants for the cubic-polynomial to be fitted in the j th sub-interval. Since Equation (1) for each sub-interval involves four constants, $4(J - 1)$ constants are needed to completely define the response of this building, which in turn implies that $4(J - 1)$ equations are required to uniquely solve for these constants. For this purpose, $2(J - 1)$ equations are obtained by matching the response from Equation (1) to the recorded response at the $2(J - 1)$ locations. The remaining $2(J - 1)$ equations may be obtained by forcing continuity conditions at the junctions of two adjacent sub-intervals and by utilizing the boundary conditions (or the known values of derivatives of the response) at the base and top of the building. Since the derivatives of the response at the bottom and top of the building are usually not available, one of the most commonly used boundary condition is the “not-a-knot” condition. With this boundary condition, the remaining $2(J - 1)$ equations are obtained as follows: (a) $2(J - 2)$ equations by forcing the first and second derivatives of the response to be equal at the $(J - 2)$ junctions of the $(J - 1)$ sub-intervals; (b) one equation by forcing the third derivative of the response to be equal at the top of the first sub-interval and bottom of the second-sub-interval; and (c) one equation by forcing the third derivative of the response to be equal at the top of the last-but-one sub-interval and bottom of the last sub-interval. The computation of the needed constants then requires solution of a tri-diagonal system of linear equations (see Appendix I).

A summary of the PWCPI procedure, adopted from Beatson (1986), is presented in Appendix I for estimating the motions at non-instrumented floors. This procedure may be used to interpolate the floor displacements (e.g., Naeim, 1997; De la Llera and Chopra, 1997) or floor accelerations (Limongelli, 2003). A convenient implementation of the PWCPI procedure is possible in MATLAB (MathWorks, 2006) with the use of “spline” function.

2. Mode-Based Interpolation (MBI) Procedure

For a linearly elastic building, idealized as an N degree-of-freedom system, the floor displacements and accelerations can be calculated by the superposition of modal displacements and accelerations (Chopra, 2007) as

$$\{u(t)\} = \sum_{i=1}^N \Gamma_i \{\phi_i\} D_i(t) \quad \text{and} \quad \{\ddot{u}(t)\} = \sum_{i=1}^N \Gamma_i \{\phi_i\} \ddot{D}_i(t) \quad (2)$$

in which $\{u(t)\}$ and $\{\ddot{u}(t)\}$ are the vectors containing the time-variations of relative floor displacements and accelerations, respectively; $\{\phi_i\}$ is the i th mode-shape vector; $\Gamma_i = \{\phi_i\}^T [m] \{1\} / \{\phi_i\}^T [m] \{\phi_i\}$ is the i th modal participation factor with $[m]$ being the mass matrix and $\{1\}$ being the influence vector

describing the influence of support displacements on structural displacements; and $D_i(t)$ and $\ddot{D}_i(t)$ are the time-variations of displacement and acceleration of the i th-mode single-degree-of-freedom system, as computed from

$$\ddot{D}_i(t) + 2\zeta_i\omega_i\dot{D}_i(t) + \omega_i^2D_i(t) = -\ddot{u}_g(t) \tag{3}$$

with ω_i and ζ_i being the i th-mode frequency and damping ratio, and $\ddot{u}_g(t)$ being the time-variation of ground acceleration. Denoting $q_i(t) = \Gamma_i D_i(t)$ as the modal displacement and $\ddot{q}_i(t) = \Gamma_i \ddot{D}_i(t)$ as the modal acceleration, Equation (2) leads to

$$\{u(t)\} = \sum_{i=1}^N q_i(t)\{\phi_i\} \quad \text{and} \quad \{\ddot{u}(t)\} = \sum_{i=1}^N \ddot{q}_i(t)\{\phi_i\} \tag{4}$$

Let us now consider a building in which recorded motions are available at K floors, in addition to the base. Let the locations of floors with recorded motions be designated as k_1, k_2, \dots, k_K . Considering the first K modes in the modal superposition, the motions at the instrumented floors may be described as

$$\{\bar{u}(t)\} = [\Psi]\{\bar{q}(t)\} \quad \text{and} \quad \{\ddot{\bar{u}}(t)\} = [\Psi]\{\ddot{\bar{q}}(t)\} \tag{5}$$

in which $\{\bar{u}(t)\} = \{u_{k_1} \ u_{k_2} \ \dots \ u_{k_K}\}^T$ and $\{\ddot{\bar{u}}(t)\} = \{\ddot{u}_{k_1} \ \ddot{u}_{k_2} \ \dots \ \ddot{u}_{k_K}\}^T$ are the vectors of relative displacements and relative accelerations, respectively, at the K floors; $\{\bar{q}(t)\} = \{q_1(t) \ q_2(t) \ \dots \ q_K(t)\}^T$ is the vector of modal displacements for the modes 1 to K ; $\{\ddot{\bar{q}}(t)\} = \{\ddot{q}_1(t) \ \ddot{q}_2(t) \ \dots \ \ddot{q}_K(t)\}^T$ is the vector of modal accelerations for the modes 1 to K ; and $[\Psi]$ is the matrix containing mode-shape components at the instrumented floors. It may be noted that the matrix $[\Psi]$ differs from the complete mode-shape matrix $[\Phi]$, as the former contains the components of mode shape only at the instrumented floors. For the selected system, the matrix $[\Psi]$ of dimensions $K \times K$ is given by

$$[\Psi] = \begin{bmatrix} \phi_{k_1,1} & \phi_{k_1,2} & \dots & \phi_{k_1,K} \\ \phi_{k_2,1} & \phi_{k_2,2} & \dots & \phi_{k_2,K} \\ \vdots & \vdots & & \vdots \\ \phi_{k_K,1} & \phi_{k_K,2} & \dots & \phi_{k_K,K} \end{bmatrix} \tag{6}$$

If $\{\bar{u}(t)\}$ or $\{\ddot{\bar{u}}(t)\}$, and the mode-shape component matrix $[\Psi]$ are available, the modal displacements $\{\bar{q}(t)\}$ and modal accelerations $\{\ddot{\bar{q}}(t)\}$ can be computed by solving Equation (5) at each time-instant. The relative displacements and accelerations at any non-instrumented floor j can then be computed from

$$u_j(t) = \sum_{i=1}^K q_i(t)\phi_{ji} \quad \text{and} \quad \ddot{u}_j(t) = \sum_{i=1}^K \ddot{q}_i(t)\phi_{ji} \tag{7}$$

The total displacements and accelerations at any non-instrumented floor can thus be computed from

$$u_j^t(t) = u_j(t) + u_b(t) \quad \text{and} \quad \ddot{u}_j^t(t) = \ddot{u}_j(t) + \ddot{u}_b(t) \tag{8}$$

in which $u_b(t)$ and $\ddot{u}_b(t)$ are the displacements and accelerations, respectively, recorded at the base of the building. Equations (5) to (8) represent the MBI procedure.

The MBI procedure requires that mode-shape component matrix $[\Psi]$ be well conditioned. Since the mode shape matrix of all modes is rank-deficient by one, the MBI procedure cannot include all modes, even if it is possible, in Equation (5). In fact, the largest number of modes that can be included in the MBI

procedure is equal to the total number of instrumented floors excluding the base. Furthermore, the modes which have a “node” (or zero mode-shape component) at or near one or more of the floors with recorded motions must be avoided in the MBI procedure, because including those modes would lead to poorly conditioned $[\Psi]$ matrix. For the buildings considered in this investigation, three to four modes were found to be sufficient for the MBI of recorded motions.

The MBI procedure described so far is for estimating the translational displacement and accelerations at non-instrumented floors from the recorded translational displacements and accelerations at limited number of instrumented floors. However, this procedure could easily be extended to estimate the rotational (or torsional) displacements and accelerations as well if recorded torsional motions were available. It is useful to note that torsional motions are almost never directly recorded; they are typically computed from the differential translational motions at two ends of the building. Implementation of the MBI procedure including torsional motions would require that the matrix $[\Psi]$ (see Equation 6) also contains the mode-shape components corresponding to the torsional degrees of freedom, and relative torsional displacements and accelerations be computed from Equation (7), with ϕ_{ji} representing the torsional component of mode shape at the i th floor. However, care must be exercised in attempting to estimate torsional motions of a building with little or no coupling between the translational and torsional modes because of the possibility of poorly conditioned $[\Psi]$.

The MBI procedure requires mode shapes of the building. These mode shapes may either be computed from the eigenanalysis of a computer model of the building, estimated from the system identification methods (e.g., Mau and Aruna, 1994), or be computed from the approximate formulas for mode shapes (Miranda and Taghavi, 2005; Miranda and Akkar, 2006; Miranda and Reyes, 2002; Taghavi and Miranda, 2005). Among these three procedures to compute the mode shapes, the eigenanalysis is obviously the most complicated and time-consuming procedure. However, computer models of many instrumented buildings have already been developed for the purposes other than the eigenanalysis alone (e.g., to evaluate the current analytical procedures). These models have been carefully calibrated against the recorded data. Mode shapes from the eigenanalysis are therefore readily available for such buildings and have been utilized in the MBI procedure implemented in this investigation. If such computer models were not available, the other two procedures might be used to estimate the mode shapes needed in the MBI procedure.

The above development of the MBI procedure assumes complete uncoupling between the modal responses. This assumption is strictly valid for the buildings remaining in the linearly elastic range. However, the MBI procedure may be extended to estimate the response of buildings deformed slightly beyond the linearly elastic range because of weak modal coupling (Chopra, 2007). Clearly, the MBI procedure should not be applied to interpolate motions of buildings deformed far beyond the linearly elastic range, where significant modal coupling may occur. But application of an interpolation procedure is not necessary for the performance evaluation of such buildings, because performance may be evaluated visually in the case of large damage.

3. Error Function

The effectiveness of the PWCPI or MBI procedure to provide accurate estimates of the motions at non-instrumented floors is quantitatively measured by an error function defined by Limongelli (2003) as

$$\varepsilon_j = \sqrt{\frac{\sum_{i=1}^{\text{NPT}} (r_{r,j}(t_i) - r_{c,j}(t_i))^2}{\sum_{i=1}^{\text{NPT}} (r_{r,j}(t_i))^2}} \quad (9)$$

In this ε_j is the error function at the j th floor; $r_{r,j}(t_i)$ and $r_{c,j}(t_i)$ are the recorded (or exact) and interpolated values, respectively, of a response—floor displacement, story drift, or floor acceleration—at the j th location at the i th time-instant; and NPT is the number of time-instants for which the response is available. A lower value of the error function for a selected interpolation procedure is indicative of better estimate of the interpolated motion compared to the other interpolation procedure(s).

The error function defined by Equation (9) is the sum of squares of differences between the “exact” and interpolated responses at each time-instant. Therefore, the value of the error function is expected to be

larger for rapidly varying functions, such as acceleration, with many more peaks and valleys (and thus with the possibility of a much larger numerator in Equation (9)) compared to the less rapidly varying functions, such as displacement, with fewer peaks and valleys.

SELECTED BUILDINGS

Two reinforced-concrete (RC) buildings have been selected for this investigation. The first building is a 13-story commercial building in Sherman Oaks, California. This building has two basements. Designed in 1964, its vertical load carrying system consists of 2.4-in (61-mm) thick one-way slabs supported by concrete beams, girders, and columns. The lateral load system consists of moment-resisting concrete frames in the upper stories and concrete shear walls in the basement. The foundation system consists of concrete piles. This building is instrumented by the California Strong Motions Instrumentation Program (CSMIP) to measure horizontal accelerations at the 2nd sub-basement level, ground level, 2nd floor, 8th floor, and at the roof level (see Figure 1).

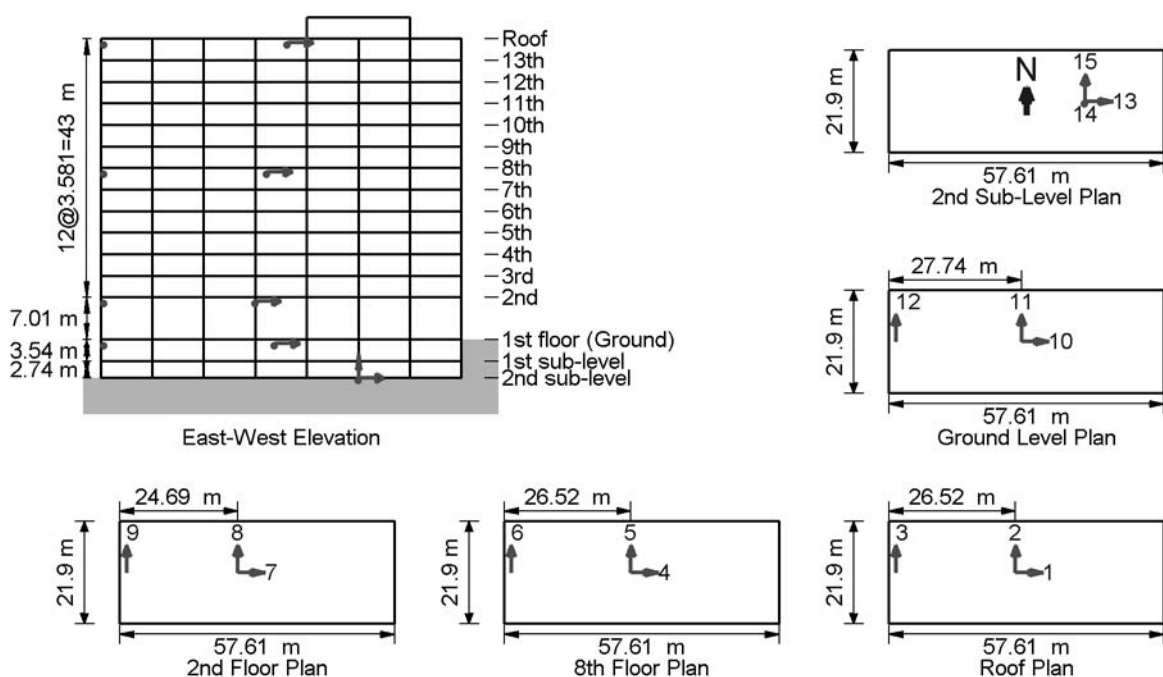


Fig. 1 The Sherman Oaks 13-Story Commercial Building

The second building selected is a 20-story hotel in North Hollywood (see Figure 2). This building has just one basement. Designed in 1966, its vertical load carrying system consists of 4.5–6 in (115–152 mm) thick RC slabs supported by concrete beams and columns. The lateral load system consists of moment-resisting concrete frames in the upper stories and concrete shear walls in the basement. The foundation system consists of spread footing below the columns. This building was instrumented by the CSMIP in 1983 with 16 sensors on five levels of the building. The sensors in the building measure horizontal accelerations at the basement level, 3rd floor, 9th floor, 16th floor, and at the roof level.

These two buildings have been selected in this investigation because of significant stiffness discontinuities and because three-dimensional computer models of these buildings are available from a recently completed study (Goel and Chadwell, 2007). Both of these buildings have very stiff shear walls in the basement and flexible moment-resisting frames in the upper stories. Furthermore, the Sherman Oaks building has soft-story condition between the ground and 2nd floor because the height of this story is much higher compared to those of the other stories (see Figure 1).

Motions of the two selected buildings are available from the Center for Engineering Strong Motion Data¹. The motions used in this investigation are the translational motions recorded during the 1994 Northridge earthquake in the longitudinal (east-west) direction of the Sherman Oaks 13-Story

¹ Website of the Center for Engineering Strong Motion Data, [http:// www.strongmotioncenter.org](http://www.strongmotioncenter.org)

Commercial Building, and in the transverse (north-south) direction of the North Hollywood 20-Story Hotel. Of the two selected buildings, the Sherman Oaks 13-Story Commercial Building was deformed slightly beyond the linearly-elastic range and the North Hollywood 20-Story Hotel remained within the linearly-elastic range during the 1994 Northridge earthquake (Goel and Chadwell, 2007).

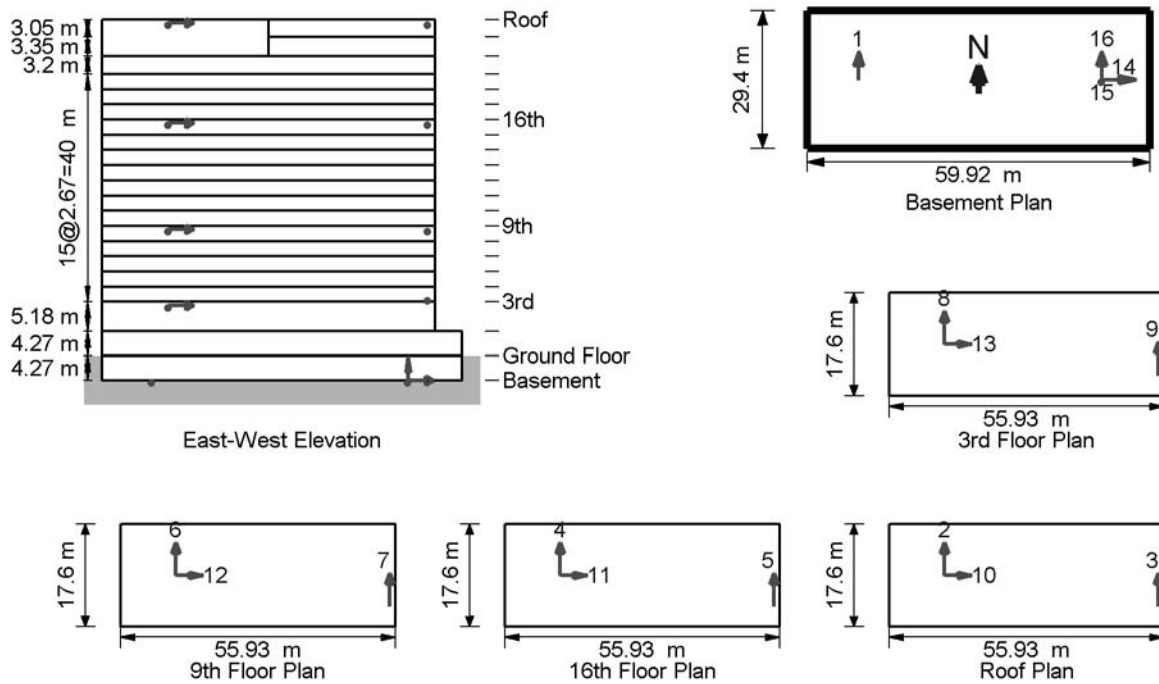


Fig. 2 The North Hollywood 20-Story Hotel

The relative floor motions obtained by subtracting the base motion from the floor motions recorded during the 1994 Northridge earthquake are shown in Figures 3 and 4 for the Sherman Oaks and North Hollywood buildings, respectively; motions recorded at the 2nd sub-level of the Sherman Oaks building (see Figure 1) and at the basement of the North Hollywood Hotel (see Figure 2) are considered as the base motions.

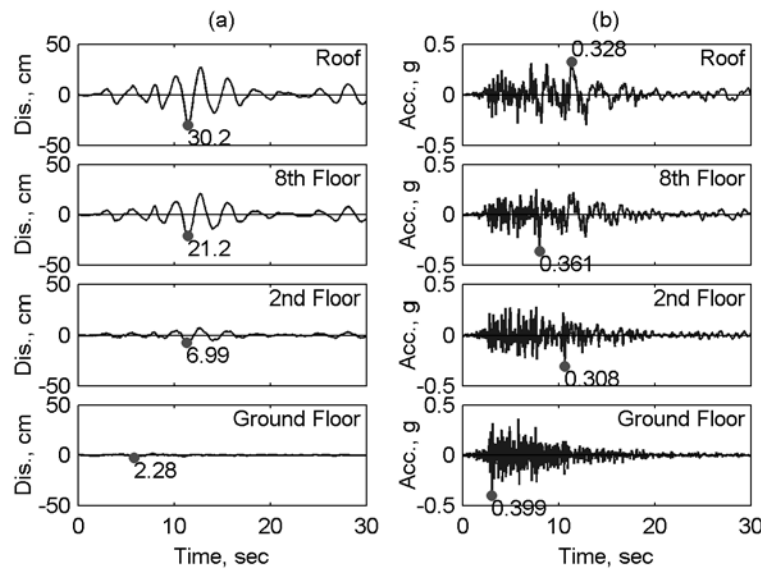


Fig. 3 Motions of the Sherman Oaks 13-Story Commercial Building in the longitudinal (east-west) direction during the 1994 Northridge earthquake: (a) Floor displacements relative to the base; and (b) Floor accelerations relative to the base

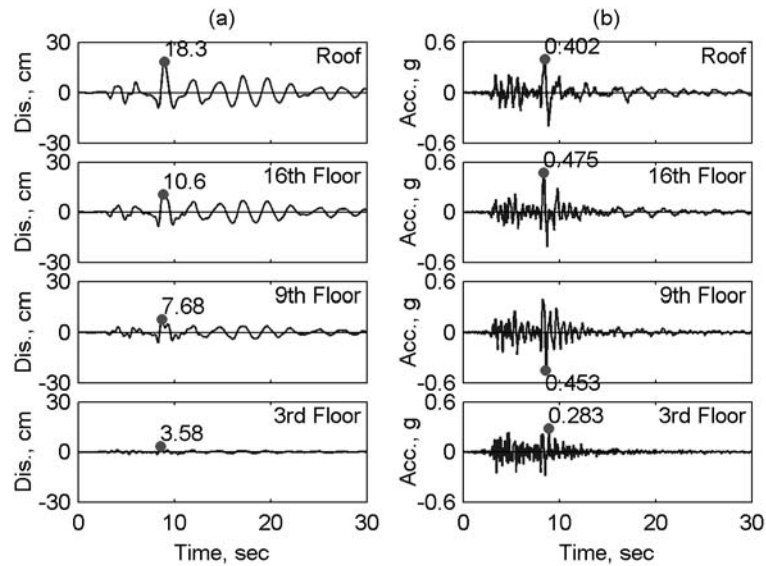


Fig. 4 Motions of the North Hollywood 20-Story Hotel in the transverse (north-south) direction during the 1994 Northridge earthquake: (a) Floor displacements relative to the base; and (b) Floor accelerations relative to the base

The motions used in this investigation are the corrected (or processed) strong motions recorded during the 1994 Northridge earthquake. The data processing procedure (see Shakal et al., 2003) attempts to eliminate the errors associated with noise in the actual recorded (or unprocessed) data. However, some errors may still remain in the processed data and may thus affect the accuracy of various interpolation procedures.

RESPONSE QUANTITIES

Response quantities investigated here are the floor displacement and floor acceleration at the center of the building relative to its base. Also considered is the story drift—defined as the relative displacement between two adjacent floors. It is useful to emphasize that while floor displacements and floor accelerations are recorded, albeit at a limited number of floors, story drift is not directly recorded but is “derived” from the recorded floor displacements. Torsional motions were not considered because the selected buildings are essentially symmetric; recorded motions indicated that these buildings experienced some torsional motions but those were very small.

MODE SHAPES

Needed in the MBI procedure are the mode shapes of the selected buildings. These mode shapes are computed by the eigen-value analyses of the linearly elastic models of the selected buildings. For this purpose, three-dimensional linear-elastic models of the two buildings were developed in Open System for Earthquake Engineering Simulation (OpenSees) (McKenna and Fenves, 2001). The effective flexural and shear stiffnesses of beams and columns were specified initially according to the FEMA-356 recommendations (FEMA, 2000). The first three mode shapes of the two selected buildings from the eigen-value analyses are shown in Figure 5. It may be noted that only the longitudinal component (in the east-west direction) of the mode shapes for the Sherman Oaks building and transverse component (in the north-south direction) of the mode shapes for the North Hollywood building are included in Figure 5. These components are extracted from the three-dimensional mode shapes of these buildings as in Goel and Chadwell (2007).

ACCURACY OF THE PWCPI PROCEDURE

The PWCPI procedure may be sensitive to the relative size of the interpolation segment (Beatson, 1986). Furthermore, the interpolated motions obtained from the PWCPI procedure may be sensitive to the significant stiffness discontinuities in buildings. This section examines sensitivity of the interpolated

motions from the PWCPI procedure to such conditions. It is useful to emphasize that this investigation is not concerned about a complete sensitivity analysis of the PWCPI interpolation with the number and combinations of instrumented floors but with demonstrating the possible limitations of the PWCPI procedure and presenting an improved procedure. A detailed sensitivity analysis of the PWCPI procedure and optimal location of sensors for interpolation is available elsewhere (Limongelli, 2003).

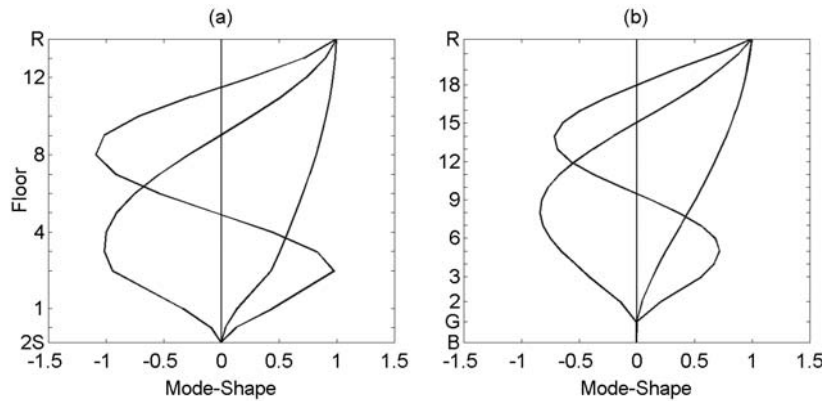


Fig. 5 Mode shapes of the selected buildings: (a) Sherman Oaks 13-Story Commercial Building; and (b) North Hollywood 20-Story Hotel

1. Interpolation of the Recorded Motions

Motions of the two selected buildings are available at five floors: motions of the Sherman Oaks building in the longitudinal direction were recorded at the 2nd sub-level (2S), ground floor (G), 2nd floor, 8th floor, and at the roof by the sensors, 13, 10, 7, 4, and 1, respectively (see Figure 1); and motions of the North Hollywood 20-Story Hotel in the transverse direction at the east edge were recorded at the basement (B), 3rd floor, 9th floor, 16th floor, and at the roof by the sensors, 16, 9, 7, 5, and 3, respectively (see Figure 2). The motions at the non-instrumented floors were first interpolated by the PWCPI procedure considering motions at all the five floors. The motions were then interpolated by dropping one of the intermediate instrumented floors; motions at the base and the roof of the building were always included in the interpolation. For the Sherman Oaks building, either the G or the 2nd floor was dropped from the set of instrumented floors; dropping the 8th floor led to unacceptable motions at the non-instrumented floors and is, therefore, not considered here. For the North Hollywood building, either the 3rd floor or the 9th floor was dropped from the set of instrumented floors. The peak floor displacements, story drifts, and floor accelerations obtained by these three interpolations are presented in Figures 6 and 7. Also included are the values of the error functions for the floors, which were dropped in the interpolation procedure, i.e., ε_G and ε_2 for the Sherman Oaks building, and ε_3 and ε_9 for the North Hollywood building. It may be noted that error function is computed only for those floor displacements and floor accelerations, for which the recorded data is available at the floor dropped in the interpolation procedure. Error function is not computed for the story drifts because recorded story drift data is not directly available.

The results presented in Figure 6 for the Sherman Oaks building indicate that peak values of interpolated motions depend noticeably on the instrumented floors selected in the interpolation procedure. The differences appear to be much larger for the story drifts (see Figure 6(b)) and floor accelerations (see Figure 6(c)) compared to the floor displacements (see Figure 6(a)).

When compared with the interpolated motions obtained from considering all the five floors, ignoring recorded motion of G or 2nd floor leads to an under-prediction of displacements at the floors 2 to 7 and to an over-prediction of displacements at the floors 9 to 13 (see Figure 6(a)). However, the discrepancy for the first case is smaller compared to that for the second, as indicated by a slightly lower value of ε_G compared to that of ε_2 (see Figure 6(a)). It may be recalled that ignoring the 2nd floor implies ignoring motion at a location of the soft-story condition. The floor displacements are identical for the three cases at 2S, 8th floor, and roof, because these three floors are included in each of the three sets of floors considered during the interpolation procedure.

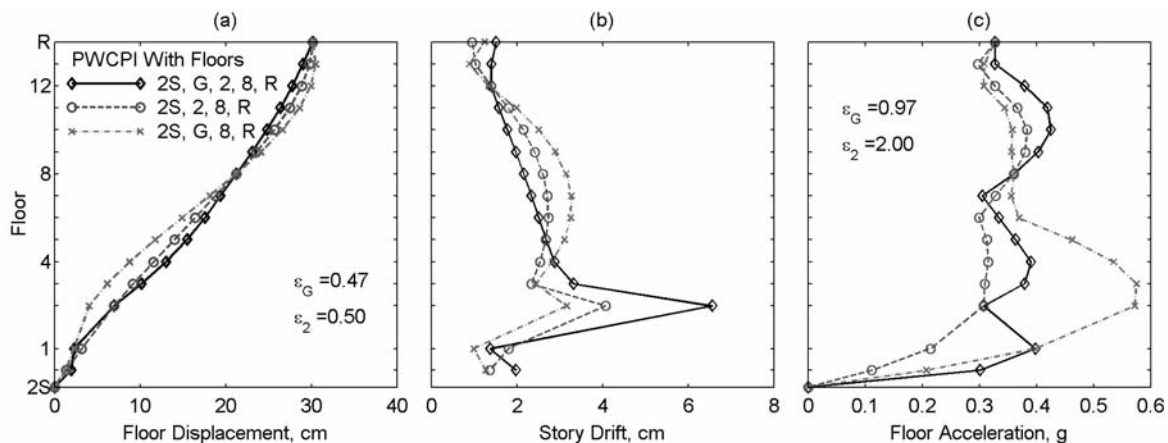


Fig. 6 Height-wise distribution of the peak response from the PWCPI procedure using recorded motions of the Sherman Oaks 13-Story Commercial Building for three different sets of sensors

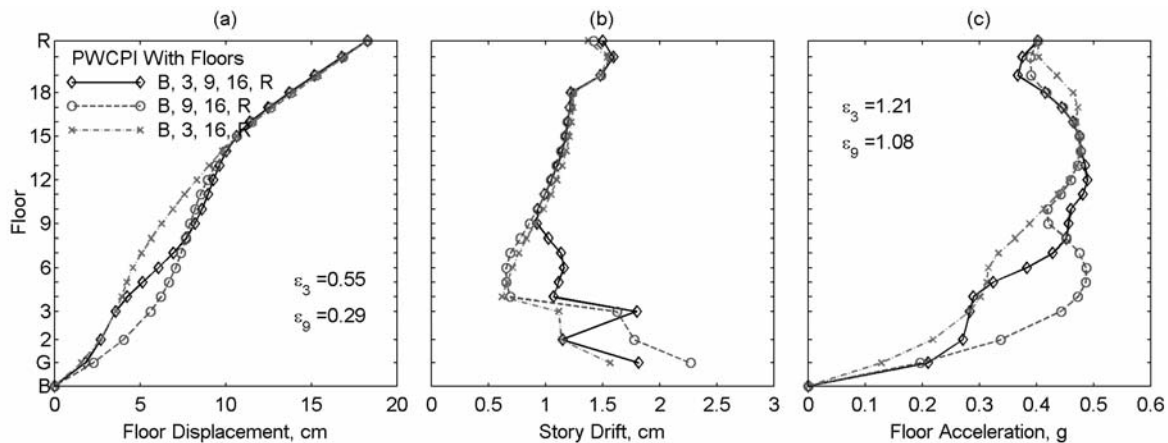


Fig. 7 Height-wise distribution of the peak response from the PWCPI procedure using recorded motions of the North Hollywood 20-Story Hotel for three different sets of sensors

The peak story drifts from the three sets of interpolation also differ significantly (see Figure 6(b)). When compared to the values from considering all the floors, ignoring the G or 2nd floor leads to a significant under-prediction for the stories 1–3 and an over-prediction for the stories 5–12. In particular, the differences are extremely large for the 2nd story drift—location of the soft-story condition. Unlike the floor displacements, which match at the common instrumented floors for the three cases (see Figure 6(a)), the story drifts appear to have the largest discrepancy at or near these floors (see Figure 6(b)). This is the case because story drifts, which are indicative of the slope of the displacement profile, differ the most at the common instrumented floors even though displacements match at these floors.

Similar to the story drift, peak floor accelerations from the three sets of interpolation also differ significantly (see Figure 6(c)). In particular, dropping either the G or 2nd floor leads to a significant under- or over-prediction of the floor accelerations, when compared with the interpolation using all the five floors. These differences tend to be larger in the lower floors compared to the upper floors.

The error functions for interpolated accelerations are much larger than those for the interpolated displacements: $\epsilon_G = 0.47$ for the displacements, and $\epsilon_G = 0.97$ for the accelerations; and $\epsilon_2 = 0.5$ for the displacements, and $\epsilon_2 = 2.0$ for the accelerations (see Figures 6(a) and 6(c)). As mentioned previously, a larger value of the error for accelerations is in part due to the rapidly varying nature of the acceleration function.

The results for the North Hollywood building (see Figure 7) indicate that the interpolation using three sets of instrumented floors provides almost identical floor displacements and story drifts in the upper part of the building—above floor 15 for the displacements (see Figure 7(a)), and above story 9 for the drifts

(see Figure 7(b)). In the lower part of the building, however, both interpolated displacements and drifts depend on the selection of instrumented floors. Compared to the case in which all the five floors are considered, ignoring the 3rd floor tends to over-predict displacements in the floors 2–6 (see Figure 7(a)), and over-predict drift in the story 1 and under-predict drifts in the stories 3–8 (see Figure 7(b)). Ignoring the 9th floor under-predicts the displacements of floors 1–13 (see Figure 7(a)) and the drifts of stories 3–8 (see Figure 7(b)). The floor accelerations, however, differ throughout the building height (see Figure 7(c)). For this building, ignoring the recorded motions at the 9th floor leads to a lower error function for both displacements and accelerations compared to the values when recorded motions at the 3rd floor are ignored. As noted previously, error function for the interpolated accelerations is much larger than that for the interpolated displacements (see Figures 7(a) and 7(c)).

2. Interpolation of Simulated Motions

The results presented in the preceding section indicate that interpolated motions may depend noticeably on the locations of instrumented floors. However, these results do not indicate which set of instrumented floors would provide the most accurate prediction of motions, because the recorded motions for the selected buildings are available only at a limited number of floors. For this purpose, data is needed from the buildings with motions available at all floors. Unfortunately, the mid- or high-rise buildings, such as those considered in this investigation, are almost never instrumented at each floor. In the absence of the data from buildings instrumented at each floor, data simulated from the response-history analysis (RHA) of carefully calibrated computer models of buildings provides the best-available option. It is useful to note that this approach has been used previously by Taghavi and Miranda (2005) to evaluate an interpolation scheme developed to estimate the floor acceleration demands in multistory buildings.

In this investigation, the motions at each floor were simulated by the RHA of building models due to the motions that were recorded at the base of the building. For this purpose, three-dimensional computer models of the two selected buildings were developed using the structural analysis software “OpenSees” (McKenna and Fenves, 2001). The beams, columns, and shear walls were modeled with the “nonlinearBeamColumn” element with fiber section in “OpenSees”. The damping was defined as the classical damping with damping ratios in the first and second modes to be 5%. The base input motions were taken as those recorded at the base of these buildings during the 1994 Northridge earthquake, and soil-structure interaction effects were ignored. Further details of the modeling of the selected buildings are available elsewhere (Goel and Chadwell, 2007).

The RHA motions at a limited number of floors were then used to interpolate motions at the remaining floors. The sets of floors used to interpolate were selected to be the same as those in the preceding section. The accuracy of the interpolation procedure is evaluated by comparing the motions simulated from RHA with those from the PWCPI procedure.

While accuracy of an interpolation procedure may be evaluated by considering numerous combinations of instrumented floors, only a few practical combinations are considered in this investigation. These combinations include the locations of significant stiffness discontinuities and nearly evenly distributed locations over the remaining height of the building. Combinations with one of the intervals being much larger than the others, such as those obtained by dropping the 8th floor in the Sherman Oaks building, lead to unacceptable results and are not considered in this investigation.

The height-wise variations of the peak values of floor displacements, story drifts, and floor accelerations from RHA are compared with those from the PWCPI procedure in Figure 8 for the Sherman Oaks building and in Figure 9 for the North Hollywood building. The PWCPI procedure uses the same three sets of floors for interpolation as those considered in the preceding section. The error functions are computed for the floor displacements, story drifts, and floor accelerations at each of the floors not used in the interpolation procedure. The means of these errors are also reported in Figures 8 and 9.

The presented results for the Sherman Oaks building indicate that one of the three interpolations—the case in which the motions at 2S, G, 2nd floor, 8th floor, and roof are used in the PWCPI procedure—provides reasonable predictions of the floor displacements (see Figure 8(a)) and floor accelerations (see Figure 8(c)) when compared with the RHA results. Ignoring one of the floors leads to further deterioration of the accuracy of the predictions from the PWCPI procedure when compared to the results from the RHA. The mean error function is the lowest for floor displacements and accelerations for the interpolation based on the motions at 2S, G, 2nd floor, 8th floor, and roof, but becomes larger when one of these floors is ignored in the interpolation procedure. The story drifts from the PWCPI procedure differ

significantly from the RHA values (see Figure 8(b)): the PWCPI procedure considering the motions of aforementioned five floors leads to an under-prediction in the mid-portion of the building (i.e., for the stories 6 to 10) and to an over-prediction in the lower- and upper- portions (i.e., for the stories 3 and 13) of the building. The mean error function for story drifts is also much larger compared to the values for floor displacements and accelerations. Ignoring one of the five floors in the interpolation procedure tends to provide slightly better correlation of story drifts with the values from RHA but the mean error still remains quite high.

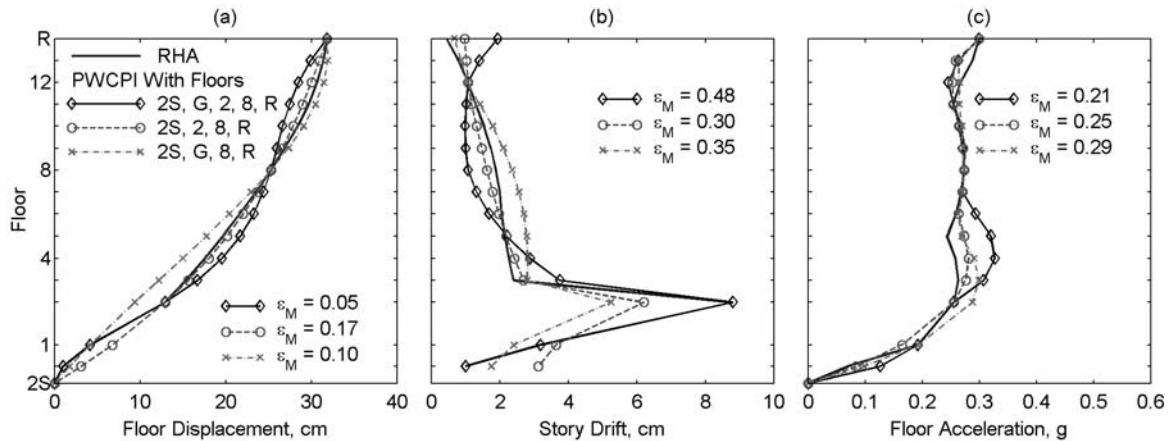


Fig. 8 Height-wise distribution of the peak response from the PWCPI procedure using simulated motions of the Sherman Oaks 13-Story Commercial Building for three different sets of monitored floors

The results for the North Hollywood building (see Figure 9) indicate that the case in which the motions at basement, 3rd floor, 9th Floor, 16th floor, and roof are used, the PWCPI procedure generally provides very good predictions of the floor displacements throughout the building height (see Figure 9(a)). The predictions for the story drifts and floor accelerations, however, may be poor in some portions of the building (see Figures 9(b) and 9(c)). Furthermore, the accuracy of the predictions deteriorates significantly if one of the floors is ignored in the interpolation procedure as indicated by the significant increase in the mean error.

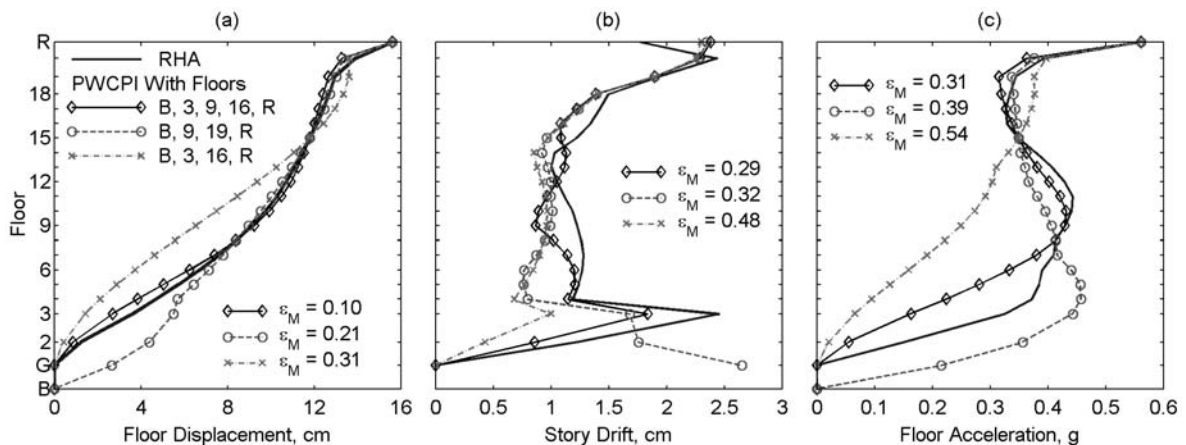


Fig. 9 Height-wise distribution of the peak response from the PWCPI procedure using simulated motions of the North Hollywood 20-Story Hotel for three different sets of monitored floors

The results presented in this section indicate that the PWCPI procedure may provide reasonable predictions of the floor displacements at non-instrumented floors if (1) the building is instrumented at a regular interval over its height, and (2) additional instruments are located in the building where stiffness changes significantly either due to the very-stiff condition resulting from the basement shear walls or due

to the soft-story condition resulting from a taller story compared to the other stories. This becomes apparent from the displacements in Figures 8(a) and 9(a) where ignoring one of the five floors—a case which results in non-uniform locations of the instrumented floors—or ignoring the 1st floor in the Sherman Oaks building and ignoring the 3rd floor in the North Hollywood building—a case which leads to ignoring the floor near the stiff-story condition due to the basement shear wall—or ignoring the 2nd floor in the Sherman Oaks building—a case which leads to ignoring the floor near the soft-story condition—results in significant discrepancies between the results from the PWCPI procedure and the RHA. The story drifts and floor accelerations, however, may not still be accurately predicted by the PWCPI procedure. It may be noted that the mean errors for story drifts and floor accelerations tend to be much larger compared to those for the floor displacements.

RELATIVE ACCURACY OF PWCPI AND MBI PROCEDURES

The interpolated seismic demands from the two interpolation procedures—PWCPI and MBI—are compared with those from the RHA procedure (or simulated seismic demands) in Figure 10 for the Sherman Oaks building and in Figure 11 for the North Hollywood building. The “known” motions at the selected floors in both the interpolation procedures are taken same as the simulated motions from the RHA. The motions at 2S, G, 2nd, 8th, and roof of the Sherman Oaks building and the motions at B, 3rd, 9th, 16th, and roof of the North Hollywood building are used in the interpolation procedures. The estimates from the MBI procedure are based on the first four modes of the two selected buildings.

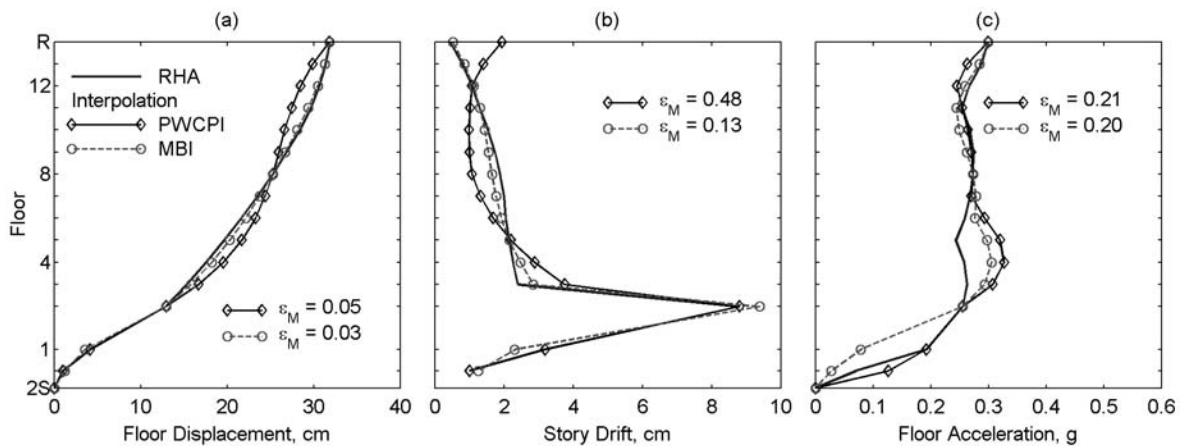


Fig. 10 Comparison of the height-wise distributions of peak response from two interpolation procedures—PWCPI and MBI—with those from RHA for the Sherman Oaks 13-Story Commercial Building

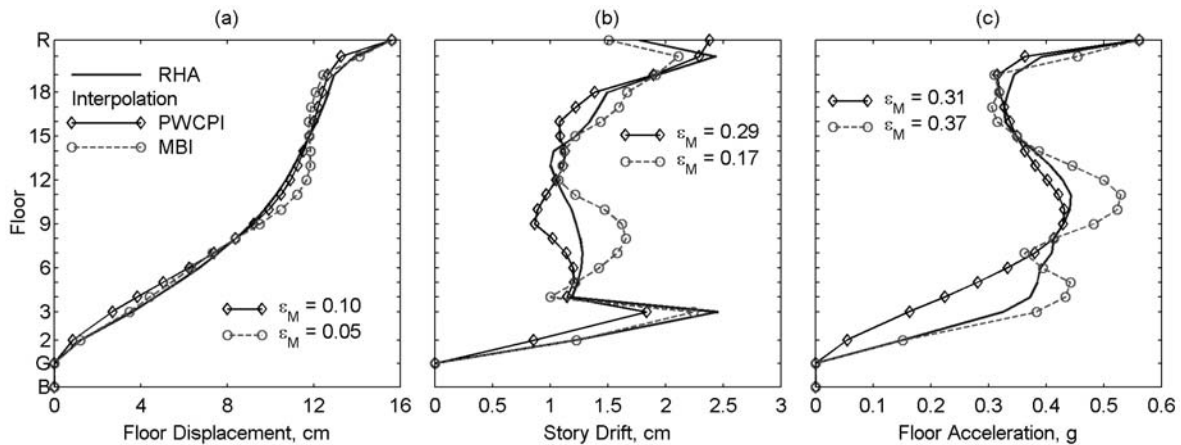


Fig. 11 Comparison of the height-wise distributions of peak response from two interpolation procedures—PWCPI and MBI—with those from RHA for the North Hollywood 20-Story Hotel

The height-wise distributions of floor displacements indicate that both the PWCPI and MBI procedures provide reasonable estimates of the floor displacements over building height (see Figures 10(a) and 11(a)). However, the MBI procedure provides slightly better estimates of the floor displacements, as indicated by a lower mean error for the MBI procedure in comparison with the PWCPI procedure: the mean error from the MBI procedure is 0.03 and 0.05 for the Sherman Oaks and North Hollywood buildings, respectively, compared to the values of 0.05 and 0.1 from the PWCPI procedure (see Figures 10(a) and 11(a)).

The estimates of story drifts from the MBI procedure are much better compared to those from the PWCPI procedure. In particular, the PWCPI procedure under-predicts story drifts in the middle stories and over-predicts story drifts in the upper stories of the Sherman Oaks building, whereas the MBI procedure closely tracks the story drifts from the RHA (see Figure 10(b)). With one exception, similar trends are apparent for the story drifts of the North Hollywood building (see Figure 11(b)); the exception occurs for the top-story drift where the MBI may slightly under-predict the drift compared to the RHA procedure. The mean error in story drifts from the MBI procedure is significantly less than that from the PWCPI procedure: the mean error in story drifts from the MBI procedure is 0.13 and 0.17 for the Sherman Oaks and North Hollywood buildings, respectively, compared to the values of 0.48 and 0.29 from the PWCPI procedure (see Figures 10(b) and 11(b)).

The accuracy of both the MBI and PWCPI procedures for estimating floor accelerations appears to be similar as apparent from the similar mean errors (see Figures 10(c) and 11(c)). However, the discrepancies in floor accelerations from the two procedures may occur at different locations when compared with the results from the RHA.

The preceding results indicate that for the same selection of instrumented floors the MBI procedure provides improved estimates of the floor displacements and story drifts compared to the PWCPI procedure. The two procedures, however, provide similar estimates of the floor accelerations.

SENSITIVITY OF MBI PROCEDURE

Sensitivity of the MBI procedure, i.e., the dependence of results from the MBI procedure to the sensor distribution—number and locations of sensors—is investigated next by comparing the results from RHA with those from the MBI procedure using two sets of floor motions for the two selected buildings. For the Sherman Oaks building, the first set consist of the motions at all floors—G, 2nd, 8th, and roof—whereas the second set consists of motions only at two floors—G, 8th and roof. Obviously, first four modes were included in the MBI procedure using the first set of motions, and first three modes were included in the MBI procedure using the second set. For the North Hollywood building, the first set consists of motions at four floors—3rd, 9th, 16th, and roof—permitting the use of first four modes in the MBI procedure, and the second set includes the motions at three floors—9th, 16th, and roof—allowing the use of first three modes.

The results for the Sherman Oaks building indicate that both sets of motions lead to very good estimates of floor displacements, story drifts, and floor accelerations when compared with the RHA results (see Figure 12): the mean errors from the two sets are generally very similar. More importantly, the dependence of results from the MBI procedure on the locations and number of instrumented floors is much less, as apparent from the much smaller variation in mean error with selection of floors in the interpolation procedure, compared to that of the results from the PWCPI procedure (compare Figure 12 with Figure 8). Similar to the Sherman Oaks building, both sets of motions provide very good estimates of the floor displacements for the North Hollywood building (see Figure 13(a)), and the dependence of results from the MBI procedure on the locations and number of instrumented floors is much less than that of the results from the PWCPI procedure (compare Figure 13(a) with Figure 9(a)). While the story drifts and floor accelerations from the MBI procedure using the second set of motions are much better than those from the PWCPI procedure using the same set (compare Figure 13(b) with Figure 9(b), and Figure 13(c) with Figure 9(c)), noticeable differences occur in the results from the MBI procedure when compared with the RHA results at few locations in the building. Such is the case because higher modes contribute much more to the response quantities like story drifts and floor accelerations of the flexible North Hollywood building, and dropping one floor from the set of motions leads to the inclusion of one less mode in the MBI procedure, which in turn leads to a loss of accuracy.

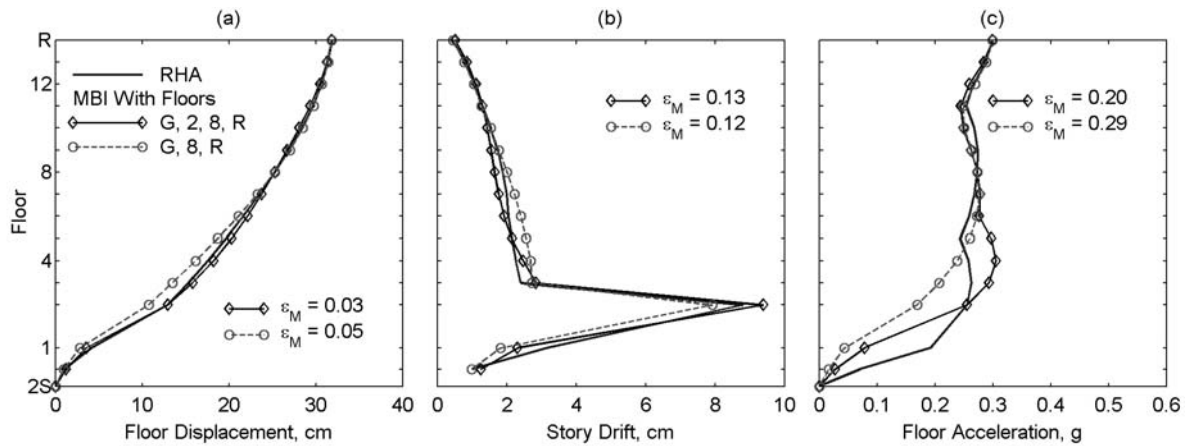


Fig. 12 Height-wise distribution of peak response from the MBI procedure, for the motions from RHA of the Sherman Oaks 13-Story Commercial Building, for two different sets of monitored floors

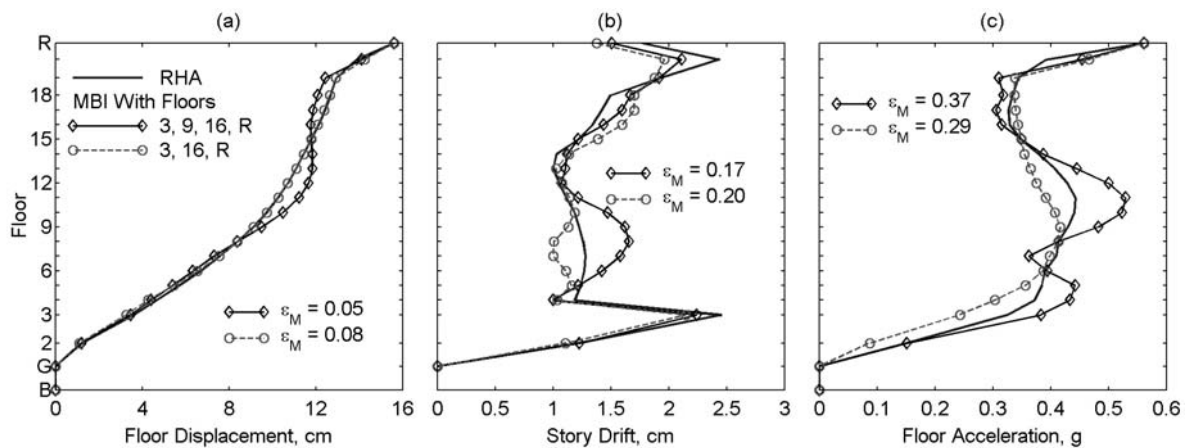


Fig. 13 Height-wise distribution of peak response from the MBI procedure, for the motions from RHA of the North Hollywood 20-Story Hotel, for two different sets of monitored floors

SUMMARY AND CONCLUSIONS

Investigated in this paper is the accuracy of the piece-wise cubic polynomial interpolation (PWCPI) procedure to estimate the motions—floor displacements, story drifts, and floor accelerations—at non-instrumented floors in the buildings with significant stiffness discontinuities. Based on the interpolation of recorded motions of two buildings, it has been shown that the results from the PWCPI procedure may depend noticeably on the locations of instrumented floors. Since recorded motions are typically available only at a few floors, this did not clearly indicate which locations in the PWCPI procedure would provide the most accurate estimates of the motions at non-instrumented floors. Therefore, the motions at each floor of the selected buildings were simulated from the response history analysis (RHA) of the computer models of these buildings. The RHA motions at a limited number of floors were then used to investigate the accuracy of the PWCPI procedure. It has been shown that the PWCPI procedure may provide good estimates of the displacements at non-instrumented floors if (1) the building is instrumented at a regular interval over its height, and (2) additional instruments are located in the building where stiffness changes significantly. The story drifts and floor accelerations, however, may not be accurately predicted by the PWCPI procedure.

The mode-based interpolation (MBI) procedure presented in this paper provides much-improved estimates of the motions—floor displacements, story drifts, and floor accelerations—at non-instrumented floors compared to those from the PWCPI procedure. Furthermore, the dependence of results from the

MBI procedure on the number and locations of the instrumented floors is much less compared to that from the PWCPI procedure.

It is useful to emphasize that the observations and conclusions in this paper are based on a limited set of data: two buildings and only a few combinations of the number of sensors and their locations. Clearly, a much larger dataset is needed to develop further confidence in these conclusions. Furthermore, the MBI procedure in this investigation has been applied to interpolate only the translational motions. Since the recorded motions of even essentially symmetric buildings have been known to include some level of torsional motions, it would be useful to extend the MBI procedure to estimate torsional motions as well. A comprehensive investigation to address this issue is currently underway, and the results would be reported upon completion.

ACKNOWLEDGEMENTS

This investigation is supported by the California Department of Conservation, California Geological Survey, Strong Motion Instrumentation Program under Contract No. 1005-832. This support is gratefully acknowledged. Also acknowledged is the useful insight provided by Dr. Praveen Malhotra on various interpolation procedures.

APPENDIX I: PIECE-WISE CUBIC POLYNOMIAL INTERPOLATION PROCEDURE

Let us consider a building with sensors at J locations and sub-divided into $J - 1$ sub-intervals. Also, let r_j be the recorded response from the j th sensor located at height h_j ; response r_j is available for $j = 1, 2, \dots, J$. Using the piece-wise cubic polynomial interpolation, the response r at height h located in the j th sub-interval may be expressed as

$$r(h) = a_j \bar{w}_j + b_j w_j + c_j \frac{(\Delta h_j)^2}{6} (\bar{w}_j^3 - \bar{w}_j) + d_j \frac{(\Delta h_j)^2}{6} (w_j^3 - w_j) \tag{A.1}$$

in which $w_j = (h - h_j) / (h_{j+1} - h_j)$; $\bar{w}_j = (h_{j+1} - h) / (h_{j+1} - h_j)$; $\Delta h_j = h_{j+1} - h_j$; and a_j , b_j , c_j , and d_j are the cubic-polynomial constants for the j th sub-interval.

The polynomial constants for each of the $J - 1$ sub-intervals are $a_j = r_j$, $b_j = r_{j+1}$, $c_j = \sigma_j$, and $d_j = \sigma_{j+1}$. The J values of σ_j for the piece-wise cubic polynomial interpolation with “not-a-knot” end conditions are computed from the following set of linear equations (Beatson, 1986):

$$\begin{aligned} -\bar{\theta}_1 \sigma_1 + \sigma_2 - \theta_1 \sigma_3 &= 0 \\ \theta_{j-1} \sigma_{j-1} + 2\sigma_j + \bar{\theta}_{j-1} \sigma_{j+1} &= \frac{6}{h_{j+1} - h_{j-1}} \left[\left(\frac{r_{j+1} - r_j}{h_{j+1} - h_j} \right) - \left(\frac{r_j - r_{j-1}}{h_j - h_{j-1}} \right) \right]; \quad j = 2, 3, \dots, J - 1 \\ -\bar{\theta}_{J-2} \sigma_{J-2} + \sigma_{J-1} - \theta_{J-2} \sigma_J &= 0 \end{aligned} \tag{A.2}$$

in which

$$\begin{aligned} \theta_j &= \frac{h_{j+1} - h_j}{h_{j+2} - h_j}; \quad j = 1, 2, \dots, J - 2 \\ \bar{\theta}_j &= \frac{h_{j+2} - h_{j+1}}{h_{j+2} - h_j}; \quad j = 1, 2, \dots, J - 2 \end{aligned} \tag{A.3}$$

In the matrix form, the solution for J values of σ_j involves solving the following system:

$$[A]\{\sigma\} = \{b\} \tag{A.4}$$

in which $\{\sigma\} = \{\sigma_1 \ \sigma_2 \ \dots \ \sigma_J\}^T$,

$$[A] = \begin{bmatrix} -\bar{\theta}_1 & 1 & -\theta_1 & 0 \\ \theta_1 & 2 & \bar{\theta}_1 & 0 \\ 0 & \theta_2 & 2 & \bar{\theta}_2 \\ & & & \vdots \\ & \theta_{J-3} & 2 & \bar{\theta}_{J-3} & 0 \\ & 0 & \theta_{J-2} & 2 & \bar{\theta}_{J-2} \\ & 0 & -\bar{\theta}_{J-2} & 1 & -\theta_{J-2} \end{bmatrix} \quad (\text{A.5})$$

and

$$\{b\} = \begin{Bmatrix} 0 \\ \frac{6}{h_3 - h_1} \left(\frac{r_3 - r_2}{h_3 - h_2} - \frac{r_2 - r_1}{h_2 - h_1} \right) \\ \frac{6}{h_4 - h_2} \left(\frac{r_4 - r_3}{h_4 - h_3} - \frac{r_3 - r_2}{h_3 - h_2} \right) \\ \vdots \\ \frac{6}{h_{J-1} - h_{J-3}} \left(\frac{r_{J-1} - r_{J-2}}{h_{J-1} - h_{J-2}} - \frac{r_{J-2} - r_{J-3}}{h_{J-2} - h_{J-3}} \right) \\ \frac{6}{h_J - h_{J-2}} \left(\frac{r_J - r_{J-1}}{h_J - h_{J-1}} - \frac{r_{J-1} - r_{J-2}}{h_{J-1} - h_{J-2}} \right) \\ 0 \end{Bmatrix} \quad (\text{A.6})$$

Once σ_j s have been computed from Equation (A.4), constants c_j and d_j can be determined, and the motion at any non-instrumented floor can be estimated from Equation (A.1). It may be noted that the formulation presented here differs slightly from Equation (2). However, this formulation is presented as it permits a much more convenient computation of the polynomial constants. The formulation presented here has been verified against the “spline” function in MATLAB (MathWorks, 2006) with “not-a-knot” end conditions.

REFERENCES

1. Beatson, R.K. (1986). “On the Convergence of Some Cubic Spline Interpolation Schemes”, SIAM Journal on Numerical Analysis, Vol. 23, No. 4, pp. 903–912.
2. Chopra, A.K. (2007). “Dynamics of Structures: Theory and Applications to Earthquake Engineering”, Prentice-Hall, Upper Saddle River, U.S.A.
3. De la Llera, J.C. and Chopra, A.K. (1997). “Evaluation of Seismic Code Provisions Using Strong-Motion Building Records from the 1994 Northridge Earthquake”, Report UCB/EERC-97/16, University of California, Berkeley, U.S.A.
4. FEMA (2000). “Prestandard and Commentary for the Seismic Rehabilitation of Buildings”, Report FEMA 356, Federal Emergency Management Agency, Washington, DC, U.S.A.
5. Goel, R.K. (2005). “Evaluation of Modal and FEMA Pushover Procedures Using Strong-Motion Records of Buildings”, Earthquake Spectra, Vol. 21, No. 3, pp. 653–684.
6. Goel, R.K. (2007). “Analysis of Strong Motion Records from Reinforced-Concrete Buildings”, Proceedings of the 2007 Structures Congress, Long Beach, U.S.A. (on CD).
7. Goel, R.K. and Chadwell, C. (2007). “Evaluation of Current Nonlinear Static Procedures for Concrete Buildings Using Recorded Strong-Motion Data”, Data Utilization Report, California Strong Motion Instrumentation Program, California Geological Survey, California Department of Conservation, Sacramento, U.S.A.

8. Limongelli, M.P. (2003). "Optimal Location of Sensors for Reconstruction of Seismic Responses through Spline Function Interpolation", *Earthquake Engineering & Structural Dynamics*, Vol. 32, No. 7, pp. 1055–1074.
9. Limongelli, M.P. (2005). "Performance Evaluation of Instrumented Buildings", *ISET Journal of Earthquake Technology*, Vol. 42, No. 2-3, pp. 47–61.
10. MathWorks (2006). "MATLAB—The Language of Technical Computing", The MathWorks, Natick, U.S.A.
11. Mau, S.T. and Aruna, V. (1994). "Story-Drift, Shear, and OTM Estimation from Building Seismic Records", *Journal of Structural Engineering*, ASCE, Vol. 120, No. 11, pp. 3366–3385.
12. McKenna, F. and Fenves, G.L. (2001). "OpenSees Command Language Manual: Version 1.2", Pacific Earthquake Engineering Center, University of California, Berkeley, U.S.A.
13. Miranda, E. and Akkar, S.D. (2006). "Generalized Interstory Drift Spectrum", *Journal of Structural Engineering*, ASCE, Vol. 132, No. 6, pp. 840–852.
14. Miranda, E. and Reyes, C.J. (2002). "Approximate Lateral Drift Demands in Multistory Buildings with Nonuniform Stiffness", *Journal of Structural Engineering*, ASCE, Vol. 128, No. 7, pp. 840–849.
15. Miranda, E. and Taghavi, S. (2005). "Approximate Floor Acceleration Demands in Multistory Buildings. I: Formulation", *Journal of Structural Engineering*, ASCE, Vol. 131, No. 2, pp. 203–211.
16. Naeim, F. (1997). "Performance of Extensively Instrumented Buildings during the January 17, 1994 Northridge Earthquake: An Interactive Information System", JAMA Report 97-7530.68, John A. Martin & Associates, Los Angeles, U.S.A.
17. Naeim, F., Lee, H., Bhatia, H., Hagie, S. and Skliros, K. (2004). "CSMIP Instrumented Building Response Analysis and 3-D Visualization System (CSMIP-3DV)", *Proceedings of the SMIP04 Seminar on Utilization of Strong-Motion Data*, Sacramento, U.S.A., pp. 83–102.
18. Shakal, A., Huang, M. and Graizer, V. (2003). "Strong-Motion Data Processing" in "International Handbook of Earthquake & Engineering Seismology, Part B (edited by W.H.K. Lee, H. Kanamori, P.C. Jennings and C. Kisslinger)", Academic Press, New York, U.S.A.
19. Taghavi, S. and Miranda, E. (2005). "Approximate Floor Acceleration Demands in Multistory Buildings. II: Applications", *Journal of Structural Engineering*, ASCE, Vol. 131, No. 2, pp. 212–220.